Peptide-mediated oligonucleotide delivery into eukaryotic cells

Inaugural-Dissertation

zur

Erlangung des Doktorgrades

der Mathematisch - Naturwissenschaftlichen Fakultät

der Universität zu Köln

vorgelegt von

Stephanie Natividad-Tietz

aus Bonn

2016

Abstract

Nucleic acids are promising molecules to treat genetic diseases in the field of molecular medicine. However, the clinical application is still restricted due to low serum stability and poor cellular uptake resulting from the high molecular weight, the negative charges and the hydrophilic character of the nucleic acids. Furthermore, before applying the nucleic acid to a patient, the generation of appropriate *in vitro* systems are mandatory to study the impact of the nucleic acid on the cells. Therefore, many viral and non-viral systems have been developed to facilitate the transfer of the nucleic acid across the cell membrane. Hence, the development of nucleic acid carriers with good efficiency and low toxicity are strongly needed. Among all available non-viral delivery systems, cell-penetrating peptides (CPPs) emerged as versatile carriers to deliver a wide range of cargoes into a large spectrum of different cell types *in vitro* as well as *in vivo*.

This thesis focuses on the development of appropriate *in vitro* systems and novel peptide-based vectors that can be utilized for intracellular delivery of nucleic acids through non-covalent nanoparticle formation. For this purpose, different CPPs derived from the human peptide hormone calcitonin (hCT) and additionally from the C-terminal domain of the cationic antimicrobial peptide CAP18 (sC18), were investigated concerning their ability to act as transporters in different fields of research that still need novel methods for gene modulation.

As a result of this thesis, the herein presented cell-penetrating peptides were able to transport nucleic acids into different cell lines (MCF-7, HEK-293 and hTERT RPE-1) without inducing cytotoxicity. Furthermore, remarkebly high transfection rates of non-differentiated hTERT RPE-1 cells could be obtained for the CPP N-E5L-hCT(18-32)-k7, even exceeding the results obtained by lipofection. Besides, N-E5L-hCT(18-32)-k7 was able to translocate into small single-cell protists (choanoflagellates).

Zusammenfassung

Nukleinsäuren sind viel versprechende Moleküle um genetisch bedingte Erkrankungen zu behandeln. Die unzureichende Serumstabilität und die schlechte Zellaufnahme aufgrund des hohen Molekulargewichts, der negativen Ladung und des hydrophilen Charakters der Nukleinsäure, erschweren jedoch die klinischen Anwendungen. Des Weiteren müssen bevor die Nukleinsäuren einem Patienten verabreicht werden können, geeignete *in vitro*-Systeme entwickelt werden, um die Auswirkungen der Nukleinsäure auf die Zellen zu untersuchen. Daher wurden zahlreiche virale als auch nicht-virale Transportsysteme entwickelt, um den Transport der therapeutischen Nukleinsäuren in die Zellen zu erleichtern. Da jedoch die Anwendung von viralen Vektoren mit vielen Nachteilen verbunden ist, werden nicht-virale Transportsysteme mit einem guten Wirkungsgrad und einer geringen Toxizität dringend benötigt. In den letzten Jahren sind sogenannte zellpenetrierende Peptide (cell penetrating peptides, CPP) als effektive, nicht-virale Vektoren für den Nukleinsäure-Transfer in den Fokus der Forschung getreten. Sie sind in der Lage, Moleküle in das Zellinnere zu transportieren, welche aufgrund ihrer Ladung, Größe und Hydrophilie normalerweise nicht die Zellmembran passieren können.

Ziel dieser Arbeit war die Etablierung von geeigneten *in vitro*-Systemen sowie die Entwicklung von neuen peptid-basierten Transportmolekülen, die über eine nicht-kovalente Verbindung in der Lage sind, die Nukleinsäuren in die Zellen zu transportieren. Hierfür wurden verschiedene CPPs im Hinblick auf ihre Transportfähigkeit für Forschungsbereiche untersucht, die noch geeignete Transporter benötigen. Die untersuchten CPPs wurden sowohl von dem humanen Calcitonin (hCT) als auch von dem kationischen antimikrobiellen Peptid CAP18 (sC18) abgeleitet.

Die in dieser Arbeit untersuchten CPPs waren in der Lage, Nukleinsäuren erfolgreich in verschiedene Zelllinien (MCF-7, HEK-293 und hTERT RPE-1) zu transportierten, ohne dabei die Vitalität der Zellen zu beeinflussen. Des Weiteren konnte für das CPP N-E5L-hCT(18-32)-k7 eine bemerkenswert hohe Transfektions-Effizienz erzielt werden, nachdem nicht-differenzierte hTERT RPE-1 Zellen damit transfiziert wurden. Die Effizienz überschritt sogar die von Lipofectamin, welches als positiv Kontrolle verwendet wurde. CPP N-E5L-hCT(18-32)-k7 war zudem in der Lage in einzellige Protisten (Choanoflagellate) zu internalisieren.

Table of Contents

1. Introduction

1.1 Gene therapy – Now and then

The idea of treating inherited and/or acquired diseases by shuttling therapeutic nucleic acids into a patient´s cell, aroused the first time in 1972 by Friedman and Roblin [1]. They cited a publication from Stanfield Roger, where he proposed that "good DNA" could be used to treat genetic disorders. This was the birth of the concept of gene therapy [1]. Twelve years later, scientists succeeded in developing a retrovirus vector that might shuttle foreign genes in an efficient manner into mammalian chromosomes [2]. Only six years later, in 1990, the first approved gene therapy was performed at the National Health Institute (NIH) in the United States of America (USA) by treating a four-year old girl that suffered from a genetic disorder (ADA-SCID) causing an inability of fighting infections. The doctors extracted her white blood cells and inserted them with the corrected genes that were able to produce the missing enzyme, adenosine deaminase, subsequently reinjected the corrected white blood cells. Unfortunately, the effect was only temporary [3]. In the following years, several other successful applications to treat genetically disorders were reported, leading the scientists to unrealistic expectations and overestimating their skills. In 1999, the death of Jesse Gielsinger caused an abrupt stop of gene therapy research in the USA. After he was treated with a trillion of adenoviruses as a vector that was directly injected to his liver, he died. Differentially than expected, the infection spread and infected other important organs. Gelsinger´s immune system showed an more intensive response by blasting all infected cells causing his death [4]. As a result, several clinical trials were suspended and scientists were forced to rethink their research. However, the faith and hope in gene therapy never died. In the following years, several successful approaches where published with a turning point in 2008, when eight-year old Corey Haas, suffering from a degenerative retina disorder, was healed after gene therapy [5]. In 2011, a further successful gene therapy application was reported. A man who was treated with a hematopoietic stem cell transplantation was cured from HIV [6].Despite all success, gene therapy is still in the fledgling stages and needs further improvement concerning safety and efficiency. One of the bottlenecks is the successful delivery of the nucleic acids into the host cells, and to their target. Therefore, many efforts have been done to develop effective delivery vectors.

However, before applying a nucleic acid to a patient, it is first of all mandatory to perform the experiments *in vitro*. For this purpose, generating *in vitro* studies for transfections are of enormous importance to elucidate potential toxicities or side-effects.

1.2 Viral *vs*. non-viral vectors for nucleic acid delivery

The delivery of large and hydrophilic molecules, such as nucleic acids, to the intracellular compartments is restricted due to their poor ability to permeate the plasma membrane. Only compounds within a narrow range of molecular size, net charge and polarity are able to directly cross the barrier into the cell [7]. For compounds that are not able to translocate the cell membrane on their own, various delivery systems were developed. Once, the gene delivery system is administrated, it is exposed to a harsh environment. The system must survive degrading serum nucleases and be protected against possible interactions with blood components, serum proteins and antibodies, which may cause the loss of functional integrity [8]. The delivery can occur using either a viral or a non-viral vector to make the gene transfer safe, more efficient and specific. Viral vectors, like lentiviral vectors [9], are very effective delivery systems enabling high transduction efficiency and stable gene expression [10]. This is due to the fact that viruses evolved a large number of strategies helping them to survive the extracellular matrix and deliver their genetic material into the host cell [11]. However, the use of viral vectors has many drawbacks regarding their safety and application, for instance toxicity, mutagenicity, immunogenicity, low target cell specificity, difficulties in handling, high production costs and the inability to deliver large size genes [10, 12-15]. On the other hand, non-viral vectors provide a wide range of advantages towards viral vectors. They are easy to prepare, have less toxicity, are able to deliver large size genes, are inexpensive and moreover they are bio-safe. Unfortunately, they are usually less efficient and only transfect cells transiently compared to viral vectors [16-19]. Nevertheless, the application and development of non-viral vectors in clinical trials increases continuously, whereas the use of viral vectors decreases [16]. According to the application and the desired delivery of bioactive molecules into the cells, a large number of non-viral vectors are now available (see fig. 1). The methods are divided in physical or chemical methods, whereas the chemical methods are further subdivided into inorganic particles, lipid-based, polymer-based and peptide-based [20, 21].
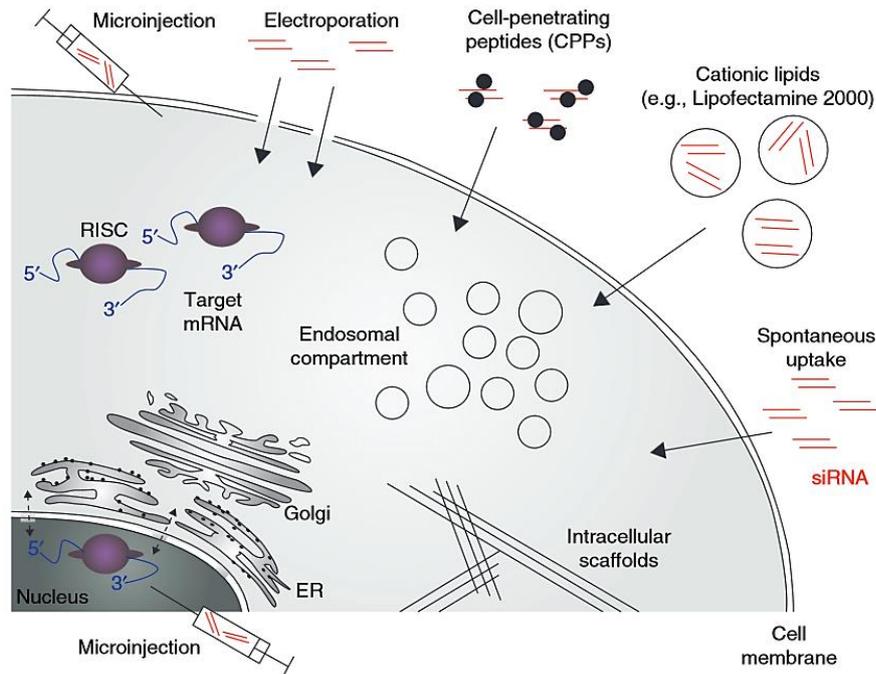
Fig. 1: Overview of transfection methods [22]

1.2.1 Physical methods

Using methods like fine needle puncture, electric impulses or high-pressure gas allow the genes to enter the cells directly, mediating direct penetration of the desired genes into the cytosol. The delivery utilizing physical methods is not restricted for small nucleic acid molecules; in fact, it is possible to deliver large nucleic acid as well as other non-permeable molecules. An overview of the different physical methods, their pros and cons is shown in table 1. However, there are a few disadvantages in using physical methods, like employing physical force to overcome the cell membrane might damage the cells irreversibly. Furthermore, it is labor-intensive and expensive equipment is needed to perform the experiments. Thus, the main drawback is the inability to deliver nucleic acid to the nucleus resulting in low transfection efficiency. This major hurdle limits the application of physical methods for clinical application [20, 23]. To overcome these impediments, a diversity of chemical delivery methods have been developed.

Table 1: Overview of physical delivery methods

Method	Procedure	Advantage	Disadvantage	Ref.
Microinjection	Direct injection of nucleic acid into a single living cell via micropipette	Easy, reproducible, delivery of large size DNA with high efficiency and non-toxic	Each cell must be individually manipulated	[21, 24]
Jet Injection	Target cells are hit by a high-speed ultrafine stream of pressurized gas with a DNA solution	Safe and easy to control, no needle is needed	Low efficiency, local tissue damage	[25]
Hydroporation	Penetration of the cell via hydrodynamic pressure	Simple, reproducible, high efficiency	Restricted clinical application due to high amount of injection volume needed	[26]
Electroporation	High-voltage electrical currents lead to temporarily nanomeric pores onto the cell membrane	Good efficiency and reproducible method	Tissue damage, expensive instruments	[27]
Needle Injection	Direct local injection of naked DNA	Simple and safe	Low transfection efficiency	[21]
Gene Gun	Heavy metals coated with plasmid DNA are fired at the target cells by high pressure gas stream	Safe and good efficiency	Tissue damage	[27, 28]
Sonoporation	Cell membrane is temporarily permeable due to ultrasound waves	Non-invasive and safe	Low transfection efficiency	[29]

1.2.2 Chemical methods

When it comes to safe and less toxic gene delivery, chemical vectors are the most widely used delivery systems among non-viral vectors. As already mentioned before, chemical methods can be classified in the use of inorganic particles, lipid-based, polymer-based and peptide-based vectors. In addition, chemical vectors can be further categorized into four subgroups depending on their function and design [20]:

a) Vectors which protect the cargo from enzymatic degradation and other components from the blood by forming condensed complexes.

b) Vectors that are developed and synthesized to enhance the delivery of the cargo into the target.

c) Vectors designed to target systematic cell tissues.

d) Vectors that enable a prolonged and controlled release of the therapeutic cargo into the cells.

Nanoparticles derived from calcium phosphate, silica, gold/silver and or quantum dots belong to the class of inorganic particles. These compounds have the advantage of easy preparation and long storage time. Moreover, the surface of nanoparticles can be modified and functionalized, increasing the portfolio of methods. However, the transfection efficiency for all inorganic particle is relatively low [30].

Lipid-based delivery vectors are for example the widely used liposomes which are synthetic lipid spheres based on cationic lipids. They are composed of fatty acids on polymers with at least one lipid bilayer. To enclose the cargo molecules, an intersection is formed in aqueous solution. The complex formation between the liposome and the cargo molecule occurs via self-assembly [16, 30, 31]. The major advantages of liposomes are their low toxicity, the possibility to deliver large size DNA, easy handling and preparation. Above all, they show a good biodegradability since they are composed of naturally occurring components, and exhibit no cell specifity meaning that they can transfect a great variety of tissues and cell types [16, 32, 33]. One major drawback of liposomes is their non-specific interaction with other negatively charged components, like enzymes and serum proteins, leading to reduced transfection efficiency and limited use in clinical applications [34, 35].

Polymer-based vectors have few advantages towards lipid-based vectors owing for instance to their higher transfection efficiency and stability. Usually, the complexes formed between cationic polymers and nucleic acids are more stable than the complexes between lipid-based vectors and nucleic acids. Additionally, cationic polymers show low toxicity, structural diversity, good biodegradability, and triggered release of the nucleic acid in the cells is possible [36, 37]. Nonetheless, *in vivo* applications are limited due to the fact that polymeric nanoparticles are artificial substances, and therefore, are recognized as intruders leading to immune response by the body [20]. Prominent representatives for polymeric based vectors are

chitosan and polyethylenimine (PEI). Chitosan is composed of natural cationic polysaccharides (see fig. 2) and exhibits low toxicity, low immunogenicity, antimicrobial activity, good biocompatibility and biodegradability. Moreover, modifications can be easily introduced to improve transfection efficiency [38-40]. However, insolubility in water at a physiological pH and insufficient charge yielding causes low transfection efficiency [41]. Therefore, the application of chitosan as a transfection method is limited.
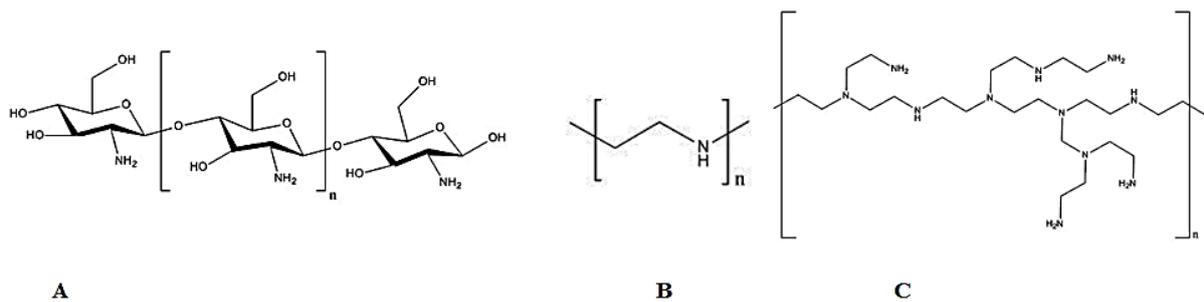
Fig. 2: Chemical structure of chitosan (A) and PEI linear (B) and PEI branched (C) [20]

Polyethylenimine (PEI) forms highly stable complexes with nucleic acids due to its strong condensation capacity. This polymer, with repeating units composed of the amine group and two aliphatic CH_2CH_2 spacers, can be synthesized either linear or branched (see fig. 2) to achieve complexation with the negatively charged nucleic acid. Benefits of using PEI are the intrinsic endosomal activity and the high transfection efficiency. Furthermore, due to an osmotic swelling, called proton sponge effect, the cargo is released from the endosomes to reach its target [42]. Usually, a PEI/DNA ratio higher than 3 is essential to yield a sufficient transfection. However, on the other hand it has been reported that higher concentrations may lead to cytotoxicity [20]. In addition, *in vivo* applications are hindered by the fact that PEI shows the tendency to aggregate red blood cells [43].

Table 2: Overview of chemical delivery methods

Method	Classification	Advantage	Disadvantage	Ref.
Calcium phosphate	Inorganic particle	Easy and cheap to prepare, good biocompatible and biodegradable	Poor efficiency and reproducibility, strict conditions	[44, 45]
Liposome	Lipid-based	Low toxicity and biodegradable	Non-specific interaction with negatively charged components	[32, 34]
Chitosan	Polymer-based	Low toxicity and immunogenicity, good biodegradability and biocompatibility	Low transfection efficiency and under physiological pH not soluble	[17, 38]
Polyethylenimine (PEI)	Polymer-based	High transfection efficiency, endosomal activity, strong condensation with DNA	Poor biodegradability, cytotoxicity can increase when transfection efficiency is enhanced	[46, 47]
Cell-penetrating peptides (CPPs)	Peptide-based	Low toxicity, good biodegradability and biocompatibility	Low tissue specificity	[48, 49]

The major obstacle in treating human diseases with gene therapy is the choice and application of the ideal delivery method that fulfills all the acquired before mentioned properties. Unfortunately, right now, all of the currently available non-viral vectors are not able to fulfill all requirements in a satisfying manner [16]. The need of developing new delivery strategies is therefore mandatory and of tremendous importance. One promising strategy that draws much attention in the last years and showed great potential is the use of so called cell-penetrating peptides.

1.3 Cell-penetrating peptides (CPPs)

In 1988, Frankel and Pabo, but also Green and Lowenstein, simultaneously reported for the first time protein transduction into cells. They demonstrated that the Trans-Activator of Transcription (TAT) protein of the Human Immunodeficiency Virus (HIV) was able to efficiently translocate tissue-cultured cells and promote the viral gene expression [50, 51]. Three years later, Prochiantz *et al.* reported on a transcription factor of *Drosophila melanogaster*, named Antennapedia homedomain, that was able to enter nerve cells and regulate neural morphogenesis [52]. In the following years, Vives *et al.* identified that a truncated sequence of the HIV-1 TAT protein basic domain, TAT_{48-60}, translocates through the plasma membrane and also accumulates in the cell nucleus [53]. In addition, Derossi postulated in 1994, that only a 16-mer peptide of the Antennapedia homeodomain, known as Penetratin or pAntp, was sufficient for intracellular delivery [54]. These discoveries marked the birth of so called cell-penetrating peptides, with its most famous representatives TAT_{48-60} and Penetratin. Ever since, a large number of new cell-penetrating peptides were identified or designed according to their application.

Cell-penetrating peptides typically consist of 5 - 30 amino acids with an amphipathic or highly cationic character, usually rich in amino acids such as arginine (Arg) and lysine (Lys) [55]. They are able to penetrate the cell membrane in an receptor-independent manner and are capable of translocating a wide range of different bioactive molecules, such as nanoparticles, peptides, proteins, liposomes, antisense oligonucleotides, small interfering RNA and double stranded DNA [56-61].

1.3.1   Classification

CPPs can be divided into diverse subgroups according to different criteria. One classification is based on the origin of the CPPs and includes protein-derived peptides, chimeric peptides and designed peptides. Protein-derived peptides, like TAT and Penetratin, are originated from natural occurring peptides or have a truncated sequence of the peptide that still has the ability to translocate the cell membrane. Chimeric CPPs are peptides that are formed by the fusion of two natural sequences, like Transportan. This CPP was constructed from the neuropeptide galanin and the wasp venom peptide toxin mastoparan [62-64]. Designed peptides, like the octa-arginine R8 [65], are rationally designed sequences usually based on structure-activity studies.

Table 3: Classification based on the origin of the peptide

Peptide	Sequence	Origin	Ref.
TAT(48-60)	GRKKRRQRRRPPQ	Protein-derived	[50]
Penetratin	RQIKIWFQNRRMKWKK	Protein-derived	[54]
sC18	GLRKRLRKFRNKIKEK	Protein-derived	[66]
Transportan	GWTLNSAGYLLGKINLKALAALAKKIL	Chimeric Galanin/ Mastoparan	[63]
MPG	GLAFLGFLGAAGSTMGAWSQPKKKRKV	Chimeric HIV-gp41/SV40-antigen	[67]
R8, R9, R10, R12	Polyarginine	Designed peptide	[65]
MAP	KLALKALKALKAALKLA	Designed peptide	[68]
N-E5L-hCT(18-32)-k7	GLLEALAELLEKFHTFPQTAIGVGAP | KKRKAPKKKRKFA	Chimeric	[69]

Another classification of CPPs is based on their physical-chemical properties according to their sequence: cationic, amphipathic and hydrophobic.

According to Milletti (2012), a CPP is considered to be cationic if the peptide contains a stretch of positive charges that does not lead to the formation of an amphipathic helix [70]. The most prominent representative is the already mentioned TAT peptide derived from the HIV-1 protein. Moreover, Futaki *et al.* investigated in their studies the necessity of positive charges in a polyarginine sequence (R_3 to R_{12}) with regard on efficient uptake and toxicity. They came to the conclusion that at least eight positive charges are necessary for an efficient uptake. They furthermore observed an increased uptake when extending the numbers of arginines [65]. On the other hand, studies revealed that longer oligomers tend to display toxicity [71]. Nuclear localization sequences (NLS) also belong to the class of cationic CPPs and are based on lysine-, arginine- or proline-rich motifs. They are able to translocate to the nucleus via the nuclear pore complex [72].

The class of amphipathic CPPs can be subdivided into primary and secondary amphipathic CPPs. Primary amphipathic CPPs, like Transportan [64], typically contain more than 20 amino acids and comprise sequentially hydrophobic and cationic residues along their primary structure [73]. Another representative of primary amphipathic CPPs is the chimeric peptide

MPG which was obtained by fusing the hydrophobic domain of HIV glycoprotein 41 to the NLS of SV40 [74].

Secondary amphipathic CPPs such as Penetratin [54] are often shorter and reveal their amphipathic α-helix structure upon interaction with the lipid membrane, in which hydrophilic and hydrophobic amino acids are located in separated faces of the helix [75, 76]. This class of CPPs possesses a highly hydrophobic patch on one site, whereas the other site can be cationic, anionic or even polar. The determination and visualization of the amphipathicity can be realized via the helical wheel projection.

According to Milleti, hydrophobic CPPs have low net charge and no amphipathic arrangements. Only a few hydrophobic CPPs are discovered so far [70].

1.3.2 CPPs used within this thesis

Human calcitonin (hCT) is a peptide hormone consisting of 32 amino acids, which is produced in the C-cells of the thyroid gland playing a crucial role in the calcium regulation [77, 78]. The cell-penetrating property of calcitonin was discovered by identifying that the effect did not only occurr after injection but also after nasal administration.

The amino acid sequence possesses at the N-terminus a disulfide-bridge between the first cysteine and the cysteine at position 7 inducing a loop-like structure [78].

$$C^1GNLSTC^7MLGTYTQDFNK^{18}FHTFPQTAIGVGAP^{32}\text{-NH}_2$$

Fig. 3: Amino acid sequence of human calcitonin

Amino acids 1-8 of the N-terminus are responsible for the receptor-interaction. The core sequence of human calcitonin consists of hydrophobic amino acids, which are arranged in regular intervals of 3-4 residues. This core sequence is composed of an amphipathic α-helix, which interacts with the lipid bilayer of the cell membrane. CPPs derived from human calcitonin do not have the N-terminus for the receptor recognition but they still show translocation through the cell membrane, thus excluding receptor-interaction. Despite,

experiments confirmed this ability to cross the cell membrane in a receptor independent-manner for this class of CPPs by showing that uptake occurs also in cells that do not express calcitonin receptors [79].

Table 4: Overview of published CPPs derived from human calcitonin

Peptide	Sequence	MW [Da]
hCT(9-32)	LGTYTQDFNKFHTFPGTAIGVGAP	2610.0
hCT(9-32)-br	LGTYTQDFNKFHTFPGTAIGVGAP | PKKKRKVEDPGVGFA	4246.0
hCT(18-32)-k7	KFHTFPGTAIGVGAP | KKRKAPKKKRKFA	3165.9
N-E5L-hCT(18-32)-k7	GLLEALAELLEKFHTFPQTAIGVGAP | KKRKAPKKKRKFA	4317,6

In this thesis, the branched chimeric peptide N-E5L-hCT(18-32)-k7 was used among other CPPs as delivery vector. This peptide possesses a truncated amino acid sequence (amino acids 18-32) of hCT. The fragment hCT(18-32) is the shortest hCT fragment that can still be internalized into cells. To increase a cytosolic uptake, the fusogenic peptide sequence N-E5L was additionally coupled to the amino acid sequence [69], which is a truncated and modified fragment of the HA2 protein. HA2 is the domain of the glycoprotein hemagglutinin of influenza virus and is responsible for the fusion with the host membrane [80]. In addition, the polycationic k7-side chain was coupled to the lysine at position 18. An introduction of side chains to an amino acid sequence enables a better transport of oligonucleotides by interaction of negatively charged nucleic acid with the positively charged side chain whereas the hCT-part is probably responsible for the internalization [81].

In addition to the CPPs derived from the human calcitonin, other CPPs were used within this work. The sC18 peptide is derived from the C-terminus of the 18 kDa cationic antimicrobial protein CAP18 (121 amino acids) and internalizes energy-, time- and concentration-independent via endocytosis into cells [66]. Previous studies have been shown that sC18 could deliver small organic molecules like fluorophores and toxic peptide sequences efficiently into different cell lines. Furthermore, Splith *et al*. could show that another

conjugate of sC18 is able to target hypoxic tumor tissues [82]. Furthermore, a branched dimer of sC18, namely (sC18)$_2$ was demonstrated to act as useful vehicle in gene delivery [66, 83].

Table 5: Peptide sequences of sC18 and (sC18)$_2$

Peptide	Sequence	MW(Da)	Net charge
(sC18)$_2$	GLRKRLRKFRNKIKEK-NH$_2$ | GLRKRLRKFRNKIKEK	4122.16	+17
sC18	GLRKRLRKFRNKIKEK-NH$_2$	2069.60	+9

1.3.3 Uptake mechanism for CPPs

The mechanisms by which CPPs translocate through the cell membrane have not been completely understood and are still controversially discussed [62, 84-87]. It has been assumed that CPPs often utilize more than one uptake pathway depending on the experimental conditions, like peptide concentration, cargo molecule, incubation time and temperature, cell line or membrane components [88]. A high peptide concentration for instance, favors probably an uptake via direct penetration whereas at low peptide concentrations, an uptake by endocytosis is favored. The two main postulated uptake mechanisms for CPPs are the direct penetration and endocytosis (see fig. 4) [62].
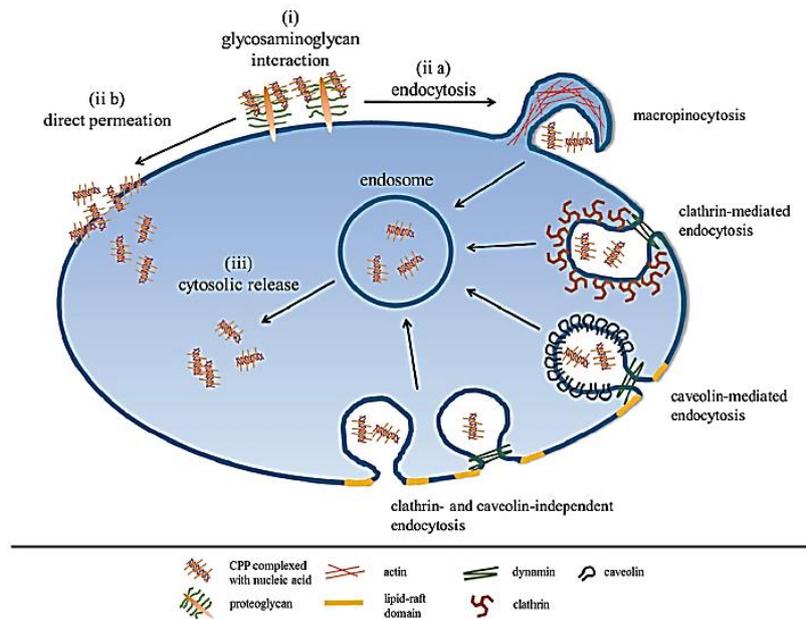
Fig. 4: Schematic overview of possible uptake mechanisms for CPPs either via direct penetration or endocytosis [89]

The first internalization step of cationic CPPs for both mechanisms is presumably an interaction of the positively charged amino acid sequence with negatively charged glycosaminoglycans, like heparin of the extracellular matrix [84].

Direct penetration can proceed via different energy-independent ways: carpet-like model, pore model or toroidol/barrel-stave. For all three mentioned mechanisms, the interaction of the CPP with the negatively charged membrane leads to a temporary destabilization of the cell membrane, which is accompanied by a peptide folding on the lipid-membrane. Direct penetration is favored for primary amphipathic CPPs with a high concentration and depends highly on the peptide sequence and lipid composition [62].

Endocytosis describes the process of molecule uptake from the extracellular area through a local cell membrane inversion [90]. Endocytosis can further be divided into macropinocytosis, caveolae-mediated endocytosis, clathrin-mediated endocytosis or clathrin- and caveolae-independent endocytosis. They differ in the composition of the coat, in the size of the detached vesicles, and in the fate of internalized particles [91]. The majority of CPPs are taken up via endocytosis, which is an energy-dependent mechanism, composed of two steps: endocytotic entry and endosomal release [89]. This uptake mechanism is presumed by CPPs applied at low concentrations, and for CPPs coupled with a cargo [62]. However, all

mechanisms used by CPPs to translocate through the cell membrane seemed to be somehow connected and can occur simultaneously. In addition, it is suggested that the down-regulation of one pathway with inhibitors might lead to an up-regulation of another pathway [92]. Furthermore, it is important to emphasize that the uptake mechanism of CPP-cargo complex depends highly on the properties of the CPP and numerous other parameters and conditions.

1.3.4 Application of cell-penetrating peptides as delivery vectors

Since the discovery of cell-penetrating peptides, they have been used for various applications, e.g. the delivery of nucleic acids or nanomaterials. For this purpose, the cargo molecule can be either covalently or non-covalently linked to the CPP [92]. A covalent conjugation between the cargo and the CPP can be achieved by a disulfide bond, an amide bond or via specific linkers. This is the case for neutral cargos, like PMOs (Phosphorodiamidate morpholino oligomers) or PNAs (Peptide nucleic acid), proteins, small organic molecules, etc. If the cargo molecule is negatively charged (siRNA or pDNA), a non-covalently conjugation can be formed via electrostatic interaction with the positively charged CPP [93].

Conjugating anticancer drugs to CPPs have shown great potential in *in vitro* as well as *in vivo* studies by increasing the solubility, biodistribution and pharmacokinetic profiles of chemotherapeutic drugs. Various publications have reported on the covalent conjugation of the chemotherapeutic drug, doxorubicin, to well-described CPPs, like TAT. The treatment of several cancer cell lines with CPP/doxorubicin showed higher apoptotic efficiency compared to the application of doxorubicin alone [94].

Besides the delivery of bioactive molecules, the transport of nanomaterials via CPPs into tissues emerged as a versatile tool. In 2009, Pujals *et al.* reported on the delivery of gold nanoparticles with the sweet arrow peptide SAP ((VRLPPP)$_3$) into the cancer cell line Henrietta Lacks (HeLa). For this purpose, an additional cysteine was synthesized at the N-terminus to enable the attachment of the gold nanoparticles due to the highly favorable thiol chemisorption on gold [95].
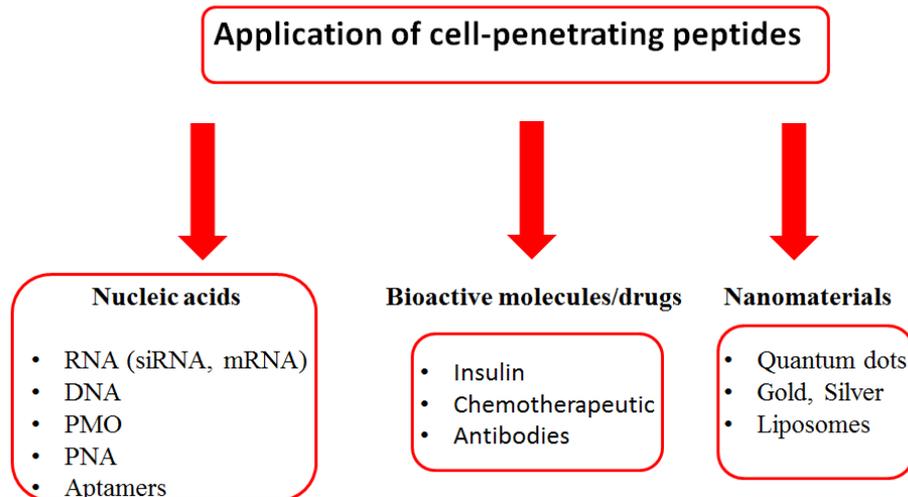
Fig. 5: Application of cell-penetrating peptides as delivery vectors

The delivery of nucleic acids via CPPs represents the majority of CPP-based applications. Morris *et al*. were one of the first who complexed a CPP (MPG) with fluorescein-labeled single oligonucleotides and achieved an improved gene delivery in human fibroblasts cells [67]. In 2001, Futaki *et al*. were able to show that the introduction of a fatty acid to the CPP octaarginine (R8) led to an enhancement of the transfection efficiency. Stearylated octaarginine yielded in transfection experiments with pDNA comparable results as the widely used lipofectamine [96]. Tönges *et al*. then used the stearylated octaarginine to deliver siRNA into primary hippocampal neurons. To demonstrate the capability of gene silencing, the hippocampal neurons were first transfected with an EGFP-expressing DNA plasmid by nucleofection. After applying anti-EGFP siRNA complexed with stearylated octaarginine to the primary neurons, they were able to detect efficient silencing of the EGFP expression [97]. Hayashi *et al*. reported in 2011 on the successful gene knock-down using (R8)-modified lipid nanoparticles *in vivo*. They used polyarginine functionalized lipoplexes to deliver siRNA, which efficiently silenced an endogenous gene [98]. Recently, we designed branched CPPs derived from the C-terminal domain of the cationic antimicrobial peptide CAP18 as delivery vectors. In preliminary studies, the fluorescently-labeled branched CPP (sC18)$_2$ showed a drastically enhanced uptake into the cancer cell line MCF-7 cells compared to the monomeric peptide sC18 [132].

1.4 Different fields of research that need novel methods for gene modulation

1.4.1   Ciliopathie

Many cell types of multicellular organisms exhibit primary non-motile cilia which are located on the apical surface of the cell [99]. This microtubule-based organelle is surrounded by a membrane lipid bilayer which is in continuity with the plasma membrane but is functionally separated from it by a diffusion barrier that limits the exchange between the cilium and the rest of the cell [100, 101]. Cilia are involved in the regulation of several central signal transduction pathways such as Wnt- and Shh-signaling that are key players in a row of cellular processes e.g. growth, differentiation, tissue maintenance, polarity and proliferation. A quickly growing number of proteins are known to be involved in the formation, maintenance and function of primary cilia. Due to their central role in cell biology of most tissues, mutations in the genes encoding ciliary proteins affect various organ systems. These developmental and degenerative diseases, like nephronophthisis and retinitis pigmentosa are summarized as ciliopathies [101]. Cell culture studies regarding ciliary biology are hampered by the fact that differentiated ciliated cells cannot easily be transfected using current state-of-the art transfection techniques due to limited efficiency and significant toxicity inducing not only cell death but also loss of primary cilia.

1.4.2   Evolution of multicellularity studied in choanoflagellates

Choanoflagellates are free-living, single-cell and colony forming eukaryotes ubiquitous in all aquatic environments with a size of 3-10 μm. These protists possess a spherical or ovoid cell body with a single apical flagellum used for locomotion and also food intake. The flagellum is additionally surrounded by a collar of microvilli. Via wavelike movements of the flagellum they are able to move through the water or to create a water current which they use to filter bacteria to their sticky collar, which are then taken up via food vacuoles [102, 103].
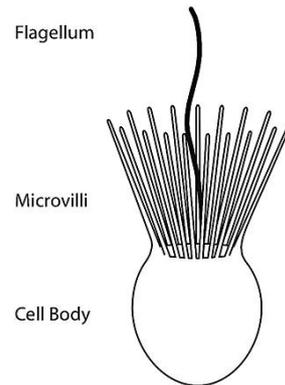
Fig. 6: Simplified structure of choanoflagellates (© Stephen Fairclough, www.tolweb.org/Choanoflagellates)

Till 2011, choanoflagellates were morphologically divided by their outer structure into three families regarding their periplast: Salpingoecidae, Codosigidae and Acanthoecidae. Members of Salpingoecidae were defined by the possession of an organic shell which is called theca and encloses the protoplast. It consists of micro-fibrils and can either be bottle-, cup- or tubular-shaped. Choanoflagellates of the Acanthoecidae, which only occur in marine waters or in brackish water, own a siliceous basket, called lorica. The lorica consists of rib-like silicate-containing rods that form a basket. The Acanthoecidae are further divided into two subgroups: the *nudi* and the *tecti* form. Regarding the morphological definition, choanoflagellates of the Codosigidae family had a thin layer of fibrils called glycocalyx. They neither have a theca nor lorica [102].

This classification into three families, which is based only on certain external characteristics, for example, the lack of a lorica, was corrected and improved in 2011 by Nitsche *et al*.

Based on molecular biology studies of the small and large subunits of ribosomal DNA (SSU and LSU), the chaperone HSP 90 and α-tubulin, the taxonomic classification is now divided into two orders,:the Craspedida and Acanthoecida. The former families of Salpingoecidae and Codosigidae are now summarized as Craspedida based on genetic studies that revealed a synapomorphy and form a monophyletic group by sharing the same ancestors. The family of the Stephanoecidae (*tecti* form) and the family of Acanthoecidae (*nudi* form) now form the order the Acanthoecida [104].
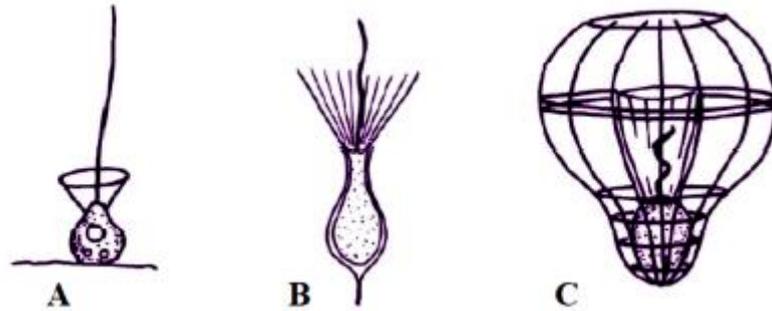
Fig. 7: (A) Codonsigidae, (B) Salpingoecidae with theca and (C) Acanthoecidae with lorica [105]

Choanoflagellates are considered to be the next living relatives of metazoans [106, 107]. Comparison of the mitochondrial genomes of choanoflagellates, sponges and other metazoans, and phylogenetic analysis show that they have all shared a common ancestor about 600 million years ago [106]. The transition from unicellular to multicellularity most likely occurred due to numerous factors, such as external environmental influences, natural selection, genomic innovation, but also simply by chance [108].
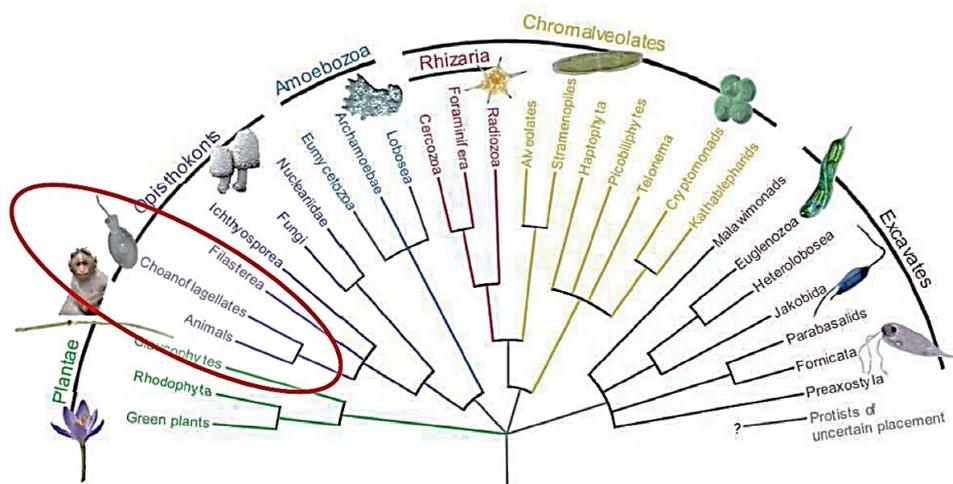
Fig. 8: Tree of life [109]

King *et al.* investigated the genome of choanoflagellate *Monosiga brevicollis* which was almost equally rich in introns as the human genome (6.6 introns per *M. brevicollis* gene and 7.7 introns per human gene). Furthermore genome analysis of *M. brevicollis* revealed the presence of many tyrosine kinases [106]. The phosphorylation of tyrosine kinases plays an

essential role in signal transduction and the cell growth of multicellular animals. These tyrosine kinases have not been found in plants, yeasts and fungi, so that it was assumed that these enzymes occur only in the metazoan [110].

A comparison of the genomes of metazoans and choanoflagellates showed not only similarities, but also significant differences, such as the lack of components of other intracellular signaling pathways and transcription factors that are essential for the development of animals. Thus, genomic analysis of *M. brevicollis* showed the absence of MAP-kinase ERK3 and the protein Notch [106]. MAP-kinases (mitogen-activated protein-kinases) are serine / threonine-kinases, which play an essential role in signal transmission of extracellular pulses by controlling important cellular processes (differentiation, migration and apoptosis) [107]. Notch is a transmembrane receptor in the Notch-signaling pathway, which plays a fundamental role in the development of metazoans [111].

2. Aim of the study

The main goal of this thesis was to develop and apply novel peptide-based vectors that can be utilized for intracellular delivery of nucleic acids through non-covalent nanoparticle formation for *in vitro* studies. For this purpose, different cell-penetrating peptides (CPPs) were synthesized and investigated concerning their delivery ability using different cell lines and choanoflagellates as model organisms.

In part I of the thesis (**"Studying the potency of novel CPPs as transfection vectors"**), the impact of cyclization and dimerization of the CPP sC18 on the ability to transfect mammalian cells were investigated. Besides complex formation, the transfection efficiency was qualified by fluorescent microscopy and quantified by flow cytometry.

Choanoflagellates are considered to be the closest living relatives of animals. They have the potential to serve as model organism to illuminate fundamental and ancient aspects of animal origins. Hence, the development of methods to genetically manipulate choanoflagellates is mandatory. In part II of the thesis (**"Analyzing toxicity, internalization capacity and selectivity of CPPs when in contact with choanoflagellates"**), the *in vivo* application of CPP N-E5L-hCT(18-32)-k7, derived from our group, and the well-characterized CPP TAT(48-60) were studied. The CPPs were investigated upon their toxicity, uptake mechanism and their nucleic acid transfection ability generating new methods.

Cell culture studies regarding ciliary biology are hampered by the fact that differentiated ciliated cells cannot easily be transfected using current state-of-the art transfection techniques due to limited efficiency and significant toxicity inducing not only cell death but also loss of primary cilia. Therefore, in part III (**"Peptide-mediated oligonucleotide delivery into ciliated retinal pigment epithelium cells (hTERT RPE-1)"**), different CPPs, which were developed in our group, were examined upon their toxicity, complex formation activity, internalization and nucleic acid delivery ability in retinal epithelium cells (hTERT RPE-1). Furthermore, the capability of delivering a functional plasmid via CPP into differentiated hTERT RPE-1 cells was investigated using fluorescent microscopy.

3. Materials and Methods

The chemicals, reagents and consumables used in this thesis were obtained from the companies Fluka (Taufkirchen, Germany), Merck (Darmstadt, Germany), Sarstedt (Nümbrecht, Germany), Sigma-Aldrich (Taufkirchen, Germany) and VWR (Darmstadt, Germany).

All N^{α}-Fmoc protected amino acids were purchased from IRIS Biotech (Marktredwitz, Germany). The side chains of trifunctional amino acids are equipped with a protecting group in order to prevent side reactions and the formation of byproducts. These protecting side chains are orthogonal to the base-labile Fmoc-group using acid-labile protecting groups: Pbf for Arg; Trt for Asn, Gln, His, Cys; Boc for Trp and Lys; *tert*-Butyl for Asp, Glu, Ser, Thr, and Tyr. In order to introduce a side chain to an amino acid sequence, lysine was used as Fmoc-Lys(Dde)-OH.

Peptides still attached to the resin or lyophilized peptides were stored at 4 °C whereas dissolved peptides were stored at -20 °C.

In order to calculate the concentration of a peptide solution it was taken into account that free amine groups and the side chains of lysine and arginine have a TFA-molecule as a counter ion. Therefore, the molecular weight of the peptide is increased.

Buffers and media

<u>LB-broth (Luria/Miller)</u>

For 1 L:

25 g Luria/Miller in 1 L H_2O_{dd}

<u>sp-media</u>

For 2 L:

NaCl	56.30 g
KCl	1.34 g
$MgCl_2$	11.01 g

$MgSO_4$	13. 4 g
$CaCl_2$	2.90 g
KNO_3	0.20 g
K_2HPO_4	0.02 g

Trypanblue sodium acetate (pH 4.33)

6.5 mM in sodium acetate buffer:

38% (v/v) 0.1 M CH_3COONa

62% (v/v) 0.1 M CH_3COOH

Müller-Hinton-agar plates

For 1 L:

21 g Müller-Hinton and 15 g agar in 1 L H_2O_{dd}

Buffers & solutions for Western Blot

IP Buffer (Storage: 4 °C):	**IP-Buffer** (Storage: 4 °C)
20 mM Tris 7.5	50 mL 10% Triton X-100
1% Triton X-100	10 mL 1M Tris HCl (pH 7,5)
50 mM NaCl	12.5 mL 2 M NaCl
12.5 mM $Na_4P_2O_7$	50 mL 0.5 M NaF
25 mM NaF	30 mL 0.25 M $Na_4P_2O_7$
Addition of Na_3VO_4, PMSF, PIM to 10 mL: • PMSF $\rightarrow$ 44 μL ,(t ½ in H_2O: ~ 30 min) • Na_3VO_4 $\rightarrow$ 200 μL (pY-Phosphataseinhibitor) (100 mM stock solution)	$\rightarrow$ Addition 500 mL H_2O_{dd}
Lämmli 2x 33.3 mL 1.5 M Tris-HCl (pH 6.8) 100 mL 20% SDS	

100 mL Glycerol 1 g Bromphenol blue → Addition 500 mL H_2O_{dd}	
Resolving gel buffer A: 1000 mL 180 mL 2 M Trizma Hydrochloride 570 mL 2 M Trizma Base 20 mL 20% SDS → Addition 1 L H_2O_{dd} pH 8.8	**Stacking gel buffer B:** 1000 mL 24 mL 2M Trizma Hydrochloride 8 mL 2M Trizma Base 20 mL 20% SDS → Addition 1 L H_2O_{dd}
10x Running buffer: 5000 mL 720 g Glycine 50 g SDS 150 g Trizma Base → Addition 5 L H_2O_{dd}	**10x Protein wash buffer** 1530 mL 1 M Tris HCl (pH 7.5) 3060 mL 5 M NaCl 153 mL Tween 20 → Addition 5 L H_2O_{dd}
10x Transfer buffer: 5000 mL 150 g Trizma Base 50 g SDS 705 g Glycine → Addition 5 L H_2O_{dd}	**1x Transfer buffer** 305 mL 10x Stock solution 525 mL Methanol 2625 mL H_2O_{dd}
Blocking buffer: 50 mL 5% Bovine serum albumin (Fraction V) in 1x protein wash buffer Kept at 4 °C to prevent bacterial contamination.	

3.1 Methods

3.1.1 Solid phase peptide synthesis

The solid phase peptide synthesis (SPPS) was developed in 1963 by B. Merrifield and revolutionized the peptide chemistry [112]. In this case, amino acids can be synthesized fully automated via a linker from the C- to the N-terminus to a solid polymeric carrier. As solid polymeric carriers Wang and Rink-amide resins are widely used.
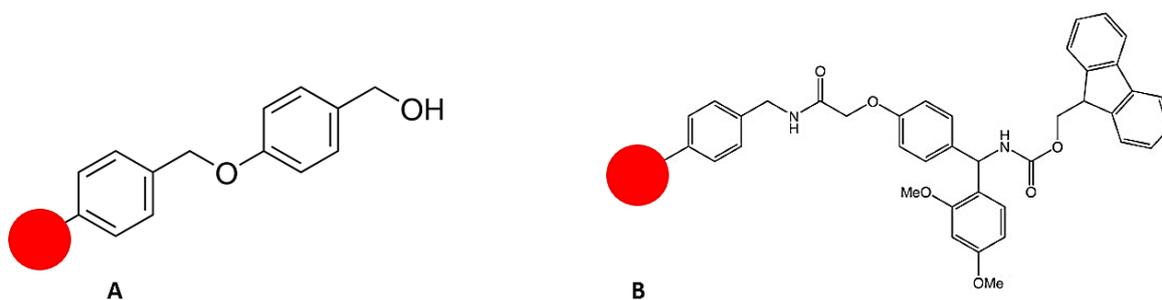
Fig. 9: Chemical structure of Wang-linker (A) and Fmoc-Rink amide-linker (B)

The first step in SPPS is the loading of the resin with an N-terminally Fmoc-protected amino acid. After basic cleavage of the amino protecting group, a coupling of another protected amino acid is followed, whose carboxylic group was activated for coupling. This sequence can be repeated, until the peptide has the desired length. After completion of the peptide sequence, the whole peptide can be cleaved from the resin (see figure 10).

Fig. 10: Schematic representation of the SPPS workflow

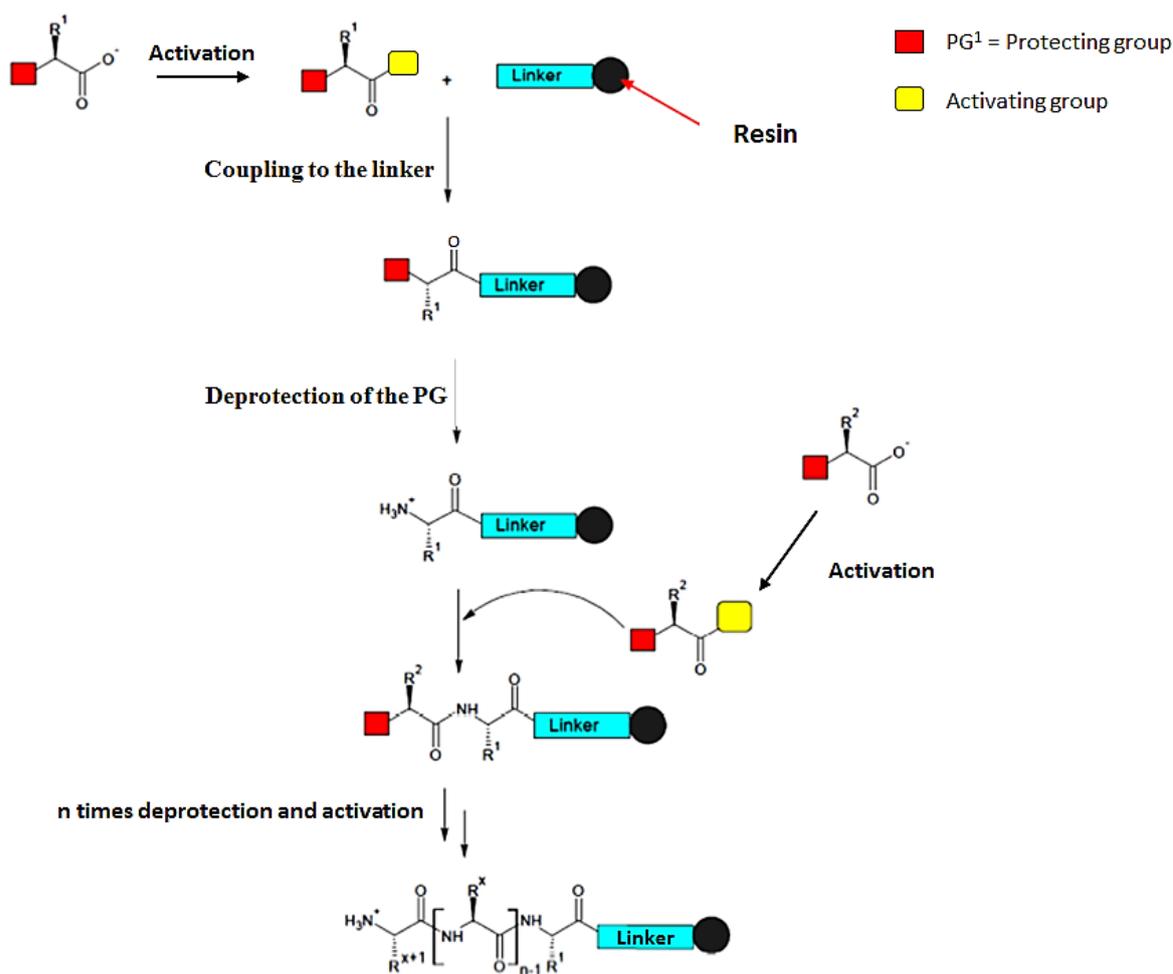In order that the desired coupling can take place, it is mandatory that the N-terminus of amino acid 1 is reversibly protected, so that whose free carboxyl-group can react with the free amino group of amino acid 2. Additionally, it is necessary to protect the carboxyl-group of amino acid 2. The coupling between the two amino acids can only take place after the activation of the inert carboxyl-group of amino acid 2. For this purpose, activation reagents like Oxyma Pure ® or HOBt are added to the reaction.

In this thesis, the Fmoc/tert-butyl strategy was used in SPPS. It has the advantage of orthogonality meaning that the protecting groups can be cleaved selectively under certain conditions, while all other protecting groups remain intact. Thus, as a base-labile N^{α}-protecting group Fmoc is chosen, which can be cleaved under basic conditions whereas the acid-labile protecting groups ^{t}Bu, Pbf, Trt and Boc are stable under these conditions. They are cleaved using trifluoroacetic acid (TFA). Furthermore, all side chains of trifunctional amino

acids (Lys, Arg, His, Glu, Asp, Ser, Thr, Tyr und Cys) must be protected to avoid undesired side reactions [113].

All peptides used in this thesis were synthesized by automated solid-phase peptide synthesis on a multiple Syro I peptide synthesizer (MultiSynThech, Bochum, Germany) using a Rink amide as resin.

3.1.2 Automated solid phase peptide synthesis

The Fmoc-protected amino acids were dissolved at 0.4 M in DMF (Fmoc-Phe-OH in 0.4 M NMP).

The synthesis runs in open polypropylene reactor vessels (2 mL) equipped with a Teflon frit. They are accepted by a reactor block provided with a vortexer that guarantees an optimal mixing of the reactants. The software SyroXP calculates the amounts of amino acids (0.4 mol/L) and solvents required for the complete synthesis run. Thus, Fmoc-Rink amide resins (30 mg, 0.5 mmol/g loading) were first swollen in 800 µL DMF for at least 15 min, then the Fmoc protecting groups cleaved using 40% piperidine in DMF (400 µL, 3 min) and afterwards with 20% piperidine in DMF (400 µL, 10 min). After four washing steps with 600 µL DMF, the N^{α}-Fmoc protected amino acids were introduced in 8-fold excess by using *in situ* activation with DIC and oxyma. First 50 µL oxyma (2.4 M in DMF) was added to the resin followed by 3 min incubation. Then 50 µL DIC (2.4 M in DMF) was added to the reaction solution and incubated for further 40 min at rt. Each coupling of an amino acid was performed as a double coupling step (2 x 40 min). The reaction vessels were then washed twice with 800 µL DMF and the next coupling of an amino acid could proceed till the desired sequence was reached.

3.1.3 Manual coupling of amino acids and fatty acids

The resin (1 eq, 15 µmol) was swelled for at least 15 min in 1 mL DMF. After removing the solvent, the Fmoc-protected amino acid (3 eq, 45 µmol) and oxyma (3 eq, 45 µmol) were dissolved in 300 µL DMF and added to the swollen resin. DIC (3 eq, 45 µmol) was added immediately to the reaction solution. The reaction was carried out under vigorous shaking for 2 h at room temperature. The resin was washed with DMF and a second coupling step was performed. For the fatty acid coupling HATU (MW = 380.23 g/mol)/DIPEA (each 5 eq.,

75 µmol) was used instead of oxyma/DIC. After the incubation, the resin was washed five times with DMF, CH$_2$Cl$_2$, MeOH and Et$_2$O and dried for 10 min under reduced pressure. To monitor whether the coupling was successful, a Kaiser test was performed.

3.1.4 Ninhydrine test (Kaiser Test)

A few dried resin beads are transferred to a 1.5 mL reaction vessel. One drop of the solutions I to III (table 6) was added in quick succession to the sample and then incubated at 95°C for 5 min. An emerge of blue color indicated the presence of primary amines and thus incompletion of the reaction. A primary amine compound (e.g. aminohexane) served as control [114].

Table 6: Composition of the Kaiser Test solutions

Solution I	1 g ninhydrin in 20 mL EtOH (abs.)
Solution II	80 g phenol in 20 mL EtOH (abs.)
Solution III	0.4 mL 1 mM aqueous KCN-solution in 20 mL piperidine

3.1.5 Boc-protection of primary amines

The resin was swollen for at least 15 min in 1 mL DCM. After removing the solvent, a solution containing di-*tert*-butyl-dicarbonate (10 eq., 150 µmol) in 500 µL DCM and DIPEA (1 eq., 15 µmol) was added to the resin. The syringe was sealed with parafilm to prevent the solvent from volatilizing and incubated over night at room temperature on a shaker. After incubation the solvent was removed and the resin washed five times with DCM, MeOH and Et$_2$O, successively. The resin was then dried for 10 min under reduced pressure.

3.1.6 CF-labeling of primary amines

The resin was swollen for at least 15 min in 1 mL DMF. After removing the solvent, CF and HATU (each 3 eq., 45 µmol) were dissolved in 300 µL DMF and added to the resin. Subsequently, DIPEA (3 eq., 45µmol) were added directly to the syringe. The reaction was carried out over night at room temperature on a shaker. After the incubation, the resin was

washed five times with DMF, CH$_2$Cl$_2$, MeOH and Et$_2$O, successively and dried under reduced pressure. To determine whether the coupling was successful, a Kaiser test was performed. For the cleavage of CF-polymers the resin was swollen in 1 mL DMF for at least 15 min. After removing the solvent, 20% piperidine in DMF was added and the reaction was carried out at room temperature for 45 min. Subsequently, the reaction mixture was removed; the resin washed five times with DMF, CH$_2$Cl$_2$, MeOH and Et$_2$O, successively and dried under reduced pressure. Coupling of CF was achieved as a double coupling step.

3.1.7 Trt-protection of CF-hydroxy group

The CF-peptide-resin was swollen in 1 mL DCM for at least 15 min. After removing the solvent, trityl chloride (4 eq., 60 µmol) was dissolved in 500 µL DCM and added to the swollen resin. DIPEA (4 eq., 60 µmol) was added immediately to the resin and incubated for 16 h under shaking at RT. To prevent the solvent from volatilizing, the syringe was sealed with parafilm. After the incubation the solvent was removed and the resin washed five times with DMF, CH$_2$Cl$_2$, MeOH and Et$_2$O, successively and dried under reduced pressure.

3.1.8 Cleavage of a Dde protecting group

The resin is swollen for at least 15 min in 1 mL DMF. After removing the solvent, 1 mL of a 3% hydrazine solution in DMF was added to the resin and incubated for 10 min at RT (10 times). The resin was washed with DMF (2 x) (after step 1 and 10) and the wash solution was combined with the cleavage solution. The amount of Dde from step 1 and 10 was determined by measuring the absorption at 301 nm in a photometer. As a reference a mixture of 2 mL DMF and 3% hydrazine was used. The cleavage was assumed to be complete, if the absorbance at 301 nm was under 0.1. Otherwise the procedure was repeated as long as necessary. After the successful cleavage, the resin was washed five times with DMF, CH$_2$Cl$_2$, MeOH and Et$_2$O, successively and dried under reduced pressure

3.1.9 Sample cleavage

To monitor the success of the peptide synthesis a few dry resin beads were transferred to a 1.5 mL reaction vessel and incubated for 3 h with a scavenger solution, containing 2.5 µL of water and 2.5 µL of triisopropylsilane. If the peptide contains methionine, cysteine or

tryptophan an alternative scavenger (7 µL of thioanisole and 3 µL of 1,2-ethandithiol) is needed. Afterwards the reaction mixture was filled up to 100 µL with TFA. After the incubation, 1 mL ice-cold Et_2O was added to precipitate the peptide and was left for 20 min or overnight at -20 °C for further precipitation. Afterwards, the mixture was centrifuged (4 °C for 4 min at 10,000 x g), the supernatant was discarded, the pellet resuspended in fresh 1 mL Et_2O and centrifuged again. This procedure was repeated approximately five times. The pellet was dried and then dissolved in 100 µL H_2O/*tert*-butanol(3:1, (v/v)). Finally, the sample was analyzed by HPLC-ESI-MS.

3.1.10 Full cleavage

The dry resin was incubated for 3 h with a mixture of H_2O/TIS/TFA (5:5:90, v/v/v) whereas peptides containing cysteine, methionine or tryptophan were cleaved with thioanisole/1,2-ethane dithiol/TFA (7:3:90, v/v/v). The peptides were precipitated from ice-cold Et_2O (10 mL) and collected by six centrifugation steps (4 °C, 4 min at 5,000 x g). After each step, the supernatant was discarded and the pellet was resupended in 10 mL Et_2O. Then, the pellet was dried, dissolved in 3 mL H_2O/*tert*-butanol (3:1, (v/v)) and lyophilized from H_2O/*tert*-butanol. A sample of the peptide was analyzed by HPLC-ESI-MS.

3.2 Peptide analytic

3.2.1 Analytical LC-MS

Peptides were analyzed by LC-MS using an Agilent instrument with parallel detection at 220 nm UV-absorption and electrospray-ionization mass spectrometry (ESI-MS). The reversed-phase analytical HPLC (RP-HPLC) was performed at 1.2 mL/min flow rate on a 4.6 x 100 mm Kinetex 2.6u C18 100A column (Phenomenex, Aschaffenburg, Germany). Gradients of 10 – 45 % or 10 – 60 % acetonitrile in water over 15 min (with constant 0.1 % TFA) were used.

3.2.2 Preparative RP-HPLC

Purification of the peptides was achieved by preparative RP-HPLC on a Hitachi Elite LaChrom instrument (VWR, Darmstadt, Germany) at 6 ml/min flow rate and 220 nm

detection. The chromatography was performed on a 15 x 250 mm Jupiter 4u Proteo 90A column (Phenomenex, Aschaffenburg, Germany) by using a linear gradient of 10-60% B in A (A = 0.1% TFA in water; B = 0.08% TFA in ACN) in45 min or 20-60% in 45 min at 6 mL/min. The detection was at 220 nm wavelength and the fractions containing the peptide were collected. Afterwards, TFA and ACN were removed under reduced pressure. The peptide was lyophilized overnight.

3.3 Choanoflagellates

Cultures of *Salpingoeca rosetta* and *Salpingoeca sp.* ("Mono Lake") were grown in sp-media whereas cultures of *Salpingoeca euryoecia* in commercially available spring water. All cultures were maintained at room temperature. As a carbon source a sterile wheat seed was added to the flasks.

3.3.1   Viability studies

Choanoflagellates of a confluent T25-flask were detached by scratching them off the bottom with a cell scraper, transferred into a 15 mL tube and then centrifuged at room temperature for 10 min at 1000 rpm. The supernatant was discarded and the pellet was resolved in 500 µL appropriate media. Addition of 46 µM CPP was performed and incubated for 24 h. After incubation time, 30 µL of the choanoflagellates/CPP-solution was dropped on a microscope slide and examined using a Axiophot microscope by Zeiss.

3.3.2   Agar-diffusion test

An overnight culture of the to be tested bacteria was prepared in 10 mL Müller-Hinton medium at 37 °C. Subsequently, 200 µL of the bacteria suspension was added to an antibiotic-free Müller-Hinton agar plate. To obtain a steady growth, the suspension was spread with a sterile swab by rotating the plate, followed by 5 min drying time. Afterwards, the antibiotic-impregnant filter papers were placed on the agar plate and then incubated overnight at 37 °C. The next day, the size of the bacteria-free areola are measured with a ruler.

3.3.3   Internalization and transfection of choanoflagellates with CPPs

The choanoflagellates were seeded on a glass microscope slide with a silicon attachment formed like an 8-well chamber slide (Flexiperm® 8-well slide, Sarstedt). Thus, the glass slide was cleaned first with water, ethanol and then with acetone. The silicon chamber was pressed on to the dry slide to give eight equal chambers.

To detach the choanoflagellates from the flask bottom, the flask was agitated very strongly and 200 µL of the stock solution was added to 200 µL of the appropriate medium into a chamber. The choanoflagellates were grown for three days at room temperature. The cells were then incubated at room temperature 30 min and 180 min with solutions of 5(6)-carboxyfluorescein-labeled peptides in appropriate medium at two different concentrations (10 and 25 µM). Transfection experiments were performed as described in 3.4.10. After incubation time, the choanoflagellates were washed five times with fresh medium and then analyzed via microscopy using a AxioLab A1 microscop by Zeiss.

3.4 Biological Methods

3.4.1   Production of chemically competent *E. coli* cells

Chemically competent *E. coli* cells were produced by the $CaCl_2$-Method [115]. First of all, an overnight *E. coli* culture (10 mL LB-medium) was prepared at 37 °C. In the morning, the culture was diluted with LB-medium (2 x 250 mL LB-medium with each 5 ml of the overnight *E. coli* culture). The new cultures were grown till an optical density (OD_{600}) of 0.4 – 0.5 was reached. Afterwards, the cultures were placed on ice for 15 min and then centrifuged (10 min, 5000 rpm, 4 °C). All following steps were carried out at 4 °C (all solutions were cooled down to 4 °C). The bacteria pellets were each resuspended in 60 mL of ice-cold $MgCl_2$ solution (100 mM) and centrifuged using the same settings as mentioned above. The bacteria pellets were then each resuspended in 80 mL of ice-cold $CaCl_2$ solution (1 M) and incubated on ice for 30 - 60 min. After the incubation, the cells were centrifuged again using the same setting as mentioned before and terminally resuspended in 8 mL $CaCl_2$ solution (containing 15% glycerol). This solution was aliquoted (100 – 250 µL), then immediately frozen in liquid nitrogen and then stored at -80 °C.

3.4.2 Transformation of plasmid into *E. coli* and plasmid isolation

The transformation of the plasmid pEGFP-N1 into the *E. coli* strain DH5α was performed using the heat shock method. The competent *E. coli* were taken out of the -80 °C and thawed on ice. 1 µL of pEGFP-N1 was gently mixed with 50 µL competent cells in a 2.0 mL reaction vessel and then incubated for 20 - 30 min on ice. Afterwards, the cells were heat shocked at 42 °C in a water bath for 45 sec and then immediately placed on ice again for further 2 min. Subsequently, 500 µL LB-medium without antibiotics was added to the cells and incubated at 37 °C under shaking conditions for 45 min. In the end, 10 - 25 µL of the transformation solution was plated on a LB agar plate with the appropriate antibiotic (50 µg/mL kanamycin) and incubated at 37 °C overnight. In the next morning, a colony was picked, transferred into a falcon containing 3 mL of LB-medium with 50 µg/mL kanamycin and incubated again at 37 °C overnight under vigorous shaking. The plasmid isolation was performed using a commercially available plasmid extraction kit following the manufacture´s protocol. To determine the concentration of the isolated plasmid, a NanoDrop 1000 by Thermo Scientific was used.

3.4.3 Cell lines

All cell culture work was done under sterile conditions and all cell lines were cultured in 55 cm^2 culture dishes at 37 °C in a humidified atmosphere of 5% CO_2

The cell line Human Embryonic Kidney cells (HEK-293) was grown in DMEM containing 10% fetal bovine serum (FBS) and 4 mM L-glutamine. The cell line MCF-7 was grown in RPMI 1640 containing 10% FBS and 4 mM L-glutamine. Retinal pigment epithelium (hTERT RPE-1) cells were grown in DMEM: F-12 which contained 10% FBS, 2 mM L-glutamine and 0,348% sodium bicarbonate. Each medium was also prepared without FBS for toxicity, internalization and transfection studies.

3.4.4 Splitting and seeding cells

For trypsinization of the cells, the cell layer was washed twice with DPBS. To detach the cells from the surface and from each other, 1 mL porcine trypsin (0.5 mg/mL in Hank´s balanced salt solution) was added and incubated for 3 min at 37 °C. Cells were then resuspended and mixed with 9 mL of the appropriate medium containing serum to block trypsin activity.

To split the cells, they were transferred to new culture dishes and mixed with new medium depending on the splitting ratio. HEK-293 cells were not used above the 30th passage, MCF-7 not over 40th and RPE cells not above 25th.

3.4.5   Freezing and thawing cells

To freeze the cells, they were trypsinized and then centrifuged for 5 min at 300 x g. The resulting cell pellet was resuspended in 1.5 mL freezing medium (containing additionally 10% sterile filtered DMSO). The resupended cells were transferred to a freezing tube and cooled down at 4 °C for 15 min and then stored at -20 °C for 2 - 4 h. Afterwards, the cells were incubated over night at -80 °C and then stored in liquid nitrogen.

To thaw the cells, the stock was defrosted in 37 °C water bath and directly transferred to a culture dish containing the required medium. The cells were stored for 24 h at 37 °C in a CO_2-incubator (5% CO_2). The next day, the dead cells and rests of DMSO were removed by washing the cell layer twice with fresh medium.

3.4.6   Cell viability assay on hTERT RPE-1 cells based on resazurin

For a resazurin-based cell viability assay, 5×10^4 hTERT RPE-1 cells per well were seeded in a 96-well plate and grown to 60 - 70% confluency. Cells were incubated with the different peptides using serum-free DMEM:F-12 medium for 24 h under standard growth conditions. For the positive control, cells were treated with 70% ethanol for 30 min. After washing, the cell viability was determined relative to untreated cells using the *In Vitro* Toxicology Assay Kit from Sigma-Aldrich according to the manufacture´s protocol. Measurement was performed fluorimetrically at 595 nm (λ_{ex} = 550 nm) using a Tecan infinite M200 plate reader.

3.4.7   Internalization studies on hTERT RPE-1 cells

For peptide uptake studies by flow cytometry, 2×10^5 hTERT RPE-1 cells per well were seeded on a 24-well plate and grown to 60 - 70% confluency. The cells were then incubated at 37 °C for 30 min with solutions of 5(6)-carboxyfluorescein-labeled peptides in serum-free DMEM:F-12 medium at concentrations ranging from 1 to 25 µM. After incubation time, the

cells were washed twice with DPBS, trypsinized and resuspended in standard culture medium. Analysis were performed on a BD Accuri C6 flow cytometer.

For peptide uptake studies by fluorescence microscopy, 5 x 10^4 cells per well were seeded on an 8-well µ-slide (Ibidi) and grown to 60 - 70% confluency. The cells were then incubated at 37 °C for 30 min with solutions of 5(6)-carboxyfluorescein-labeled peptides in serum-free DMEM:F-12 medium at concentrations of 5 µM and 25 µM. Staining of the nuclei was achieved by addition of 1 µg/mL Hoechst33342 nuclear dye to the cells for 10 min prior to the end of the incubation time. After treatment with 150 µM trypan blue for 0.5 min to quench extracellular fluorescence, the cells were washed twice with DPBS and then analyzed by fluorescence microscopy using a confocal laser scanning system (Nikon D-Eclipse C1) with an inverted microscope (Nikon Eclipse Ti). Images were taken with a 60x oil immersion objective, respectively and analyzed using the software EZ-C1 3.91 from Nikon. Microscope pictures were recorded in 16-bit grayscale, pseudocolored in red (channel 1), green (channel 2), and blue (channel 3) followed by processing with ImageJ.

3.4.8   Electromobility shift assay (EMSA)

A successful complexation between the CPP and the nucleic acid is mandatory for a delivery of the cargo molecule into the host cells. For the formation of nucleic acid/CPP complexes, the peptides were incubated with the plasmid/siRNA using different charge ratios in 50 µL of 37 °C warm nuclease-free water for 30 min at room temperature. Immediately after complexation, 5 µL 50% glycerin in water was added to each of the samples which were then electrophoresed for 60 min at 150 V on a 1% agarose gel stained with GelRed™ (Biotium, USA) in Tris-borate-EDTA (TBE) buffer. Naked plasmid and siRNA were used as control, respectively.

3.4.9   Labeled dsRNA delivery into hTERT RPE-1 cells

For fluorescence microscopy, 5 x 10^4 cells per well were seeded on an 8-well µ-slide (Ibidi) and grown to 60 - 70% confluency. Complex formation of the cell-penetrating peptides with Block-iT™ Alexa Fluor® Red dsRNA was performed as described in 3.4.8 using 10 µM CPP. Serum-free DMEM:F-12 was added to give a final RNA concentration of 100 nM in a total volume of 200 µL and the cells were incubated for 30 min at 37 °C. After treatment, staining of the nuclei was achieved by addition of 1 µg/mL Hoechst33342 nuclear dye to the

cells for 10 min prior to the end of the incubation time. Cells were then washed twice with DPBS and then analyzed by fluorescence microscopy using a confocal laser scanning system (Nikon D-Eclipse C1) with an inverted microscope (Nikon Eclipse Ti). Images were taken with a 60x oil immersion objective, respectively and analyzed using the software EZ-C1 3.91 from Nikon.

3.4.10 *In Vitro* transfection

For transfection studies by flow cytometry, 8×10^4 hTERT RPE-1, 1×10^5 HEK-293 cells and 5×10^4 MCF-7 cells per well were seeded on a 24-well plate and grown to 60 - 70% confluency. For the microscopical studies, 20.000 hTERT RPE-1, 50.000 HEK293 and 10.000 MCF-7 cells were seeded in a µ-slide 8-well (Ibidi).

The formation of nucleic acid/CPP complexes using different charge ratios was performed as described above (3.4.8). The complexation was carried out for 30 min at room temperature. Subsequently, the complex was added to the cells and incubated for 6 h at 37 °C. After incubation, the reaction solution was replaced by fresh medium.

3.4.11 Differentiation of hTERT RPE-1 cells

A confluent 10 cm culture dish 1:2 was seeded into a µ-slide 8-well plate or to a 12-well plate and incubated over night at 37 °C.

The day after, when the cells reached a confluency of 70 - 80%, they were serum starved for 24 h to induce ciliogenesis.

3.4.12 Cilia staining

The cells were seeded (as mentioned above) on a 18 mm coverslip in 12-well plates or in µ-slide-8-well plates for microscopy. Next day, the cells were starved in a serum free hTERT RPE-1 medium for 24 h to induce ciliogenesis.

After starvation, the cells were rinsed with 1 mL DPBS. Afterwards, DPBS was aspirated and cells were covered with freshly prepared 4% PFA. Fixation was carried out at room temperature for 10 - 15 min. Subsequently, the fixative was aspirated and rinsed three times in PBS for 5 min each. The specimen was then blocked for 1 h in 5% normal donkey serum

(NDS) (Jackson Immunoresearch) in PBS containing 0.1% Triton-X (PBTx) and thereafter washed with PBS. Primary antibody anti-Pericentrin (rabbit; 1:500; Abcam) and anti-acetylated tubulin (mouse; 1:1000; monoclonal antibody; Sigma-Aldrich) diluted in PBS were applied to the cells. The incubation was carried out for $1 - 2$ h at room temperature and then rinsed three times in PBS for approximately 5 min each. Secondary antibody diluted in PBTx (PBS + 0.1% Triton-X) was added for 30 min $- 2$ h at room temperature in the dark (cy5 conjugated Donkey Anti-Rabbit IgG (H + L); cy3 conjugated Donkey Anti-Mouse IgG (H + L) both 1:500, from Jackson Immunoresearch) and subsequently washed three times with PBS for about 5 min each. The coverslip was dipped before mounting once in distilled water. A drop ($7 - 10$ µL) of mounting medium (ProLong Gold with Dapi Invitrogen (Molecular Probes)) was added on a clean slide and dried over night at 4 °C. Visualization was performed under Zeiss Axiovert 200 microscope (Objectives: Plan Apochromat $\times 20/0.8$, C-Apochromat $\times 63/1.22$ W).

3.4.13 *In vitro* transfection of differentiated hTERT RPE-1 cells with TALEn plasmid

Puromycin selection:

Next day after transfection, cells were put under 10 µg puromycin (Invitrogen) selection when looking healthy. They were kept under selection for at least 2 weeks until colonies are visible. After having colonies, the cells were split 1:2 to a big 10 cm culture dish and put under selection as well. When reaching a confluency of 60 - 70% (after 2 - 3 days) the cells were split:

1. **Genomic DNA isolation**: cells were split on a 6-well (1:3) and gDNAwas isolated next day using either blood and tissue kit (Quiagen)
2. **For Western**: cells were split on a 6-well (1:3) for whole cell lysate preparation for Western blotting with GFP antibody.

Integration PCR

hFLCN integration PCR into AAVS locus in hTERT RPE-1 cells

Primers used:

1.   P_1CE3 + P_1DDD (empty locus ~1935 bp product size)

2.   P_1DDD + P_1DDE (integration pcr ~1180 bp product size)

Primer sequence:

P_1CE3 forward primer

CGGAACTCTGCCCTCTAACG

P_1DDD reverse primer

GTGAGT TTGCCAAGCAGTCA

P_1DDE forward primer

TATCCGCTCACAATTCCACA

Templates:

1.   293Ts gDNA (as negative control)

2.   hFLCN-Talen transfected cells in 293Ts (positive control)

3. H_2O

Table 7: PCR components

Go Taq PCR: GoTaq G2 Flexi DNA Polymerase (Promega;)	1x
5x Green flexi buffer	10 μL
$MgCL_2$ (25 mM)	3 μL
dNTPs (25 mM)	0.4 μL
P1 (1:20)	3 μL
P2 (1:20)	3 μL
Go Taq	0.25 μL
Template	1 μL
H_2O	29.35 μL

Cycling conditions:

Table 8: Cycling conditions

95 °C	2 min
95 °C	30 sec
59 °C	45 sec x 34
72 °C	2 min
72 °C	5 min
10 °C	∞

Polyacrylamide gel

The samples were electrophoresed for 40 min on a 1% agarose gel stained with ethidium bromide at 100 V for 40 min.

3.4.14 Western blotting – Immunoblotting

The whole cell lysate was prepared by harvesting the cells in 10 mL cold PBS and then centrifuged down at 190 x g at 4 °C for 5 min. The supernatant was discarded and the pellet resuspended in 300 µL IP buffer on ice. Additionally, 44 µL PMSF (stock solution 1 mg/mL) and 200 µL Na_3VO_4 (stock solution 0.1 M) per 10 mL IP buffer was added to the solution.

The supernatant was discarded and 200 µL 2x Laemmli (+DTT) were added to the pellet. The solution was then boiled at 95 °C for 5 min. Lysation of the cells was carried out on ice for 15 min, transferred into a 1.5 mL reaction vessel and then centrifuged at 14,000 rpm for 10 min at 4 °C. The supernatant was transferred to a new tube and the pellet discarded. The supernatant was used to determine the protein concentration and to run a Western gel. For protein denaturation 40 µL of Laemmli 2x (+DTT) were added to 40 µL supernatant and then boiled at 95 °C for 5 min. The solution was centrifuged at maximum speed for additionally 5 min. The gel was loaded with 30 µL sample solution whereas empty lanes were loaded with 20 µL 2x Laemmli buffer. The samples were run with constant current:

1. 70 V for 30 min. – slow run to get proteins in ‚starting position'
2. 20 mA / gel (e.g. 40 mA for 2 gels in one chamber) for 2 h : 15 min to 2 h : 30 min. to separate proteins

Polyacrylamide gel

Table 9: Composition of the Western blot gel

	5% stacking	**10% resolving**	**12% resolving**	**15% resolving**
H_2O_{dd} (mL)	3.8	5	4	2.5
40% polyacrylamide (mL)	1.2	5	6	7.5
buffer A (mL)	-	10	10	10
buffer B (mL)	5	-		
10% APS (µL)	100	200	200	200
TEMED (µL)	15	30	30	30
	10 mL	20 mL	20 mL	20 mL

(Resolving gel = separation gel)

Preparation of gel

For the Western equipment glass, Teflon plates and spacers (1.5 mm thick) were assembled. The gel was prepared using the amounts listed in table 9. The running gel (=resolving) gel was immediately poured to about 2 cm bellow the wells of the comb (~5 mL) and then sealed with isopropanol. After the gel has set, isopropanol was discarded and the stacking gel (~2.5 mL) was poured over the running gel and the comb was inserted. After the gel has solidified, the bottom of the comb was marked and then removed. The apparatus was subsequently filled with running buffer and the wells flushed out thoroughly with running buffer.

Membrane transfer and preparation

After electrophoresis, the gel run apparatus was disassembled, bottom and top cut from gel and equilibrated in transfer buffer. Then a piece of PVDF membrane was cut and wetted for about 1 min in MeOH at room temperature followed by a transfer into transfer buffer. The transfer procedure for blotting in the apparatus is carried out for 53 min at 12 V at room temperature.

Immunostaining staining

After the transfer procedure, the membrane was immersed in blocking buffer (5% BSA in protein washing buffer) and blocked on a rotating shaker for 30 min at room temperature. To keep the antibodies free from contamination, a washing step with 3 times protein wash buffer for 3 min each is mandatory. The membrane is then incubated with primary antibody (7 - 10 mL) diluted in protein wash buffer for 30 min at room temperature on a rotating platform followed by a washing step with protein wash buffer (3 x 10 min). Subsequently the membrane was incubated with the secondary antibody diluted in protein wash buffer for 30 min at room temperature. Finally, an anti-mouse (DAKO) or an anti-rabbit (Amersham) HRP 1:10.000 was diluted in the membrane solution and then washed three times for 10 min in protein wash buffer.

Detection

The detection was performed using Amersham ECLplus kit and an ECLplus and Typhoon scanner. Therefore, 1 mL of solution A and 25 µL solution B of the kit were mixed, applied on membrane for about 3 min and rotated. The membrane was then wrapped in thick plastic wrap that was prior cleaned with EtOH and examined using the laser at 457 nm. Image Quant Tools was used to analyse the results.

4. Results and Discussion

4.1 Peptide synthesis

All synthesized and by the working group provided CPPs used in this thesis are shown in table 10. Furthermore, all CPPs where additionally synthesized with a fluorophore (5(6)-carboxyfluorescein) for later fluorescence microscopy studies. The carboxyl group of the C-terminal amino acid was masked as an acid amide, to disguise the negative charge of the carboxylate, which might have a negative influence on the cell-penetrating property.
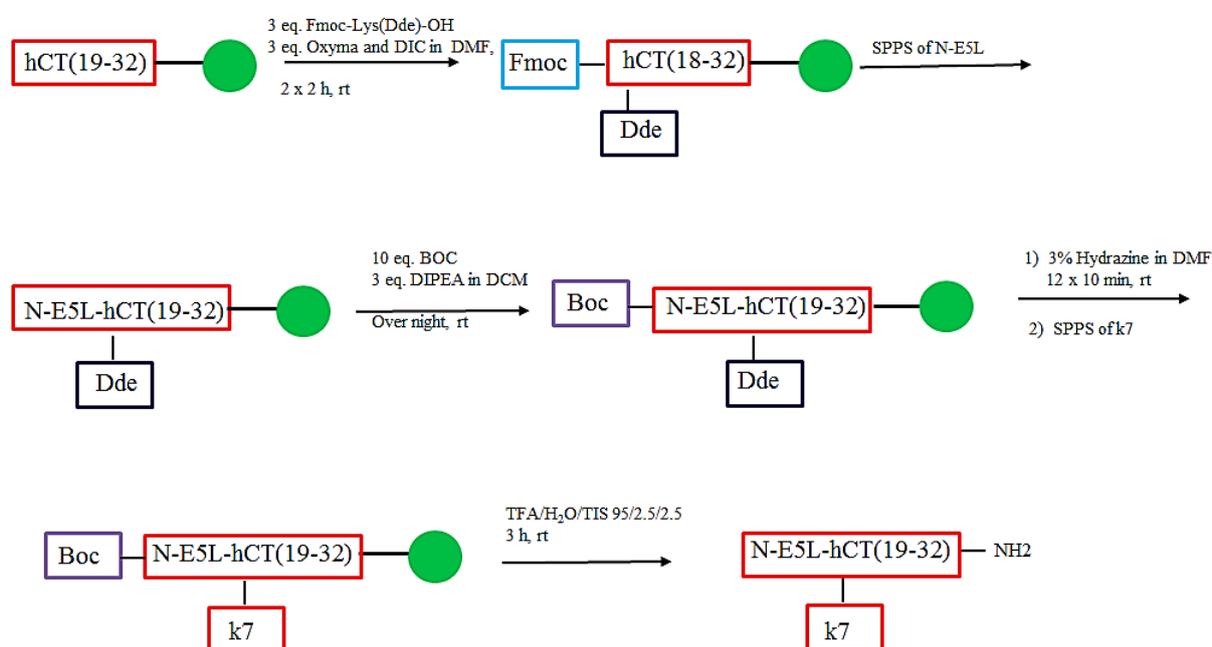

Fig. 11: Sythesis scheme of the branched CPP (**1a**)

Figure 11 shows exemplary the synthesis of a branched CPP by means of (**1a**). To synthesize the branched CPP (**1a**) the amino acid Fmoc-Lys(Dde)-OH is introduced at position 18 of the hCT(19-32) fragment. The Dde side chain protecting group can be cleaved under orthogonal conditions and thus allows branching of the peptide at this ε-position. Dde is stable under basic and acidic conditions but can selectively be removed with 2% hydrazine. After the coupling of Fmoc-Lys(Dde)-OH and subsequently cleavage of Fmoc, the amino acid sequence of N-E5L can be synthesized by the robot. It is mandatory after the Dde-cleavage that the glycine of the N-E5L sequence is either manually protected by introducing a Boc protecting group or Boc-Gly-OH is used in the robot synthesis instead of Fmoc protected

glycine. Otherwise the synthesis of the k7 chain would occur at the glycine. After the cleavage of Dde the k7-side chain was synthesized by the robot.
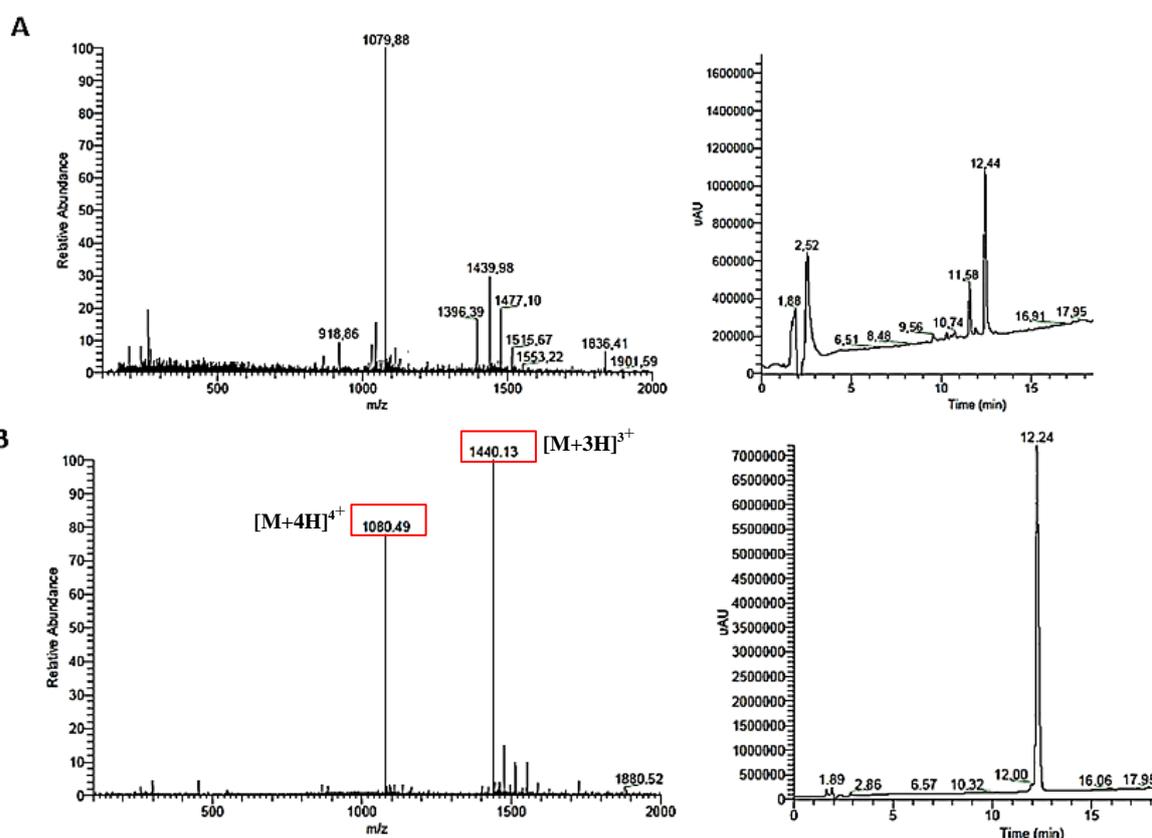
Fig. 12: ESI-MS spectrum and UV-chromatogram of (**1a**). A = After full cleavage. B = After HPLC-purification

Fig. 12 shows the ESI-MS spectrum as well as the UV-chromatogram of CPP (**1a**) once after full cleavage (A) and then after HPLC-purification (B). The retention time of the product was at 12.4 min after full cleavage and at 12.2 min after purification. The peak at m/z = 1440.13 belongs to the trifold charged molecular ion $[M+3H]^{3+}$ whereas the peak at m/z = 1080.49 to the fourfold charged species $[M+4H]^{4+}$. When taking a closer look at the UV-chromatogram after full cleavage, the smaller peak at a retention time of 11.58 min occurred before the product peak at 12.44 min. This peak possesses a m/z = 1396.88 which belongs to the trifold charged molecular ion $[M+3H]^{3+}$ and a m/z = 1048.06 beloning to the fourfold charged molecular ion $[M+4H]^{4+}$ of a byproduct weighing 4187.64 g/mol. Impurities might result from a decreasing coupling efficiency. During robot synthesis the coupling efficiency declines the longer the amino acid sequence becomes resulting in a synthesis interruption and thus various peptide fragments. Since the impurity weighs 129.49 g/mol less than the product,

most likely a glutamic acid is missing in the amino acid sequence of the byproduct. Nevertheless, after HPLC-purification, CPP **(1a)** could be obtained with over 97% purity.

All peptides listed in table 10 could successfully be synthesized via SPPS as was confirmed by mass spectrometry. After full cleavage of the peptides, a HPLC-purification was carried out. Yields and purity are also depicted in table 10.

Table 10: Overview of all peptides used in this thesis

	Peptide	Sequence	MW_{calc} [g/mol]	MW_{exp}[g/mol]	Peptide yield	purity	net charge
(1a)[2]	NE5L-hCT(18-32)-k7	GLLEALAELLEKFHTFPQTAIGVGAP-NH$_2$ | KKRKAPKKKRKFA	4317.60	4317.67	40%	>97%	+8
(1b)[2]	Capr-hCT(18-32)-k7	Capr-KFHTFPQTAIGVGAP-NH$_2$ | KKRKAPKKKRKFA	3318.09	3319.05	57%	>97%	+10
(2a)[1]	(sC18)$_{2,lin}$	GLRKRLRKFRNKIKEKGLRKRLRKFRNKIKEK-NH$_2$	4122.16	4121.81			+17
(2b)[1]	(sC18)$_{2,lin}$*	GLRKRLRKFRNKGLRKRLRKFRNK-NH$_2$	3124.91	3126.15			+15
(2c)	(sC18)$_2$	GLRKRLRKFRNKIKEK-NH$_2$ | GLRKRLRKFRNKIKEK	4122.16	4122.58	45%	>98%	+17
(2d)[2]	(sC18)$_2$*	GLRKRLRKFRNK-NH$_2$ | GLRKRLRKFRNK	3124.91	3125.04	43%	>98%	+15
(2e)	sC18	GLRKRLRKFRNKIKEK-NH$_2$	2069.60	2069.83	65%	>99%	+9
(2f)	sC18*	GLRKRLRKFRNK-NH$_2$	1570.96	1571.01	67%	>99%	+8
(3a)[1]	Cyc1[1]	<u>BLRX</u>RLRKFRNK-NH2	1635.01	1635.03			+7
(3b)[1]	Cyc2[1]	<u>BLRKRLRX</u>FRNK-NH2	1635.01	1635.06			+7
(3c)[1]	Cyc3[1]	<u>BLRKRLRKFRNX</u>-NH2	1635.01	1635.01			+7
(4)[2]	Tat(48-60)	GRKKRRQRRRPPQ-NH$_2$	1718.06	1718.15	53%	>96%	+9

[1] Provided by the Neundorf group; B: L-propargylglycine, X: L-(Ɛ-azido)-lysine; ___: amino acids involved in cyclization

[2] Peptides were also synthesized with 5(6)-Carboxyfluorescein

4.2 Studying the potency of novel CPPs as transfection vectors

4.2.1   Cyclic peptides

The therapeutic application of nucleic acids has drawn much attention due to its ability to treat inherited and/or acquired diseases. The delivery of large and hydrophilic molecules, such as nucleic acids, to the intracellular compartments is restricted based on their poor ability to permeate the plasma membrane. [7]. For the compounds that are not able to translocate the cell membrane on their own, various delivery systems were developed. Over the past years CPPs have been emerged as promising oligonucleotide delivery vectors and as an alternative to viral vectors as the use of viral vectors has many drawbacks regarding their safety and application (see chapter 1.2) [10, 12-15]. In contrast, CPPs feature advantageous properties like low toxicity, easy preparation and handling as well as good biocompatibility [49]. The majority of CPPs and CPP/cargo complex enter the cells via an endocytotic uptake mechanism. Therefore, one major obstacle in applying CPPs as delivery vectors is the cargo release out of the endosomes after an endocytotic uptake. To ensure this, various strategies have been developed to promote endosomal release or even prevent an endocytotic uptake [84]. One strategy is the cyclization of the peptide backbone. Recently, it was described that cyclization of the peptide backbone leads to an increase of cellular uptake and enhanced cytoplasmic distribution [116]. It is supposed that the guanidinium groups of arginine-rich peptides are forced into maximally distant positions leading to better membrane interaction and thus, to an increase of the cellular uptake. Moreover, the proteolytic stability is improved as an enzymatic degradation is impeded [117]. Since the initial step of the CPP/cargo uptake is the interaction of the complex with the lipid membrane of the cell [118], membrane contact is essential. Hence, the secondary structure of the CPP but also of the complex plays a crucial role. According to various reports, an appropriate arrangement of the guanidinium groups within the helical structure is beneficial for an improved uptake [119].

Recently, in our working group it was investigated whether an introduction of a triazole-bridge into the structure of the CPP sC18 would promote secondary structure arrangements. The CPP sC18 which is derived from the C-terminal domain of the 18 kDa cationic antimicrobial peptide CAP18, was developed in our group and is classified by Di Pisa *et al.* as a secondary amphipathic CPP [120].

Based on a truncated version of sC18 (see table 10), three cyclic peptide derivatives that differed in ring size and in the number of arginines were synthesized (see figure 13). Selective side-chain cyclization was performed by the copper (I) mediated alkyne-azide click (CuAAC)

reaction. Therefore, glycine and lysine was substituted by propargylglycine and azidolysine, respectively.
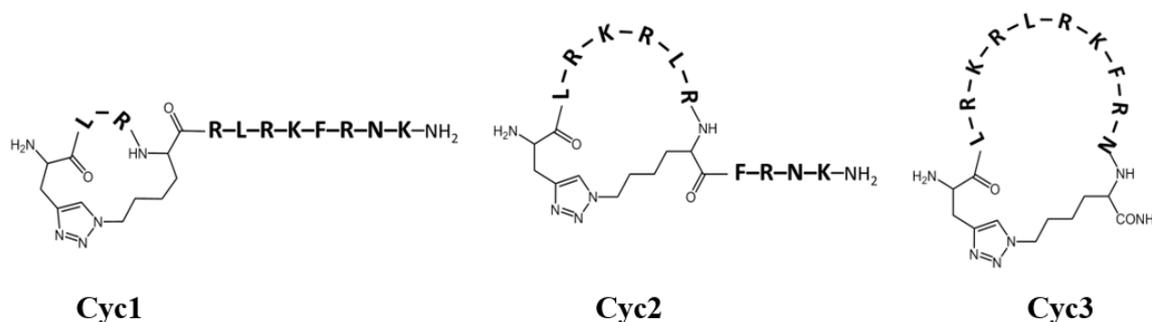

Fig. 13: Structure of the cyclic peptides used for transfection

Since confocal microscopy studies confirmed an efficient uptake of the fluorescently-labeled cyclic peptides (cyc1-cyc3) into breast adenocarcinoma cells (MCF-7) throughout the cytosol and in the cell nuclei, the cyclic CPPs were tested as potential gene delivery vectors.
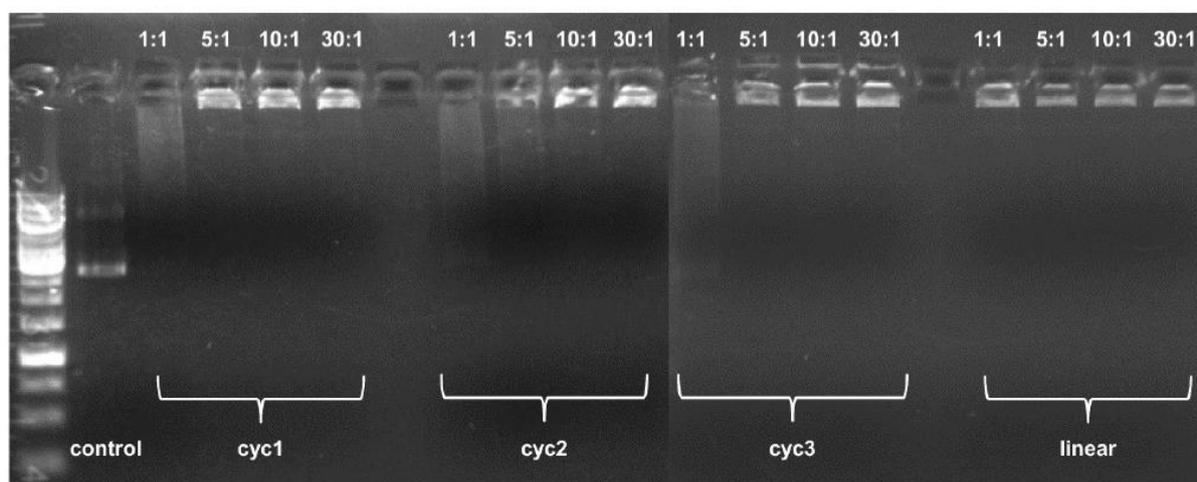

Fig. 14: Electromobility shift assay using the cyclic peptides, as well as the linear sC18 **(2e)** and pEGFP-N1 at different charge ratios Electromobility shift assay. pEGFP-N1 plasmid was complexed with the cyclic peptide conjugates and linear counterpart at various charge ratios specified on top. pEGFP-N1 plasmid served as control.

To evaluate the capability of these new cyclic peptides to achieve complete pDNA complexation and to determine optimal CPP/plasmid ratios, an electromobility shift assay

(EMSA) was performed. In principle, as the CPP is positively charged, it shields the negative charges of the plasmid upon complexation. Due to this complex formation, the electrophoretic migration rate of the plasmid pEGFP-N1 is decreased in comparison to naked DNA and hence, the mobility within the agarose gel shifts. Thus, the plasmid remains in the loading pocket of the gel when all negative charges are neutralized by the CPP. For the EMSA, CPP and plasmid were complexed for 30 min using the same conditions as for cell transfection. Four different CPP/plasmid charge ratios were analyzed, namely 1:1, 5:1, 10:1 and 30:1. The complexes were run on an agarose gel- and the plasmid was visualized by gel red staining. The results of the EMSA study are presented in figure 14. All three cyclic CPPs exhibit a net charge of +7, hence a charge ratio of 1:1 is too insufficient to shield the negative charges of the plasmid resulting in migration in the gel. The linear CPP (**2e**) possesses a net charge of +8. Charge ratios of 5:1 to 30:1 showed for all three CPPs complete band shifts to the loading pocket. This indicates a sufficient complexation of the plasmid by all three peptides. Interestingly, since all three CPPs showed the same complexation behavior, the ring size did not influence the complex formation at all. A CPP/plasmid charge ratio of 13:1 (corresponding to a CPP concentration of 20 µM) was used in the following transfection experiments. The new cyclic CPP versions were used to evaluate the potency as gene delivery vehicles to transfect MCF-7 cells with a plasmid encoding for the enhanced green fluorescent protein (eGFP). In the upper panel of figure 15, the transfection results for an incubation at 37 °C are shown, whereas in the lower panel for 1 h at 4 °C and then for further 5 h at 37 °C. Different incubation conditions were performed, since internalization studies showed an energy-independent cell entry in MCF-7 cells and peptide localization in the cell nuclei [118].
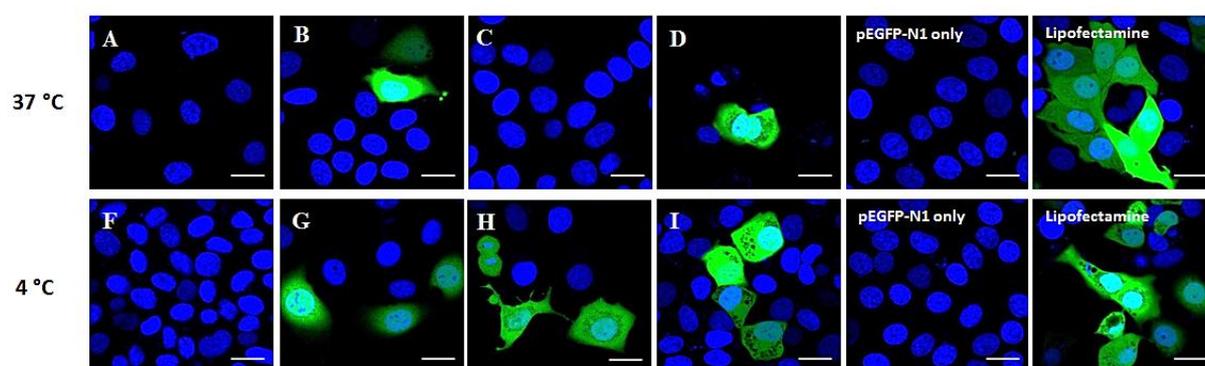

Fig. 15: Transfection of MCF-7 cells with cyclic peptides and 0.5 µg pEGFP-N1 after 48 h. (A-D: Incubation at 37 °C) A = (2e), B = cyc1, C = cyc2, D = cyc3; (F-I: Incubation at 4 °C) F = sC18, G = cyc1, H = cyc2, I = cyc3

As positive control, the commonly used standard transfection reagent Lipofectamine®2000 was used. As shown in picture **A** and **C**, no transfected cells were detectable for **(2e)** and **cyc2** whereas few transfected cells were visible for **cyc1** and **cyc3** (see picture **B** and **D** in figure 15).

In contrast, efficient plasmid transfection (cf. fig. 15) after 48 h treatment at 4 °C could be observed for all three cycles, especially for the large cycle **cyc3** which is shown in the pictures G - I. The transfection of the MCF-7 cells with the linear CPP **(2e)** led to no positive transfection results. The linear version **(2e)** (Figure 15 images A and F) did not show any activity at all, though plasmid/CPP complexation was successful as determined by electromobility shift assay. Maybe the larger dipol moment of the triazole moiety ($\mu_{triazole} = 5.5$ debye *versus* $\mu_{amide} = 3.7$ debye) compared to the one of an amide bond lead to a more efficient interaction with the plasmid and hence, to a better delivery to the nucleus. Another possible explanation concerning the good complexation of the linear version but no positive transfection might be a too strong binding to the plasmid resulting in a hindered or even prevented dissociation of the complex. CD spectroscopy of the CPP/plasmid complex showed a clear redshift, which indicates a weaker interaction between the peptides and the plasmid. A not too strong complex formation is mandatory to gain an appropriate cargo release [121]. Perhaps, owing to the tight complexation between the linear version and the plasmid, the cell-penetrating property of the peptide got lost, and therefore, the delivery of the complex into the cells failed. Considering that the uptake of the CPP/plasmid complex followed an endocytotic mechanism, the cyclic CPPs had to be able to escape from endosomal entrapment on their own, as no lysosomotropic reagents, like chloroquine was added. However, to determine how the endosomal release occurs, further investigations would be needed.

As already mentioned above, the secondary structure of the peptide, especially the α-helix plays an important role for the peptide uptake. The α-helix features 3.6 residues per complete turn. The side chains of the residues at position i, i+4, i+7 and i+11 are then orientated at the same face of the folded structure [122]. The introduction of selective cross-linkers to the peptide side-chains or the peptide backbone at these positions leads to so called "stapled" peptides [123, 124]. Therefore, these positions were taken into account when synthesizing the peptides via copper (I) mediated alkyne-azide click reaction. Cyclization in **cyc1** was introduced between position i and i+3 leading to a low flexibility of the ring. Hence, only the linear part of the peptide at the C-terminus is able to form an α-helix. Cyclization in **cyc2** was

introduced between the positions i and i+7 which results in a bigger ring size and three arginines within the ring instead of only one as in **cyc1**. In contrast, the cyclization of **cyc3** occurred between the positions i and i+11 enabling the maximum ring flexibility compared to the other two peptides. Moreover, the ring contains four arginines but no linear part. Alternative methods for side-chain cyclization of peptides are described in literature for secondary structure stabilization. For instance, Madden *et al.* synthesized stabilized α-helical peptides via photoinduced intramolecular 1,3-dipolar cycloaddition that were able to internalize into HeLa cells [123]. Hilinski *et al.* chose a bis ring-closing metathesis reaction to synthesize peptides with multiple contiguous staples. The consequential peptides showed increased thermal stabilities and a high cell-penetrating ability [125]. Further methods to synthesize α-helix stabilized peptides are disulfide bond formation and lactam formation [125, 126]. Nevertheless, in this case the CuAAC reaction worked out as the best procedure due to its easy and selective handling.

To analyze the influence of the triazole-bridge introduction on the secondary structure and thus, on the cellular uptake, Horn *et al.* performed circular dichroism (CD) spectroscopy as well as NMR spectroscopy studies with the linear peptide (**2e**) and the large sized cycle (**cyc3**). The orientation of the peptides was therefore examined in water and additionally when in contact with lipids. In phosphate buffer, all peptides showed in the CD spectra mostly unstructured forms. Although a structural rigidification of the cyclic part of the peptide was observed, CD spectroscopy revealed no matching secondary structure motif. In contrast, when in contact with large unilamellar vesicles (LUVs), an artificial lipid vesicle, **cyc3** became more structured after an interaction with neutral as well as with anionic charged lipid compositions. The capability of **cyc3** in interacting with both LUVs might be due to the flexibility of the larger ring size enabling the ring to switch between a random-coil- and an α-helix-like structure. Hence, the large ring size might enable **cyc3** to adopt the most suitable structure that favors a better interaction with the lipid composition of the cell. For this particular case, it seems that certain flexibility and therefore the orientation of the guanidinium groups outwards is more favorable than a rigidification.

In addition, NMR-based structural studies were performed by Horn *et al.* with the linear CPP (**2e**) and **cyc3**. Therefore, the peptides were examined in the presence of SDS micelles, a membrane-mimetic medium. The cyclic peptide **Cyc3** did not show any secondary structural elements, although the final structure is not completely classified. NMR spectroscopy of the

linear peptide **(2e)** in the presence of SDS micelles revealed a short helical fragment between the residues R3 - R7 at the N-terminus.

In conclusion, cyclic peptides retaining a certain flexibility like **cyc3** have a great potential as delivery vectors for plasmid DNA, making them a valuable tool for gene therapy, especially for *in vivo* studies since the addition of potentially toxic lysomotropic reagents are not required. Hence, the before assumed improvement of an endosomal release by cyclization could be proven.

4.2.2 Branched sC18-derivatives

Besides cyclization, branching and dimerization of the amino acid sequence can lead to an enhancement of cellular uptake and endosomolytic activity [127].

Rennert *et al*. showed in 2008, that branching the structure of hCT(9-32) by introducing a NLS sequence derived from SV40 large T antigen, led to an enhanced nucleic acid delivery in primary cells. Hence, these branched versions of carrier peptides are of great value for *in vivo* applications. This holds true also for other branched derivatives like hCT(18-32)-k7, and the already described N-E5L-hCT(18-32)-k7. These CPPs were used in several cell lines for efficient delivery of pDNA and siRNA [78].

Recently, it was shown that dimerization of the sC18 peptide and introduction of a branched structure led to an increased cellular uptake. The novel CPP (sC18)$_2$ was taken up in several cell lines to a 10-fold higher extent compared to the monomeric sC18. Enhancement of the positive charges associated with an increased interaction with the negatively charged plasma membrane was assumed to be the reason for the better uptake [128]. Although the peptide was shown to be promising as transporter for cytostatic drugs, the transfection ability of (sC18)$_2$ was not yet elucidated.

In this study, the impact of branching peptides on the transfection ability was investigated. Several derivatives of the already described CPP sC18 were synthesized as dimers (**2a-2d**). Version (**2a**) was synthesized in line whereas CPP (**2c**) was synthesized as a branched version. Because previous studies revealed that the truncated version of CPP sC18, lacking the amino acids IKEK, was sufficient for cellular uptake, the shorter CPP derivatives (**2b**) and (**2d**) were additionally synthesized. Furthermore, the respective monomeric versions were investigated as well. All derivatives, their sequences and some other characteristics are shown in table 11.

Table 11: Overview of sC18- derivatives.

	Peptide	Sequence	MW (Da)	Net charge
(2a)	(sC18)$_{2,lin}$	GLRKRLRKFRNKIKEKGLRKRLRKFRNKIKEK-NH$_2$	4122.16	+17
(2b)	(sC18)$_{2,lin}$*	GLRKRLRKFRNKGLRKRLRKFRNK-NH$_2$	3124.91	+15
(2c)	(sC18)$_2$	GLRKRLRKFRNKIKEK-NH$_2$ | GLRKRLRKFRNKIKEK	4122.16	+17
(2d)	(sC18)$_2$*	GLRKRLRKFRNK-NH$_2$ | GLRKRLRKFRNK	3124.91	+15
(2e)	sC18	GLRKRLRKFRNKIKEK-NH$_2$	2069.60	+9
(2f)	sC18*	GLRKRLRKFRNK-NH$_2$	1570.96	+8

* truncated sequence

All studies were carried out with the human embryonic kidney cell line HEK-293 in serum-free as well as in serum-containing media. First, the cytotoxic effects of the sC18-derivatives on HEK-293 cells using a fluorimetric resazurin-based cell viability assay were investigated. Therefore, the cells were treated for 24 h with the sC18-derivatives using concentrations ranging from 1 µM up to 25 µM. As a negative control, 70% EtOH was used. The results are shown in figure 16. No significant cytotoxicity was observed for all six CPPs when a peptide concentration of up to 10 µM was applied. When increasing the concentration to 25 µM, cell viability was reduced to almost 50% for the dimers **(2a)**, **(2b)**, **(2c)** and **(2d).** Probably, for **(2a)** and **(2c)** this might be due to their high net charge (+17) resulting in a better interaction with the plasma membrane leading to an increased membrane disruption. Hoyer *et al.* did the same experiment with **(2a)** and HEK-293 cells observing different results. CPP **(2a)** showed no toxicity using 100 µM as concentration whereas here a concentration of 25 µM already impacted the cells negatively. This might be due to different experimental conditions as Hoyer *et al.* performed their resazurin-based viability assay in serum-containing media whereas the here presented results were carried out in serum-free media. The absence of serum for 24 h and the addition of the CPP might impacted the cells more which is reflected in lower viability. On the other hand, **(2a)** revealed an enhanced toxicity towards the tumor cell line, MCF-7 [128].
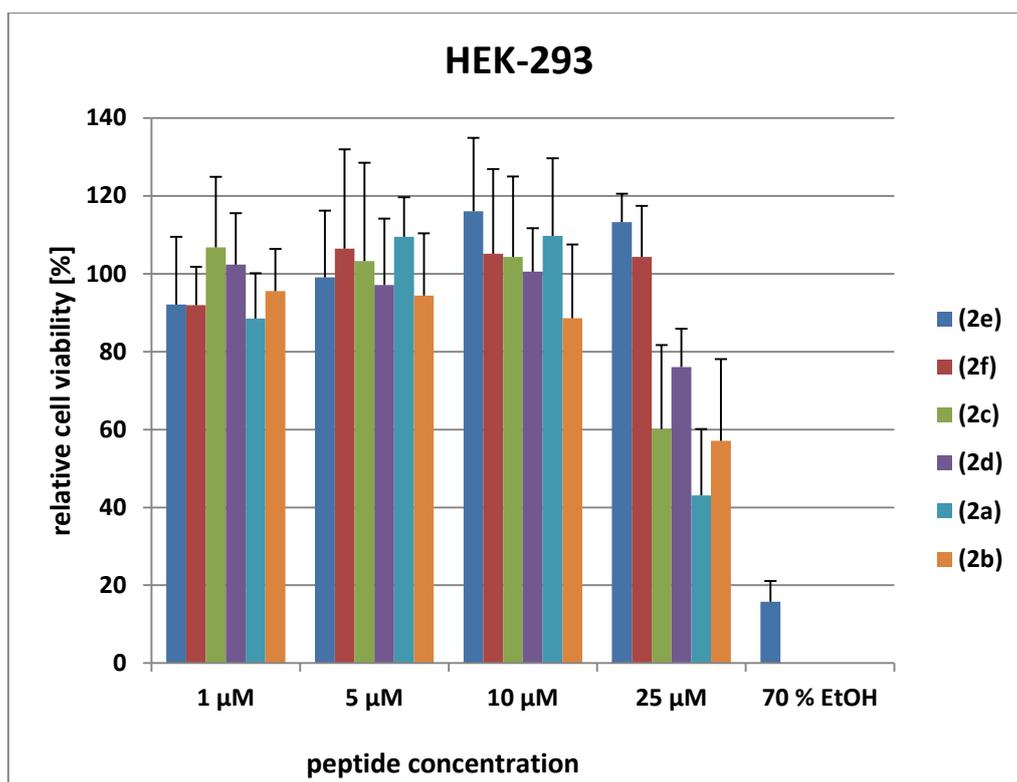
Fig. 16: Cell viability assay of HEK-293 cells using the sC18-derivatives

To determine the optimal CPP/plasmid charge ratio for the transfection experiments, an EMSA was carried out (see figure 17). The net charges of the CPPs are listed in table 11. All dimers and the monomers showed an inadequate complex formation ability using a charge ratio of 1:1 irrespective of their net charge. At higher peptide/plasmid charge ratios all CPPs showed good complex formation. A CPP/plasmid charge ratio of 10:1 was considered to be a good compromise between sufficient plasmid complexation and the prevention of toxicity. Thus, a charge ratio of 10:1 and a plasmid quantity of 0.5 µg were used in the following transfection experiments. To evaluate if a higher charge ratio and thus a higher CPP concentration has an influence on the transfection efficiency, a charge ratio of 30:1 was used as well. The concentration of each CPP for a charge ratio of 10:1 is listed in table 12 and was below 10 µM to avoid potential cytotoxic effects.
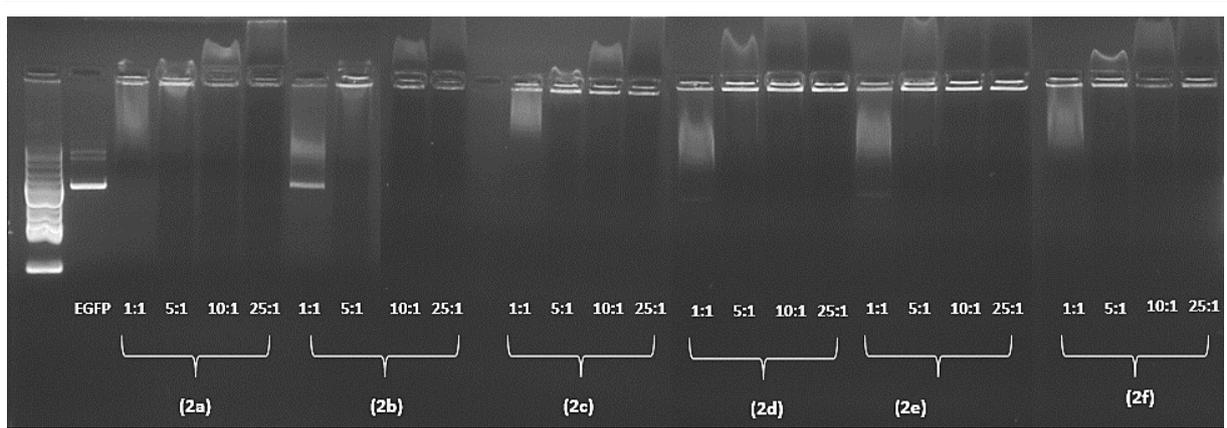
Fig. 17: Electromobility shift assay using sC18-derivatives and pEGFP-N1 at different charge ratios

However, as shown in figure 18 no efficient transfection was observed in HEK-293 cells 24 h post transfection using the plasmid pEGFP-N1. Even after 48 h of incubation the efficiency did not increase (data not shown). Nuclei were stained with Hoechst33342.
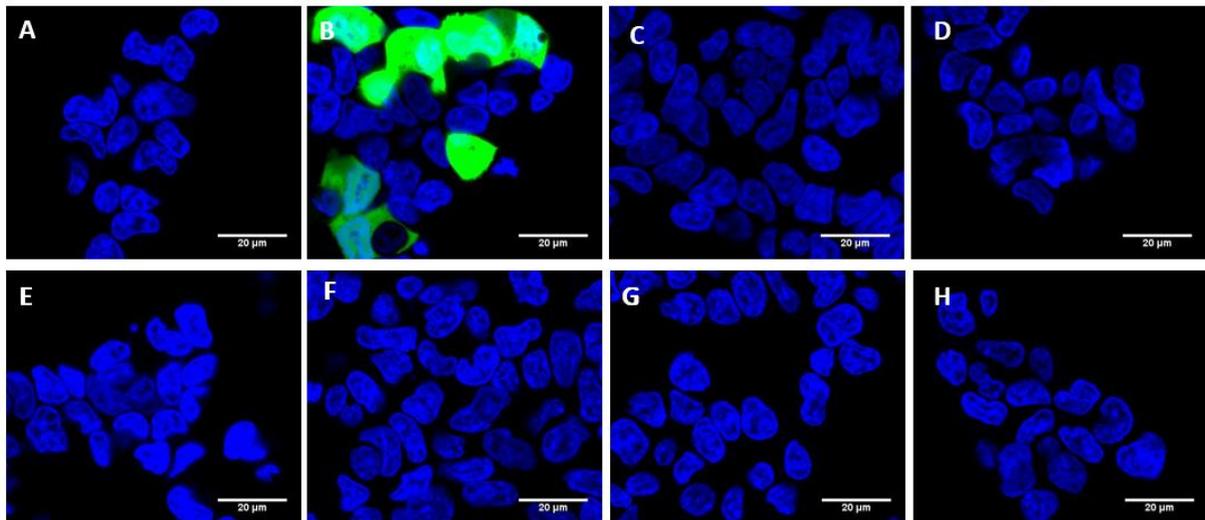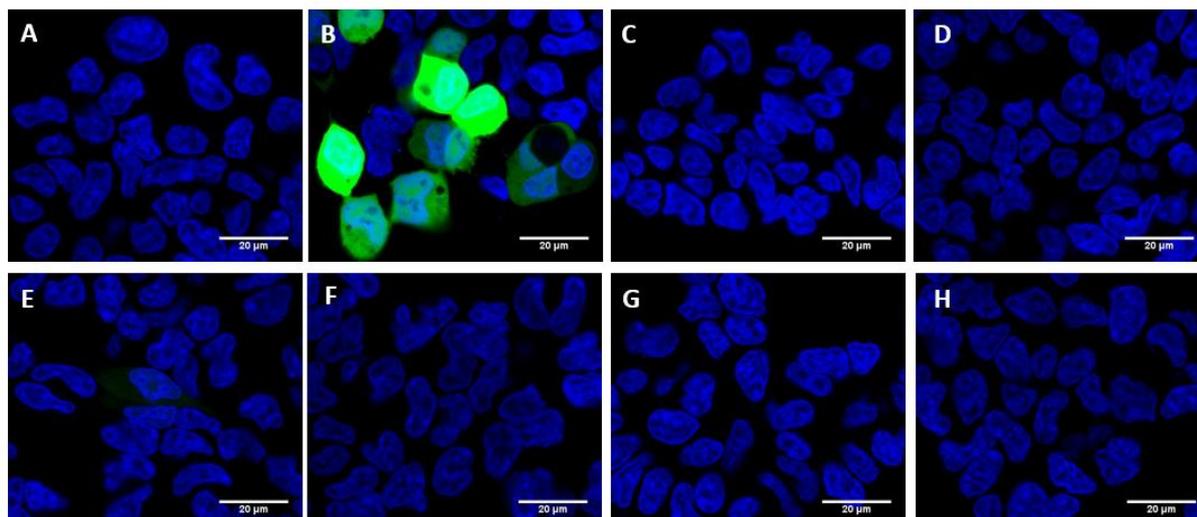

Fig. 18: Transfection of HEK-293 cells using sC18-derivatives and 0.5 µg pEGFP-N1. Charge ratio 10:1 . Scale bars, 20 µM.

Table 12: CPP concentration used to transfect HEK-293 cells

	Peptide	Charge ratio	Peptide concentration
A	Control		
B	Lipofectamine®2000		
C	(2a)	10:1	2.84 µM
D	(2b)	10:1	3.40 µM
E	(2c)	10:1	3.00 µM
F	(2d)	10:1	3.00 µM
G	(2e)	10:1	5.70 µM
H	(2f)	10:1	6.40 µM

The results altered when 100 µM of the lysosomotropic agent chloroquine (CQ) was added to the transfection mixture, which is illustrated in the fluorescent microscopy pictures in figure 19. The transfection using the monomer **(2f)** did not lead to any positive transfected cell (see picture H).
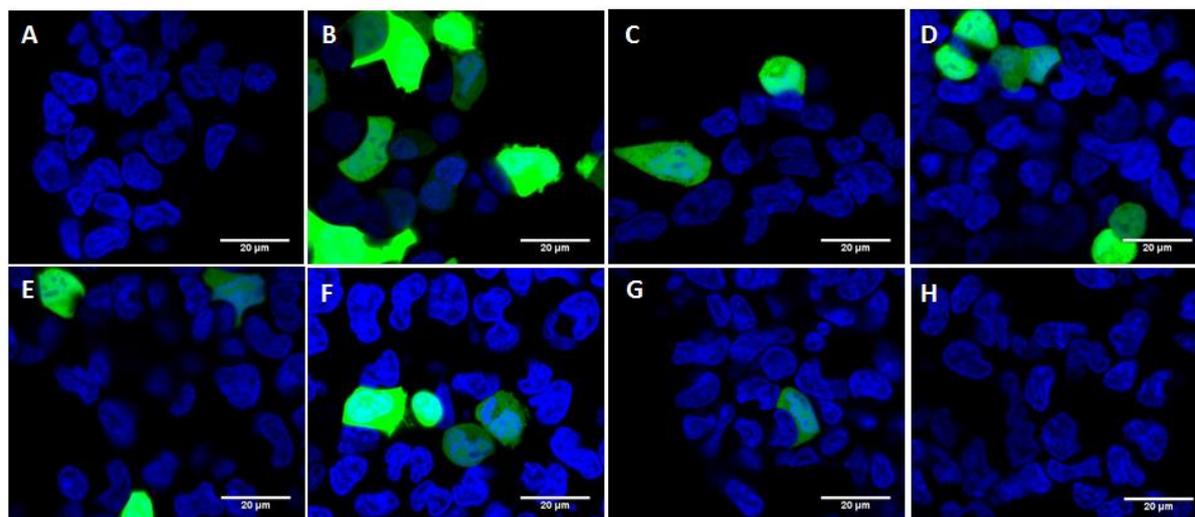
Fig. 19: Transfection of HEK-293 cells using sC18-derivatives and 0.5 µg pEGFP-N1. Addition of 100 µM chloroquine. Charge ratio 10:1. Scale bars, 20 µM.

Increasing the charge ratio from 10:1 to 30:1 did not enhance the transfection rate of HEK-293 cells at all. The applied CPP concentrations when using a charge ratio of 30:1 are listed in table 13.

Fig. 20: Transfection of HEK-293 cells using sC18-derivatives and 0.5 µg pEGFP-N1. Charge ratio 30:1. Scale bars, 20 µM.

Table 13: CPP concentration used to transfect HEK-293 cells

	Peptide	Charge ratio	[c]
A	Control		
B	Lipofectamine®2000		
C	(2a)	30:1	8.53 µM
D	(2b)	30:1	10.20 µM
E	(2c)	30:1	9.00 µM
F	(2d)	30:1	9.00 µM
G	(2e)	30:1	17.16 µM
H	(2f)	30:1	19.20 µM

However, when adding 100 µM CQ to the cells all sC18-derivatives showed a few positive transfected cells as it is shown in figure 21.
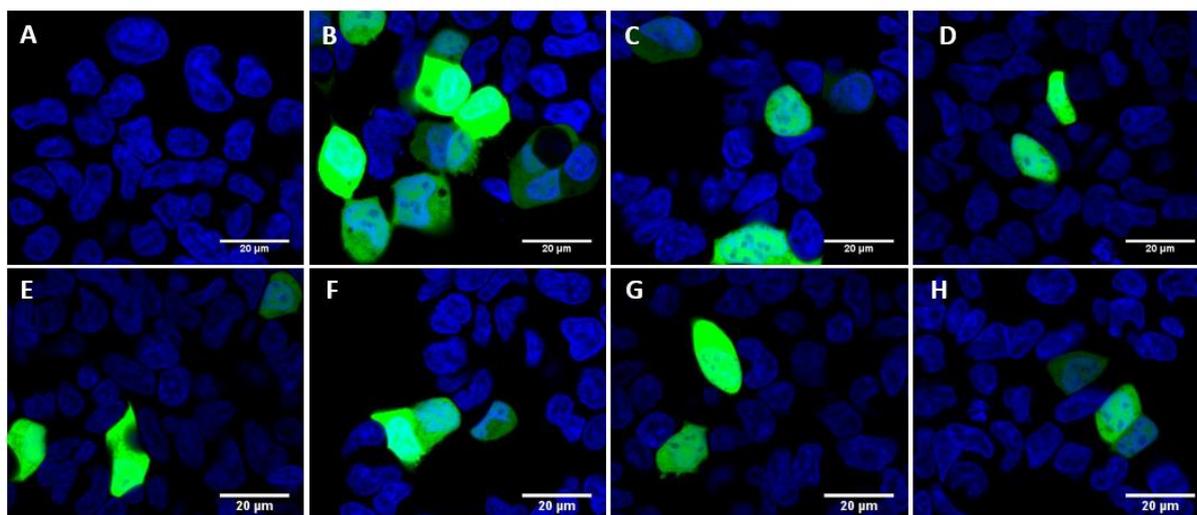
Fig. 21: Transfection of HEK-293 cells using sC18-derivatives and 0.5 µg pEGFP-N1. Addition of 100 µM chloroquine.Charge ratio 30:1.

To quantify the transfection efficiency of the sC18-derivatives, flow cytometry studies were performed. Therefore, the pDNA delivery of the sC18-derivatives was benchmarked to the transfection efficiency of the commercially available and widely used transfection reagent Lipofectamine®2000. The transfection efficiency is presented in the diagram 22. All tested derivatives showed no or poor positive transfection results, especially the monomers **(2e)** and **(2f)**. In addition to the transfection experiments in serum-free media, the transfections were also carried out in serum-containing media (indicated with *). Because one major obstacle in the application of CPPs as delivery vectors in serum-containing media might be unspecific interactions of the complex with the media components. This is important as the experimental conditions in serum-containing media are better comparable to *in vivo* conditions.

* Transfection was carried out in medium containing serum
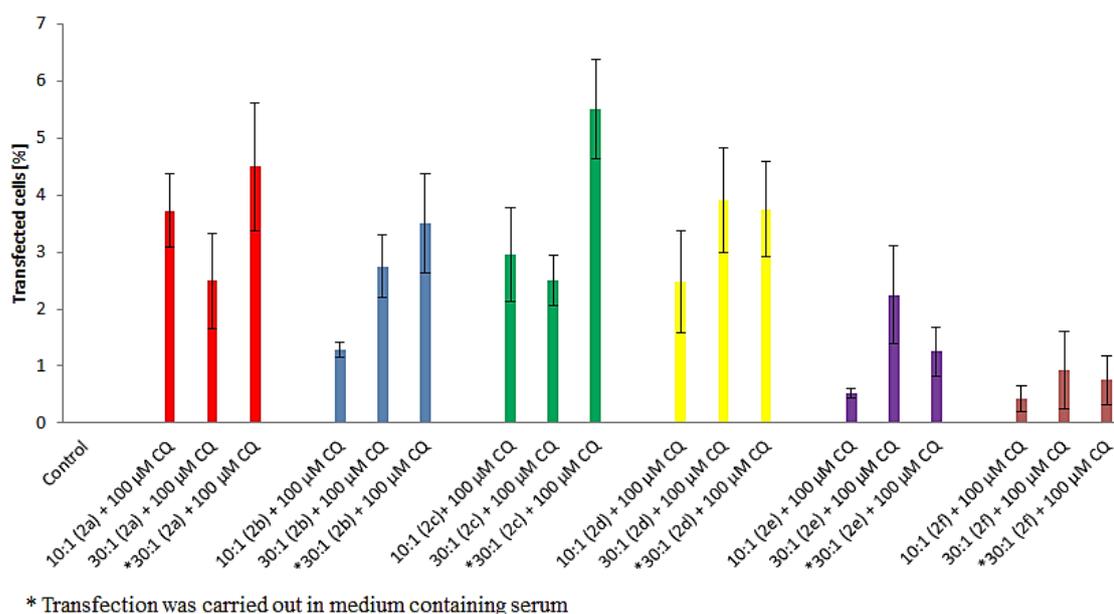
Fig. 22: Quantification of transfection efficiency after 24 h of incubation by flow cytometry. The experiment was performed at least two times in triplicate.

The before hypothesized positive impact of branching and dimerization of the parent CPP sC18 could not be approved. A slight enhancement of the transfection efficiency for the dimers (2a-2d) was observed compared to their monomers (2e) and (2f), but the results are not significant. For the dimers with the full length of sC18 (2a and 2c), increasing the charge ratio did not really influence the transfection efficiency at all. In all cases, the addition of 100 µM of chloroquine was essential for a positive plasmid transfection outcome. As already discussed before, the endosomal release is a critical step for the CPP/plasmid complex after endocytotic uptake. The complex is trapped in endosomes and must be released to reach its target. The addition of the lysosomotropic reagent chloroquine is one possibility to overcome this obstacle. The results indicate that without adding CQ, the majority amount of plasmid is still entrapped in the endosomes regardless of the applied CPP concentration and thereby did not reach the nucleus to be expressed. A significant difference in the transfection efficiency between branching the parent sC18 and just synthesizing the sequence in line could not be observed. Therefore, it is basically not necessary to branch the CPP to obtain a better efficiency. A dimerization in line is enough and, on top of that, easier to prepare since the CPP can be completely synthesized in one step by a robot. However, in terms of toxicity, the linear dimers (2a) and (2b) are more toxic than the branched dimers.when applying 25 µM.

Keeping the concentration lower, no toxic effects on HEK-293 cells were observable (see figure 16.

Nevertheless, the transfection rate for all tested sC18 derivatives were extremely poor compared to the widely used Lipofectamine®2000. Hence, further improvements concerning delivery capability are necessary.

4.3 Analyzing toxicity, internalization capacity and selectivity of CPPs when in contact with choanoflagellates

Choanoflagellates are the closest known relatives of animals. Since the progenitors of animals cannot be studied directly, choanoflagellates could serve as model organisms to investigate the evolution of multi-cellularity and the origin of animals. Therefore the development of methods to genetically manipulate choanoflagellates is of high scientific interest. Until now, common transfection methods, like electroporation or lipofection, failed in transfecting choanoflagellates. Since the application of CPPs to choanoflagellates is completely new, the focus in this part of the thesis was to generate appropriate experimental procedures to investigate the impact of CPPs, on for instance the viability. The main focus was of course the development of a CPP-based oligonucleotide delivery strategy for different choanoflagellate species.

4.3.1   Strategies to reduce bacteria

One major problem working with choanoflagellates is the presence of bacteria in the cultures. Different methods have been investigated to reduce the bacteria population in the choanoflagellate solution. First, it would be helpful to identify the strain or to narrow the group of the bacteria, to apply specific antibiotics against them. Therefore, the solution of *Salpingoeca euryoecia* was plated out on a Müller-Hinton agar plate and incubated for 24 h at 37°C. After incubation, two different looking colonies could be observed and were isolated for further experiments. By using gram staining, the two strains were identified as gram-positive bacteria. In a next step an agar diffusion test was used to determine which antibiotic would lead to reduction of the bacteria (table of applied antibiotics are listed in table 16 in the attachment).

Fig. 23: Results of agar diffusion test.

The antibiotics which showed a growth inhibition by producing a bacteria-free areola (see figure 23), were then added to the choanoflagellate cultures and examined after 24 h and 48 h, respectively, after the addition. No significant bacteria reduction could be observed for the tested antibiotics, however, the vitality of the choanoflagellates was dramatically affected after the addition.

Table 14: Overview of experiments to reduce bacteria concentration

Strategy	Result
Different antibiotic mixtures	No significant reduction of bacteria, but effects vitality of choanoflagellates
Filtration	Very slow procedure; removing choanoflagellates from the filter is difficult
Attempt to sort the choanoflagellates via cell sorter	Population during sorting could not be determined
Determination of choanoflagellates population in flow cytometer with MitoTracker® green	MitoTracker® green is also taken up by bacteria, so there are not two distinguishable populations
No food source for the bacteria	Choanoflagellates growth is slowed down and no significant reduction of bacteria concentration
Percoll-gradient	No significant reduction of bacteria concentration
Incubation on a shaker device to reduce accumulation of bacteria	No significant reduction of bacteria concentration

In another attempt, FACS (fluorescence activated cell sorting) was used to separate choanoflagellates from bacteria. In principle, the separation can take place due to different sizes as the choanoflagellates are bigger than bacteria. After cell sorting of different size clusters from the population, the collected samples were examined under a light microscope.

None of the collected samples contained the desired choanoflagellates, merely debris or pieces of bacteria biofilm were observed (data not shown).

Thus, FACS and simultaneous organelle staining was used for discriminating between bacteria and choanoflagellates. For this purpose the commercially available staining reagent MitoTracker® green was applied to the choanoflagellate solution to stain the mitochondria of the choanoflagellates. As bacteria do not contain mitochondria there should be a cluster with a green signal and one without, enabling a separation of choanoflagellates and bacteria via cell sorting.
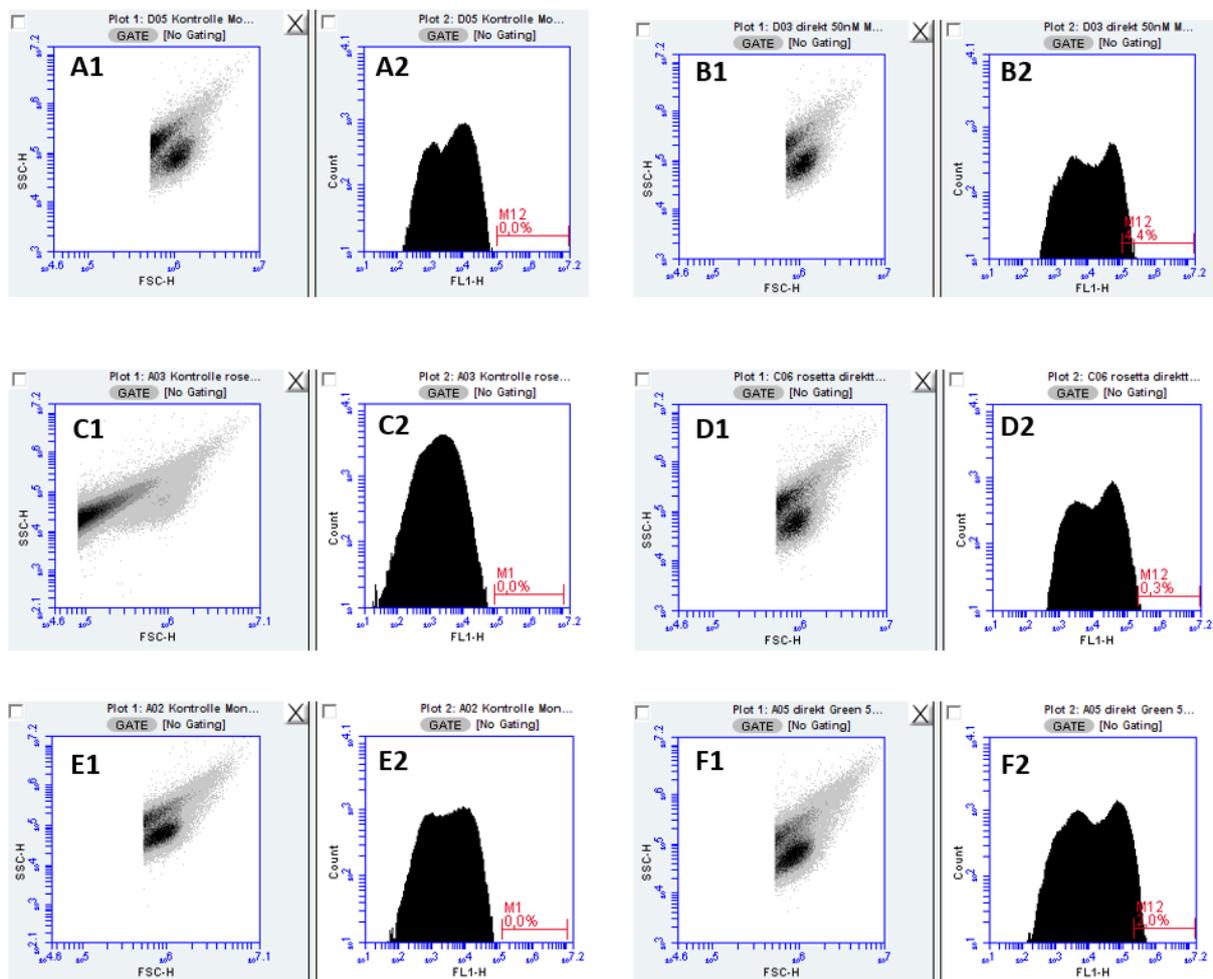
Fig. 24: 50 nM MitoTracker® green staining of *Salpingoeca euryoecia* (A-B), (C-D) *Salpingoeca rosetta* and (E-F) "Mono lake"

When adding 50 nM of MitoTracker® green to the choanoflagellates solution a slight shift of the cluster towards higher fluorescence (B2, D2 and F2 of figure 24) was detected compared to the controls (A2, C2 and E2). This result lead to the assumption that the shifted clusters belonged to the stained mitochondria of the choanoflagellates. To proof this, choanoflagellates were treated with 50 nM MitoTracker® green and then analyzed via fluorescence activated cell sorting (FACS). Untreated choanoflagellates served as a control to set the threshold and only events with fluorescence intensity over the threshold were collected into a 1.5 µL reaction vessel. The sorted events were then examined by microscopy. For unknown reason, the collected samples did not contain any choanoflagellates but pieces of the bio film and crytals from the media.

When repeating the experiment with a bacteria solution, containing the strains from *S. rosetta*, a distinct cluster shift towards higher fluorescence (see in figure 25 B2, C2, E2 and F2) was distinguishable even directly after the addition of 50 nM MitoTracker® green (B2 and E2). Actually, the staining should be highly selective as bacteria do not have mitochondria, but in some way the dye was taken up by the bacteria. Hence, it was not possible to distinguish between the choanoflagellate population and the bacteria population making the use of a cell sorter unfeasible.
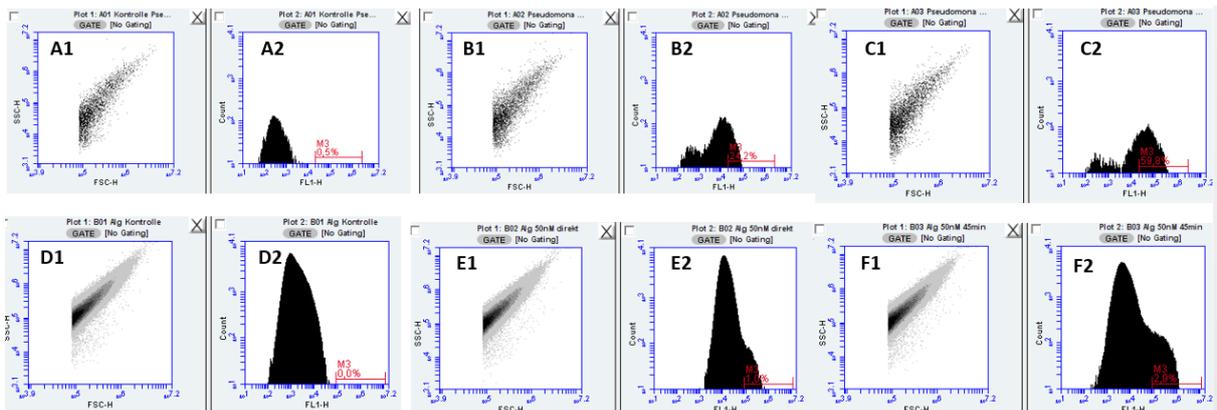
Fig. 25: 50 nM MitoTracker® green staining of *pseudomonas putida* (A-C) and *algoriphagus machipongonensis* (D-F).

A lot of effort has been made to eliminate or reduce bacteria concentration in the choanoflagellate solutions to facilitate the next experiments. An overview of all studies is

shown in table 14. Although the separation of both populations was not possible, CPP internalization and CPP-mediated nucleic acid transfection studies were performed anyway.

4.3.2 Viability studies

Recently, promising CPP-mediated transfection was shown using CPP **(1a)** [69]. Therefore, transfection experiments were carried out with this CPP using already established conditions. First, the influence of the peptides on the viability of choanoflagellates was tested. To determine the vitality of choanoflagellates the flagellum movement is observed via microscopy. Active choanoflagellates show a strong and fast movement of their flagellum whereas damaged choanoflagellates do not. As the choanoflagellates were not fixated, microscopy was strongly impacted by their movement. Established toxicity studies like a resazurin-based or MTT-based assay where not possible as the choanoflagellate solution contained a lot of bacteria which served as a food source.
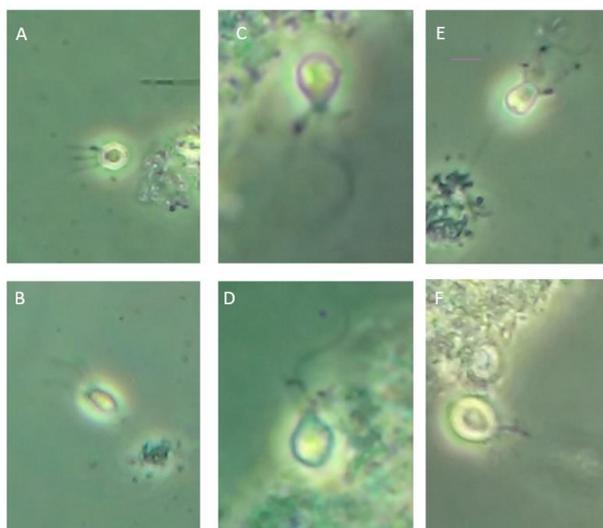
Fig. 26: Vitality of choanoflagellates 24h after treatment with the CPP **(1a)**. (A) Control *Salpingoeca sp*. ("Mono Lake"); (B) *Salpingoeca sp*.24h after treatment of 46 µM peptide; (C) Control *Salpingoeca euryoecia*, (D) *Salpingoeca euryoecia* 24h after treatment of 46 µM peptide; (E) Control *Salpingoeca rosetta*; (F) *Salpingoeca rosetta* 24h after treatment of 46 µM peptide

No toxicity or impairment could be observed when all three choanoflagellates species (*Salpingoeca euryoecia*, *Salpingoeca rosetta* and *Salpingoeca sp*.) were incubated with CPP **(1a)** solutions of up to 46 µM concentration. After 24 h treatment with the peptide, the

flagellum was visible and showed strong movements. In addition the collar was properly formed (see, Figure 26). Additionally, to proof the vitality of the choanoflagellates after the treatment, movies were taken that clearly showed the flagellum movement, and even swimmers, free living individuals, were observed.

4.3.3 Internalization

To our knowledge, there are no published studies on the uptake and effect of cell-penetrating peptides on choanoflagellates. For this purpose the CPPs **(1a)** and **(4)** were chosen for uptake studies. In addition, different choanoflagellate species, one originating from a freshwater source (*Salpingoeca euryoecia*), and two species isolated from marine water (*Salpingoeca rosetta* and *Salpingoeca sp.*), were chosen for the experiments. In addition the impact of the salt concentration on the uptake ability of the CPP was studied. All of the three choanoflagellate species studied posses a theca.

Since bacterial growth could not be prevented in the Ibidi-dishes, a strong background fluorescent occurred during microscopy, because the bacteria internalized the peptides as well.
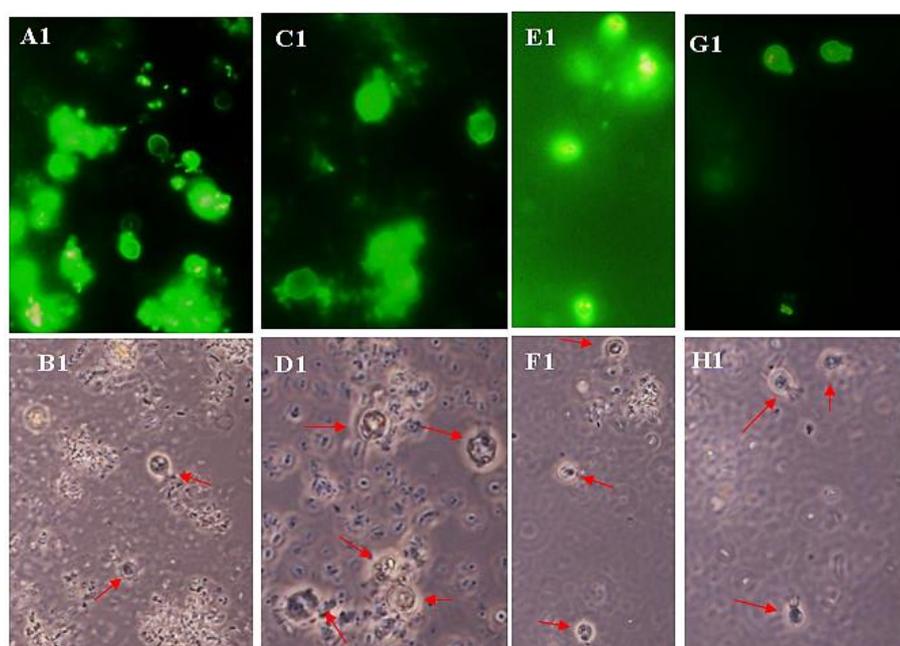
Fig. 27: Salpingoeca euryoecia. (A1-B1) 60 min 25 µM **CF-(1a)**; (C1-D1) 180 min 25 µM **CF-(1a)**; (E1-F1) 60 min 25 µM **CF-(4)**; (G1-H1) 180 min 25 µM **CF-(4)**.

After incubation of CF-labeled CPP (**1a**) for 1 h at room temperature with freshwater choanoflagellate *Salpingoeca euryoecia*, the CPP was mainly located in the theca which surrounds the cell body (Fig. 27 A1-B1). The bright field image B1 showed viable choanoflagellates, with a still present collar. This observation was important to proof that the viability is not affected. When extending the incubation time up to 3 h, the CPP (**1a**) was completely distributed in the cytosol (C1 and D1). However, taking a closer look, the bright field image D1 showed that the choanoflagellates had contracted cell bodies, since they were more rounded in their shape and no collar was visible. In contrast, an incubation of *Salpingoeca euryoecia* with CPP (**4**) did not affect the viability of them at all, even not after 3 h of incubation (Figure 28). In addition CPP (**4**) seemed to be more effective than (**1a**) when comparing image E1 with A1. After 1 h of incubation, (**4**) was fully distributed in the cytosol. Interestingly, after 3 h incubation two small bright dots in the cytosol were visible (see G1). Whether this was a food vacuole or an accumulation of the peptide in another organelle, for instance in the nucleus, could not be clarified as an *in vivo* nucleus staining did not show clear results (data not shown). The higher sensitivity of *Salpingoeca euryoecia* towards (**1a**) might be due to the composition of this CPP. It contains a fusogenic peptide sequence, N-E5L, that was derived from the HA2 domain of the influenza virus hemagglutin. Neundorf *et. al.* observed indeed an improvement of the cytosolic uptake when fusing N-E5L to CPPs, but this was simultaneously accompanied by an increase in cytotoxicity [85]. Another reason might be a too strong interaction of (**1a**) with the theca and/or the plasma membrane, causing disruption of the membrane.

The same experiments were carried out for the marine species *Salpingoeca rosetta* and for the not yet been further classified strain *Salpingoeca sp.* (referred further on as "Mono lake"), thus allowing an investigation of the impact of saline medium on the uptake ability of CPP (**1a**) and (**4**).

The addition of both CPPs affected the morphology of *Salpingoeca rosetta* irrespectively of the incubation time used (see bright field images B2-H2 of figure 28). After adding CPP (**1a**) for 1 h, the fluorescently-labeled CPP was mainly accumulated within the theca, which was also observed for the fresh-water species *Salpingoeca euryoecia* (A1). Additionally, also in the contracted collar CPP accumulation was visible. Unlike *Salpingoeca euryoecia*, the marine species *Salpingoeca rosetta* seemed to react more sensitive towards CPP (**1a**), as in image B2 strongly deformed choanoflagellates were observed. Neither the flagellum nor the collar was visible, indicating strong disturbance of viability. These effects are even stronger

when extending the incubation time. Figure D2 demonstrates that the choanoflagellates seem to be shrunken and show a rounded shape speaking for cyst formation. When environmental conditions declined, choanoflagellates may form cysts, a temporary dormant status, until an improvement of living conditions occurs. However, the exact conditions leading to cyst formation is not yet fully understood, starvation and or UV radiation were described as possible triggers [129]. CPP **(4)** showed likewise impairment after addition, but not as dramatically as **(1a)**. Furthermore, in this case, the distribution within the protoplast was different compared to the fresh-water species *Salpingoeca euryoecia.* Comparing image G1 with G2 (see image 29), there were no two bright dots observable in G2 but one big dot in the middle of the choanoflagellate. Possibly the cell body contracted and the CPP is accumulated in the cytosol. Nevertheless, after the addition of both CPPs the morphology of *Salpingoeca rosetta* seemed to be impaired.
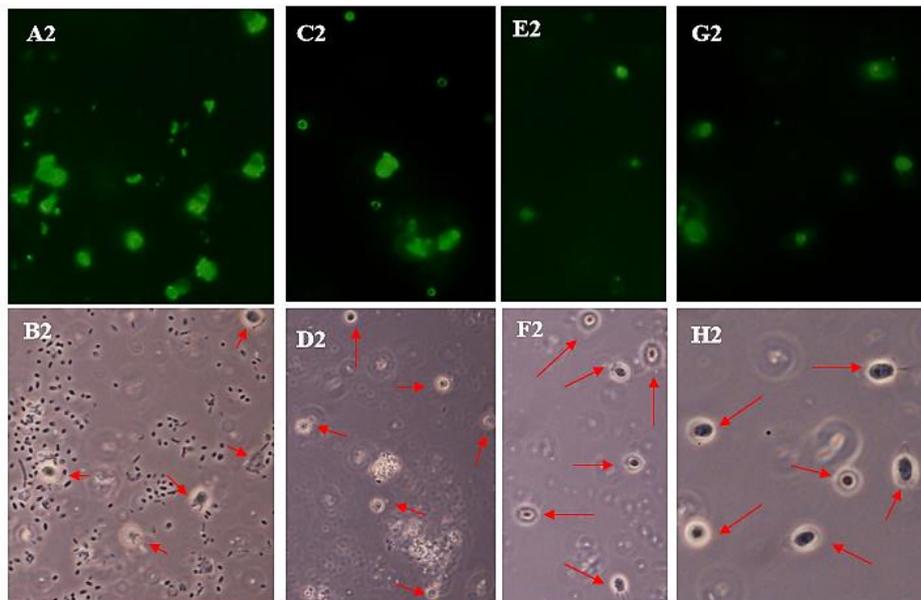
Fig. 28: Salpingoeca rosetta. (A2-B2) 60 min 25 µM (A2-B2) 60 min 25 µM **CF-(1a)**; (C2-D2) 180 min 25 µM **CF-(1a)**; (E2-F2) 60 min 25 µM **CF-(4)**; (G2-H2) 180 min 25 µM **CF-(4)**.
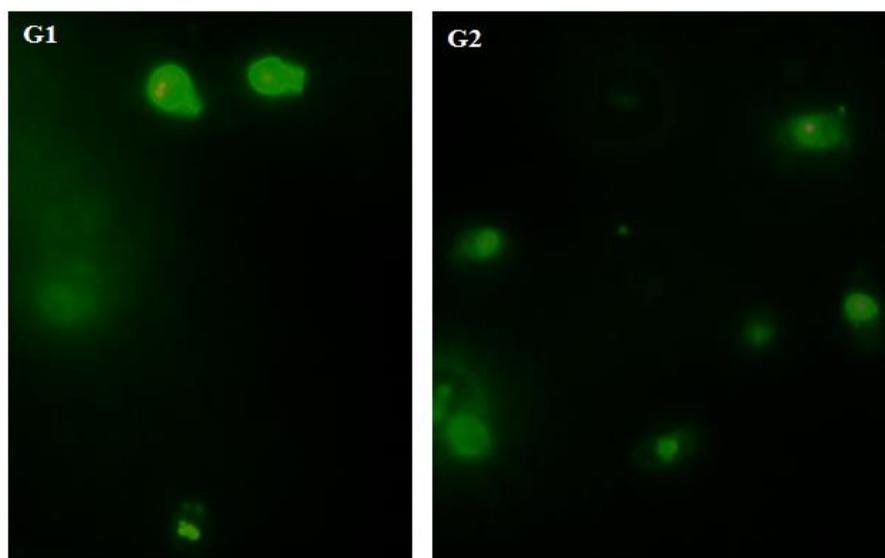
Fig. 29: Closer look at the internalization pattern of *Salpingoeca euryoecia* (G1) and *Salpingoeca rosetta* (G2) 3 h after the addition of 25 µM of (**4**).

The marine choanoflagellate species "Mono lake" that was recently isolated from the large saline soda lake, Mono Lake, was chosen for further experiments. As they are able to survive in this extreme habitat, we assumed them to be very robust towards changes in their environment. However, after the addition of CPP (**1a**) the morphology of the choanoflagellates was altered similar to *Salpingoeca rosetta*. In image B3 of figure 30, neither flagellum nor collar were visible indicating a reduction of their viability. CPP (**1a**) was again mainly accumulated in the theca after 1 h of incubation and after 3 h the shape of the choanoflagellates became more globular. Like for *Salpingoeca rosetta* this might be due to cyst formation caused by changes in their environment. Interestingly, after incubation of CPP (**4**) for 1 h (see E3), all choanoflagellates exhibit one bright fluorescent dot in their cytosol. It seemed that CPP (**4**) has been taken up by "Mono lake" and located in a specific organelle. Whether the CPP is located in the nucleus, another organelle, or a food vacuole, remained unclear. The distribution of CPP (**4**) within the choanoflagellate increased after extending the incubation time up to 3 h (see G3).
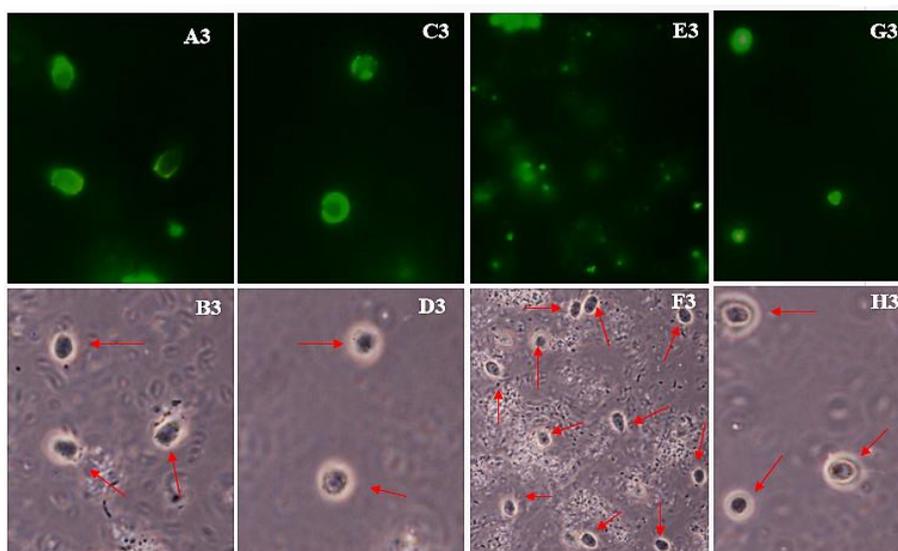
Fig. 30: "Mono lake" (A3-B3) 60 min 25 µM **CF-(1a)**; (C3-D3) 180 min 25 µM **CF-(1a)**; (E3-F3) 60 min 25 µM **CF-(4)**; (G3-H3) 180 min 25 µM **CF-(4)**.

The exact uptake mechanism for both CPPs is not yet understood, but since no punctuated distribution throughout the cytosol was visible, indicating an endocytotic uptake [80], this entry pathway might be neglected. However, the resolution of the images was not high enough to exclude an uptake of the CPPs via endocytosis. Besides the addition of trypan blue, a reagent to quench the extracellular fluorescence, was not possible since it affected the vitality of the choanoflagellates. Despite extensive washing procedures with fresh medium, CPP **(1a)** seemed to remain bound to the cell surface or the theca and not been internalized. This might explain the strong accumulation of CPP **(1a)** in image C3. To further elucidate the uptake mechanism, a microscope with a higher resolution would have been necessary as the size of the choanoflagellate used in this work is not exceeding 10 µM. Furthermore, it would be helpful to know the precise composition of the theca, to understand the interaction of the CPPs with the components of the theca. In other studies, CPP **(1a)** showed a punctuated distribution pattern in the cytosol after only 15-30 min incubation in HeLa cells [85]. If endocytosis would be the preferred uptake pathway for the CPP, an endosomal release would be necessary. In many cases the anti-malaria drug chloroquine, a lysosomotropic agent, was added to facilitate the endosomal escape [84]. This weak base accumulates in acidic organelles (lysosomes and endosomes), and due to an increased adsorption of water by binding of protons, the endosomes finally burst. This effect is also known as the proton sponge effect [130]. Since an addition of chloroquine did not occurred, direct penetration seemed to be the most presumably uptake mode. Another possible explanation might be that

the CPPs were taken up by an endocytotic pathway and the release from the endosomes occurred very fast within the incubation time. Another possibility to elucidate the uptake mechanism could be the addition of endocytosis inhibitors, like the caveolae-dependent endocytosis inhibitor filipin [131]. The consequential results should be interpreted carefully, since an inhibition of one pathway might always activate another pathway as often more than one pathway seems supposable [84]. A high resolution microscope could be used to observe an endosome staining with specific dyes to see if the fluorescently-labeled peptides are trapped in the endosomes confirming an endocytotic uptake. When comparing the effect of CPPs on the viability of the freshwater choanoflagellate *Salpingoeca euryoecia* with the two marine species, significant differences were observed. The two marine species seemed to respond more sensitive towards both CPPs, which might be due to a different membrane composition compared to freshwater choanoflagellates. One possible explanation could be the existence of pumps or channels on the cell membrane that regulate the osmotic balance. As the interaction between the CPP with the negatively charged components of the cell membrane is the initial step of internalization, a too strong binding might lead to disruption of the membrane and hence saline water could enter the cytosol causing cell death. Since CPPs **(1a)** and **(4)** showed unequal intracellular distribution patterns, the uptake mechanism must be somehow different. The uptake mode is strongly dependent on several criteria like for instance membrane composition, peptide concentration and the nature of the CPP itself [84]. Therefore it is very difficult to make specific conclusions about the mechanism. The investigation of the CPP uptake was hindered due to limited available techniques and the still poor knowledge of choanoflagellate physiology in general. In order to solve the problem of generating high-quality microscopy images, a large number of different microscopy types were used. Besides diverse confocal laser scanning microscopes, an epifluorescence and a spinning disc microscope were used. None of the used microscope achieved the desired image quality as none was able to acquire high resolution fluorescents as well as phase or DIC images. Furthermore the fact that all experiments were carried out using viable and hence moving organisms complicated the imaging studies. Nevertheless, the internalization experiments were successful for the freshwater species *Salpingoeca euryoecia* as well as for the marine species *Salpingoeca rosetta* and "Mono lake".

It should be pointed out, that all experiments were carried out under *in vivo* conditions without fixation.

4.3.4 Transfection of *Salpingoeca euryoecia*

Since preliminary uptake studies were promising, oligonucleotide delivery using CPP **(1a)** and **(4)**, were further investigated. For this purpose the CPPs were non-covalently fused by electrostatic interaction to the plasmid pEGFP-N1 encoding for the enhanced green fluorescent protein (GFP) .Complex formation was carried out at room temperature for 30 min in nuclease-free water using a peptide/plasmid charge ratio of 30:1, which correspondents to a CPP concentration of 46 μM. Subsequently, the incubation with *Salpingoeca euryoecia* and the complex was carried out for 6 h at room temperature. Detection of gene expression was done 24 h after transfection using fluorescent microscopy. As viability studies showed that 46 μM CPP did not impact the choanoflagellates at all therefore this high concentration was choosen for the transfection experiments. However, the here presented viability and transfection results are older than the internalization results. For any reason, the addition of only 25 μM of **(1a)** caused already toxic effects.

Figure 31 shows the successful gene delivery of the plasmid pEGFP-N1 using CPP **(1a)** into the freshwater choanoflagellate species, *Salpingoeca euryoecia* whereas the transfection using CPP **(4)** failed (data not shown). To our best knowledge, these are the first results on a successful gene transfection of choanoflagellates. There are no published data of an effective transfection, neither using CPP nor other transfection methods. Merely for pathogenic flagellates, like *Trichomonas vaginalis* [132] and *Spironucleus vortens* [133], successful gene transfections were published, however using electroporation as transfection method.
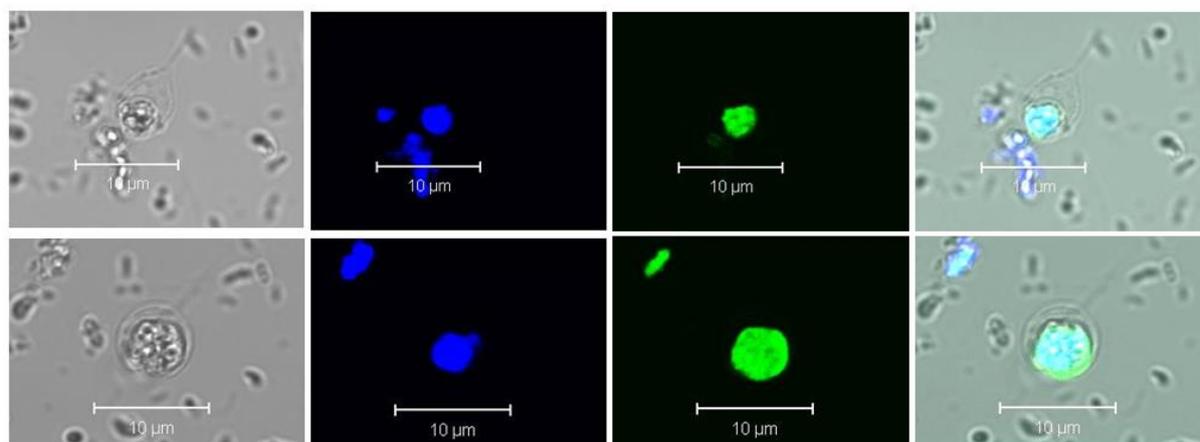
Fig. 31: Transfection of *Salpingoeca euryoecia* with CPP **(1a)** with pEGFP-N1 (30:1) after 24 h

This method and the other established transfection method failed so far in transfecting choanoflagellates. Mainly because, the harsh conditions during electroporation often lead to cell death. In 2011, Dai et al. where able to successfully transfect the unicellular ciliate *Paramecium sp.*, from the group of protozoans Alveolata, using the well described CPP octaarginine (R8). Since these ciliates have a size of about 100 µM, the handling and observation was much easier than working with choanoflagellates (size <10 µM) However, ciliates can also be transfected using other well-established methods, for instance electroporation, microinjection or particle bombardment [134].

Unfortunately, these results could not be reproduced again. Although, keeping all transfection conditions as similar as possible, no successful transfection was obtained again. Even when changing the conditions (temperature, incubation time, charge ratio, different plasmids, different salt concentrations and media or addition of $CaCl_2$ to enhance the uptake) no successful transfection was observed. Trying to transfect *Salpingoeca euryoecia* with CPP **(1a)** did not led to reliable and reproducible results, although preliminary studies showed controversial results. *Salpingoeca euryoecia* showed no impairment after the addition of the CPP/plasmid complex in one experiment, while when repeating the experiment under the same conditions, all cells died after CPP/plasmid complex addition. One more challenge was the high bacteria concentration in the media that probably impeded the CPP/plasmid complex uptake by the choanoflagellates. Since the complex has been also taken up by the bacteria, it is still unclear if enough amount of CPP/plasmid complex was provided for *Salpingoeca euryoecia*. The problem of reducing or eliminating the bacteria concentration was already elaborately discussed above.

Choanoflagellates exhibit a complex morphology, which is not comparable to mammalian cell lines. As the cell body of *Salpingoeca euryoecia* is additionally surrounded by a theca, the CPP/plasmid complex must first of all overcome this barrier to reach the membrane of the cell body. There it needs to interact with the membrane to be taken up. Finally the plasmid must be delivered to the nucleus where it must overcome the membrane of the nucleus to be successfully expressed [84]. During these processes the CPP/plasmid complex need to overcome a series of other obstacles, like potentially degradation by enzymes, strong interaction of the complex with the theca or cell membrane, or, if the complex is taken up via endocytosis, it might be kept in endosomes, where it might be degraded, too.

Concluding, choanoflagellates react extremely sensitive to slight changes in their environment. Currently the application of CPPs for transfection is rather unsuitable, whereat it

should be pointed out that so far all well-established transfection methods, like electroporation or lipofection, failed as well.

4.4 Peptide-mediated oligonucleotide delivery into ciliated retinal pigment epithelium cells

Cilia are hair-like microtubule-based organelles, which are found in most mammalian cells [99, 101]. Due to their central role in cell biology of most tissues, mutations in the genes encoding ciliary proteins affect various organ systems. The disorders caused by mutations in those genes that are encoding proteins localized to the cilium-centrosome complex are summarized as ciliopathies [101]. However, very little is known about the importance and functions of cilia, especially in the retinal pigment epithelium. This neuroepithelium is derived during organogenesis from the outer wall of the optic cup [99]. Terminally differentiated ciliated cells, like hTERT RPE-1 cells, cannot easily be transfected using current state-of-the art transfection techniques due to limited efficiency and significant toxicity inducing not only cell death but also loss of primary cilia. Therefore, the development of new strategies to transfect differentiated hTERT RPE-1 cells is mandatory.

Three different CPPs were used in the following studies: the two hCT-derived CPPs (**1a** and **1b**) and the sC18-derivative (**2d**). The aim was to gain insight into their internalization and oligonucleotide delivery capability into differentiated and non-differentiated hTERT RPE-1 cells. The peptide sequences and net charges of the CPPs are listed in table 15.

Table 15: Overview of CPPs used for hTERT RPE-1 cells experiments

Peptide	Sequence	MW [Da]	Net charge
N-E5L-hCT(18-32)-k7 (**1a**)	GLLEALAELLEKFHTFPQTAIGVGAP-NH$_2$ | KKRKAPKKKRKFA	4317,6	+8
Capr-hCT(18-32)-k7 (**1b**)	Capr-KFHTFPQTAIGVGAP-NH$_2$ | KKRKAPKKKRKFA	3318,1	+10
(sC18)$_2$* (**2d**)	GLRKRLRKFRNK-NH$_2$ | GLRKRLRKFRNK	3124,2	+15

Capr = capric acid ($C_{10}H_{20}O_2$)

4.4.1   Cell viability assay

The maximum concentration of the CPPs (**1a**), (**1b**) and (**2d**) which does not negatively impact the cells was determined by using the resazurin-based assay. The results after 24 h of CPP incubation are presented in figure 32. As a positive control, hTERT RPE-1 cells were

treated with 70% EtOH. The toxicity studies were carried out with non-differentiated hTERT RPE-1 cells since the examination of ciliogenesis requires fixation and antibody staining which is unsuitable for the resazurin-based assay.
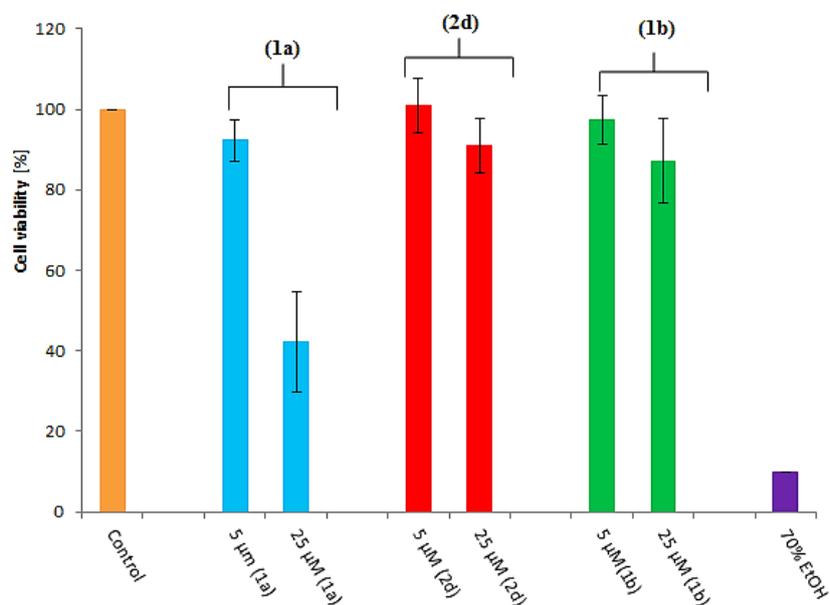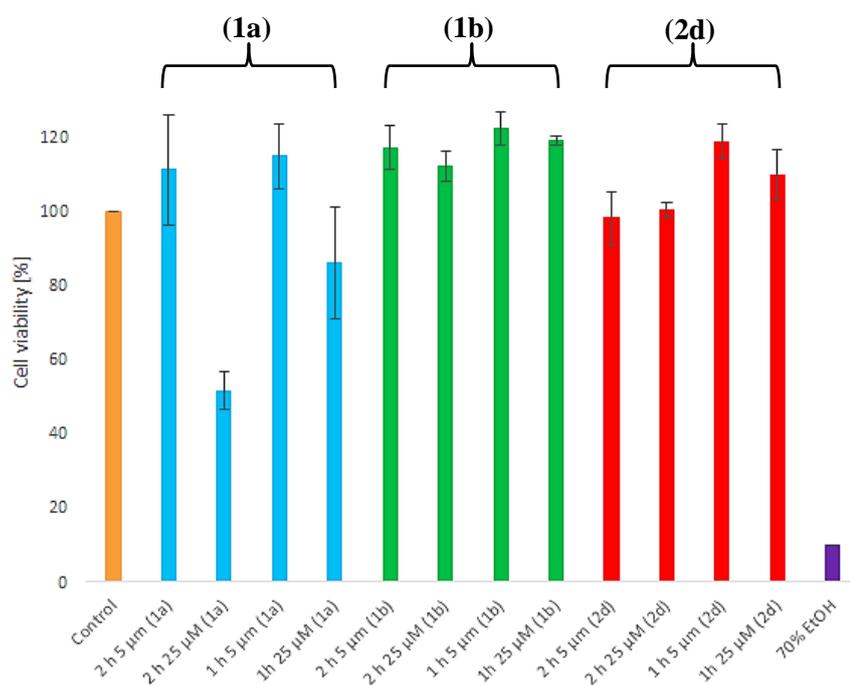

Fig. 32: Cell viability of retinal pigment epithelium (hTERT RPE-1) cells after treatment for 24 h with compounds (**1a**), (**1b**) and (**2d**). The experiment was performed at least two times in triplicate.

No toxicity was observed when incubating (**1b**) and (**2d**) at concentrations up to 25 μM for 24 h, whereas (**1a**) reduced cell viability at 25 μM to almost 60%. Therefore, when applying CPP (**1a**) for the experiments, a much lower concentration than 25 μM was used to avoid undesirable cytotoxic effects. To investigate if higher CPP concentrations of (**1a**) would be possible, hTERT RPE-1 cells were incubated for shorter times, e.g. for 1 h and 2 h, respectively (results are presented in figure 33).

Fig. 33: Cell viability of retinal pigment epithelium (hTERT RPE-1) cells after treatment for 1 h and 2 h with compounds (**1a**), (**1b**) and (**2d**). The experiment was performed at least two times in triplicate.

Even when incubating the hTERT RPE-1 cells for 2 h with 25 µM of CPP (**1a**) a significant reduction of almost 50% for the cell viability could be observed whereas 1 h incubation did not cause any significant cytotoxicity. Hence, when applying CPP (**1a**) with a concentration of 25 µM a shorter incubation time than 1 h was used.

4.4.2 Internalization studies in non-differentiated hTERT RPE-1 cells

In order to investigate whether the CPPs were able to internalize into hTERT RPE-1 cells at all, the intracellular distribution pattern of the fluorescently-labeled CPPs (**1a**), (**1b**) and (**2d**) were analyzed via fluorescence microscopy and quantified by using flow cytometry.

Fast and efficient uptake of the CPPs (**1a**), (**1b**) and (**2d**) was observed when incubating non-differentiated hTERT RPE-1 cells for 30 min at 37 °C with 5 µM and 25 µM peptide solutions, respectively. When applying CPP (**2d**) with a concentration of 25 µM at 37 °C, a complete and intense distribution of the peptide throughout the cytosol is visible (see right site of column A in figure 34). When taking a closer look at the cytosol of the cells, small punctual accumulations of (**2d**) are observable. This punctual distribution pattern indicates an

endocytotic internalization mode, which means that (2d) is still entrapped in endosomes after it has been taken up by an endocytotic mechanism [69]. Nevertheless, (2d) is highly distributed throughout the cytosol and even in the nucleus implying either a fast and efficient endosomal release within the incubation time without the addition of any lysomotropic reagents or (2d) also reached the cytosol by a simultaneously occurring direct penetration. In contrast, when adding only 5 µM of (2d) to the hTERT RPE-1 cells, a lower fluorescent signal is observable, especially in the cytosol and also in the nucleus (see left site of column A in figure 34). CPP (1a) showed a different distribution pattern compared to (2d). After the addition of 25 µM at 37 °C a likewise punctual distribution pattern is observable but there is no peptide accumulation in the nucleus or a complete distribution throughout the cytosol (see right site of column B in figure 34). Though, (1a) exhibits a fusogenic sequence (GLLEALAELLE), which facilitates an endosomal release most of the peptide seemed to be trapped in endosomes. In contrast to (2d), CPP (1a) might be longer or stronger entrapped in the endosomes, after the endocytotic uptake resulting in a lower intensity of the fluorescence signal in the cytosol. Applying only 5 µM of (1a) showed also a reduction of the peptide uptake (see left site of column B in figure 34). CPP (1b) is the hCT-derived peptide containing the fatty acid capric acid. The addition of 25 µM peptide at 37 °C displayed a complete and intense distribution throughout the cytosol and in the nuclei (see right site of column C in figure 34). Striking is the accumulation of (2d) and (1b) in the nucleus, as both CPPs not only had to overcome the lipid bilayer of the cell membrane but also the nuclear envelope. This capacity is necessary for all applications, for instance transfections, where the cargo needs to reach the nucleus. The distribution pattern for (2d) and (1b) are almost the same indicating more or less a similar uptake. Interestingly, the punctuated accumulation of (1b) is more distinct compared to (2d) and (1a). Even when reducing the peptide concentration, a high peptide distribution throughout the cytosol and even in the nucleus is visible (see left site of column C in figure 34). Since (1b) possesses a fatty acid instead of a fusogenic sequence like in (1a), the introduction of the hydrophobic moiety seemed to be more advantageous for the uptake, especially for the endosomal release. This might be, as already discussed earlier, due to a better membrane interaction between the CPP and the cell membrane [96].
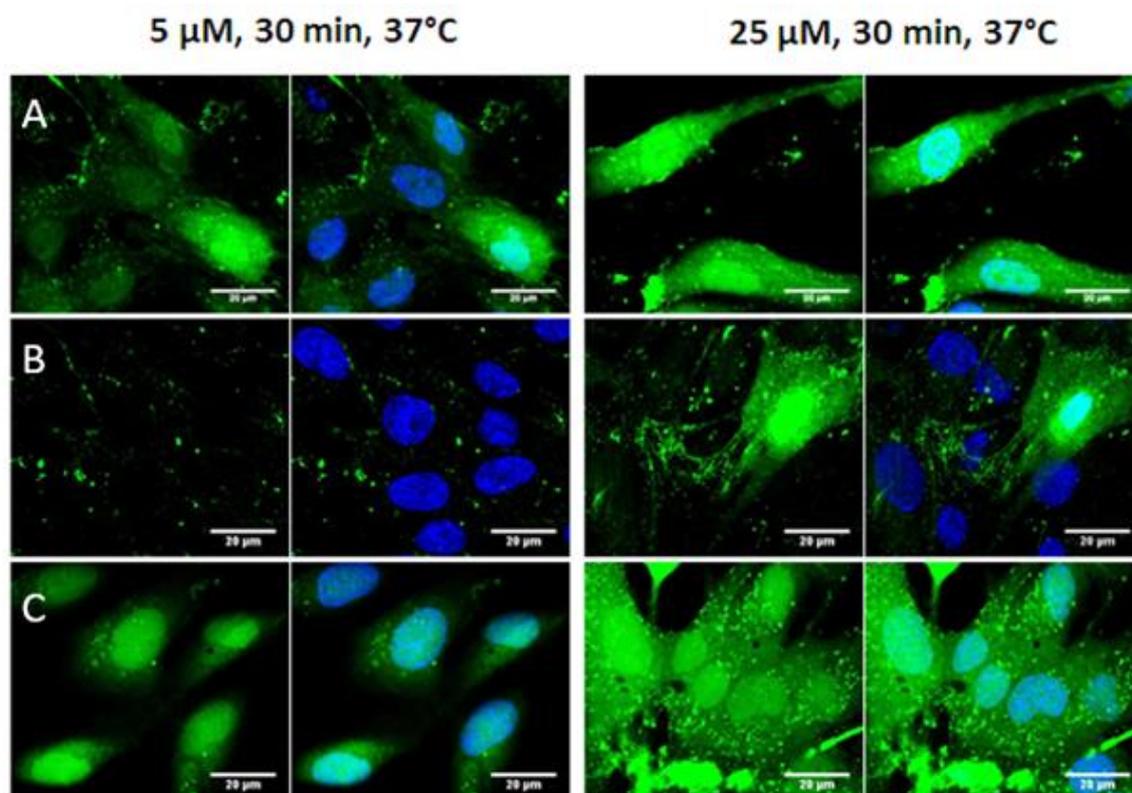
Fig. 34: Microscopy studies of hTERT RPE-1 cells at 37 °C. A = **CF-(2d)**, B = **CF-(1a)**; C = **CF-(1b)**. Cell nuclei were stained with Hoechst 33342 (blue). Scale bars, 20 µM.

Uptake quantification was done by flow cytometry. The flow cytometric studies are in good agreement with the fluorescence microscopy images, which were obtained after 30 min incubation at 37 °C. Among the three tested CPPs, **(2d)** showed the highest fluorescence intensity followed by **(1b)** which is presented in figure 35. The lowest fluorescence intensity showed **(1a)**. Even when adding 25 µM peptide to the cells, the fluorescence intensity of **(1a)** remained under the intensity of 5 µM **(2d)**. All tested CPPs showed a concentration-dependent uptake profile, where a higher CPP concentration led to an enhanced fluorescence intensity.
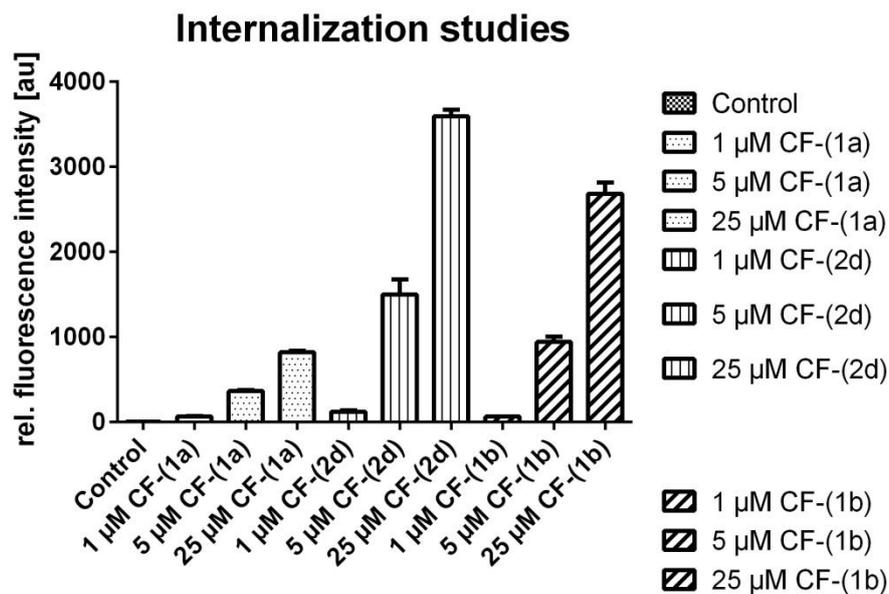
Fig. 35: Uptake quantification of 5(6)-carboxyfluorescein (CF)-labeled cell-penetrating peptides (**1a**), (**1b**) and (**2d**) after 30 min incubation. Untreated cells served as negative control. The experiment was performed at least two times in triplicate.

To evaluate the mechanism of cell entry, the internalization studies were additionally carried out at 4 °C. At this temperature, all energy-dependent uptake mechanisms are shut down [135]. The sC18-derivative (**2d**) is still able to translocate through the cell membrane of the hTERT RPE-1 cells when incubating the cells at 4 °C with 5 µM for 30 min. Interestingly, the peptide is only located in the nucleus and not in the cytosol (see figure 36, left column of picture A). Moreover, the peptide is mainly punctual accumulated within the nucleus, probably in the nucleolus. The assembly in the nucleus and in the nucleolus is even stronger when adding a 5-fold higher concentration of (**2d**) (see figure 36, right column of picture A). CPP (**1a**) showed a similar distribution pattern as presented in picture B of figure 36 after adding 25 µM peptide to the cells. A punctuated pattern is still visible indicating that though reducing the temperature and therefore inhibiting all energy-dependent mechanism, CPP (**1a**) is somehow still able to enter the cells by an endocytotic way. Maybe the temperature to shut down all energy-dependent uptake mechanism is for hTERT RPE-1 cells lower than 4 °C. The concentration reduction down to 5 µM showed likewise to the experiment at 37 °C a declined uptake of the peptide. Also, the incubation of CPP (**1b**) with 25 µM at 4 °C revealed a clearly punctuated distribution pattern in the cytosol as well as in the nucleus. Even here, a strong accumulation of the peptide in the nucleolus is still observable. Interestingly, when applying only 5 µM of (**1b**) no uptake at all is detectable. Maybe the punctuated distribution pattern for (**1a**) and (**1b**) does not show endosomes with the peptide entrapped. Another

possible explanation might be a peptide aggregation in the cytosol after a direct penetration. Since the rigidity of the cell membrane is enhanced at lower temperatures, a better binding of the CPP, in particular the guanidinium group of the arginine residues might occur. Applying a higher concentration, like 25 µM, leads to a continuously enhancement of the CPP at the cell surface causing a rearrangement of the lipid molecules. Hence, the chains of the arginine residues might translocate through the distal layer and form water pores whereby a few CPPs can diffuse into the cell interior. Finally, a pore closure completes the uptake procedure [136-138].

Since all energy-dependent uptake mechanism, like endocytosis, are shut down at 4 °C, all three CPPs must have entered the cells via an energy-independent mechanism, namely via direct penetration. Among the three tested CPPs, **(1b)** showed qualitative the highest uptake rate at 4 °C. The determination of the exact uptake mechanism of CPPs is though very difficult. The majority of uptake studies published so far used specific inhibitors to shut down pathways. However, in some cases, when shutting down one entry pathway another pathway might be suppressed as well [48]. This might also be the case for the here tested CPPs **(2d)**, **(1a)** and **(1b)**. When applying the CPPs at 37 °C, the uptake mode is mainly an endocytotic mechanism and only little amount of peptide crosses the cell membrane by direct penetration. However, the interpretation of the real uptake mechanism is hindered due to the fact that the CPPs are completely distributated through out the cytosol. Reducing the incubation temperature down to 4 °C, the rigidity of the cell membrane is enhanced and probably favors more a direct penetration.
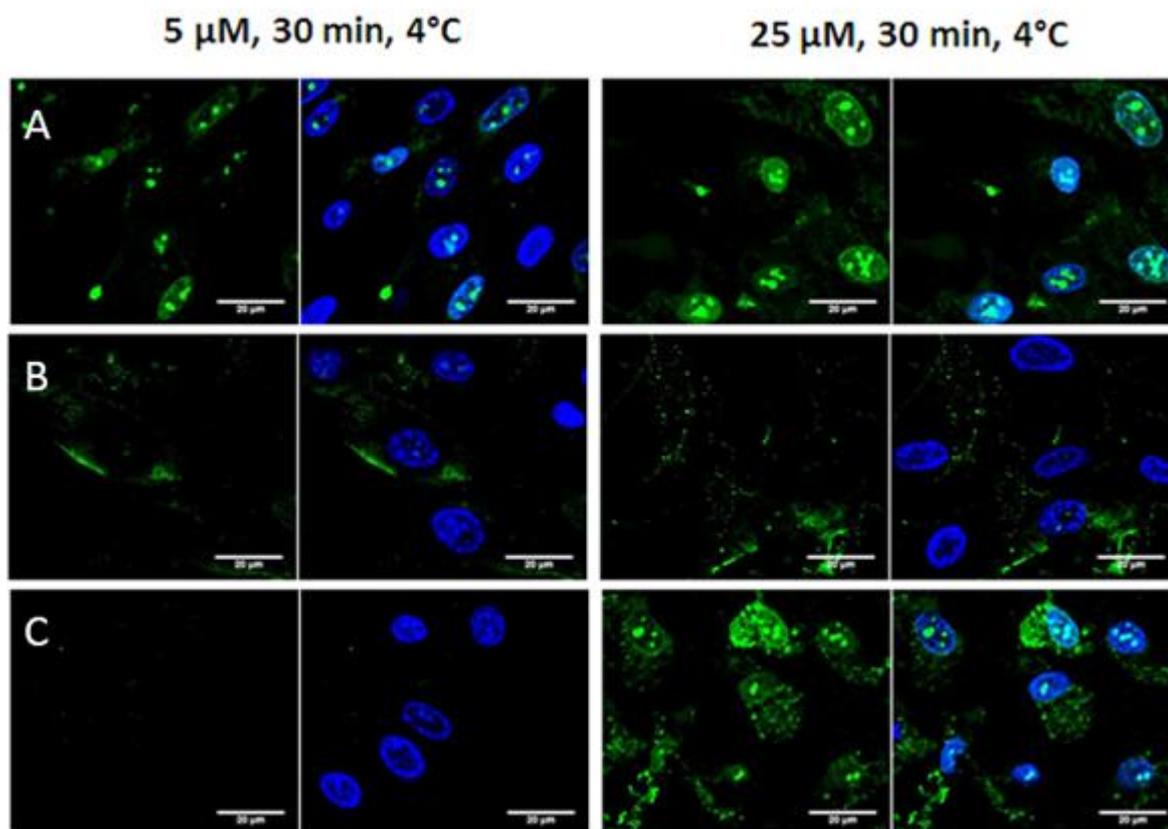
Fig. 36: Microscopy studies of hTERT RPE-1 cells at 4 °C. A = **CF-(2d)**, B = **CF-(1a)**; C = **CF-(1b)**. Cell nuclei were stained with Hoechst 33342 (blue). Scale bars, 20 µM

4.4.3 Labeled dsRNA delivery into hTERT RPE-1 cells

To check their nucleic acid delivery capability, fluorescently-labeled dsRNA was non-covalently fused to the CPPs. For these experiments, non-differentiated RPE-1 cells and untagged CPPs were used to gain insight into the delivery capability.
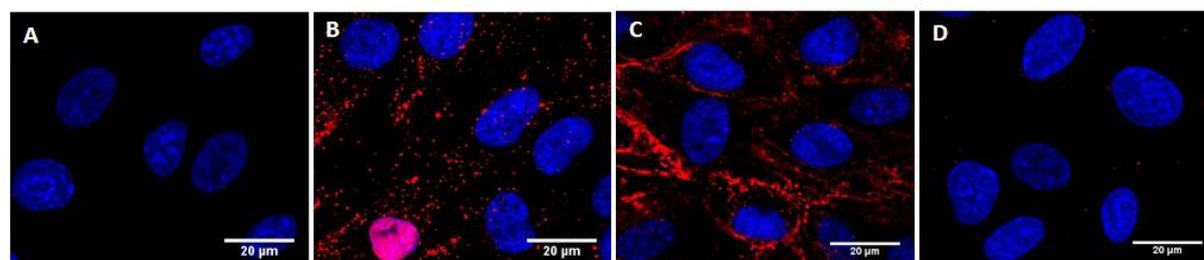
Fig. 37: Delivery of labeled dsRNA into hTERT RPE-1 cells at 37 °C using 10 µM CPP and 100 nM labeled dsRNA. A = Control, B = **(1a)**, C = **(1b)**; D = **(2d)**. Cell nuclei were stained with Hoechst 33342 (blue). Scale bars, 20 µM.

The delivery results are presented in figure 37. Picture A shows the addition of 100 nM naked fluorescently-labeled dsRNA. As expected, no fluorescence signal in the cells is visible due to the poor permeability of the nucleic acid which hinders the cell-entry. When adding the complex dsRNA/CPP **(1a)** to the non-differentiated hTERT RPE-1 cells, a similar distribution pattern as for the internalization study with fluorescently-labeled **(1a)** is visible. The punctate uptake pattern shown in picture B for CPP **(1a)** is again indicative for an endocytic entry route, which is proposed for the majority of CPP/siRNA complexes [139]. On the contrary, the CPP/siRNA complex in picture C for CPP **(1b)** seemed to be mostly aggregated in the cytosol. Surprisingly, when using **(2d)** no dsRNA delivery into hTERT RPE-1 cells was detected though internalization studies showed the best uptake results for **(2d)**. Moreover, good complexation results with pDNA was observed which is shown in figure 17. Maybe the interaction between the positive charges of the CPP and the negatively charged dsRNA led to a conformational change of the **(2d)** structure followed by the loss of its cell-penetrating property or the complexation is too strong causing an insufficient dissociation of the dsRNA from **(2d)**. Another possible explanation for the better delivery capability of **(1a)** and **(1b)** might be due to a more sufficient complexation between the dsRNA and the CPP. The positive effect on the complexation ability and moreover on the deliver capability by introducing a lipid moiety to the peptide structure has been already reported by other groups [96, 140]. The introduction of the capric acid increases the hydrophobicity of the CPP and hence, hydrophobic interactions with the dsRNA might be increased [141]. The same experiment was also done by Hoyer *et al.* using CPPs **(1a)** and **(1b)** to deliver fluorescently-labeled dsRNA into HEK-293 cells. They incubated the HEK-293 cells with the CPP/dsRNA complex for 1 h and examined them 24 h after transfection which is different to the here presented results (detection was carried out immediately after incubation). The results obtained by fluorescence microscopy are almost the same as for the hTERT RPE-1 cells. They also observed a punctuated distribution pattern within the cytosol. To elucidate the uptake mechanism, Hoyer *et al.* performed localization studies by adding a lysosomal marker. The gained results showed an overlapping between the red fluorescence signal of the labeled dsRNA and the green stained lysosomes indicating an endocytotic uptake with the entrapment of the complex in the vesicles not capable to reach the target [69]. It should be noted that no quantification by flow cytometry was performed because the amount of labeled dsRNA delivered into hTERT RPE-1 cells is irrelevant for the continuing experiments. This experiment is merely a proof of principle experiment to determine if it is in general possible to deliver oligonucleotides via CPPs into non-differentiated hTERT RPE-1 cells.

In conclusion, CPP **(1a)** and **(1b)** are able to deliver fluorescently-labeled dsRNA into non-differentiated hTERT RPE-1 cells but are still trapped in vesicles after the uptake. Therefore, the addition of endosomal releasing reagents might be necessary.

4.4.4   Transfection of non-differentiated hTERT RPE-1 cells

Since preliminary studies were promising, the CPPs were tested on their gene delivery capability as well. For this purpose, the eGFP-encoding plasmid pEGFP-N1 was again used to transfect non-differentiated hTERT RPE-1 cells. As the resazurin assay revealed a high sensitivity of the hTERT RPE-1 cells towards CPP **(1a),** it was necessary to keep the CPP concentration as low as possible, but still high enough to accomplish efficient transfection rates. Figure 38 represents the transfection results where the lower row shows the merged images of the bright field and the fluorescent images. Since CPP **(1b)** showed no successful transfection at all, the fluorescent microscopy images are not shown.
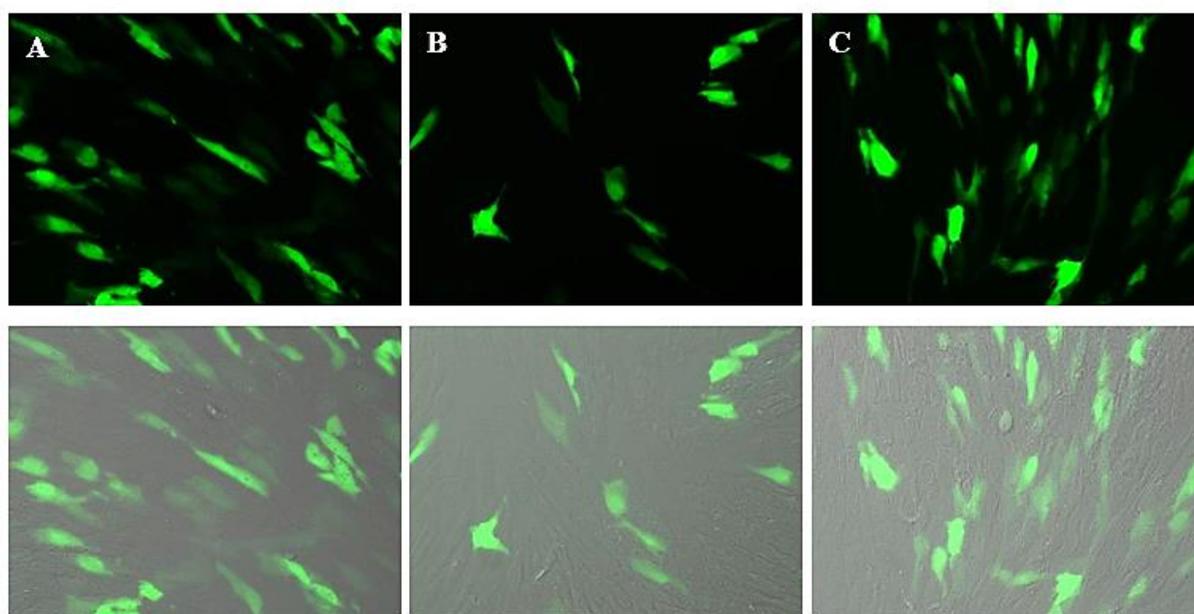
Figure 38: Microsopic images of transfected non-differentiated hTERT RPE-1 cells. A = Lipofectamine; B = 30:1; 0.5 µg eGFP and **(2d)** and 100 µM chloroquine; C = 10:1; 0.25 µg eGFP and **(1a)** und 100 µM chloroquine. The charge ratio 30:1 with 0.5 µg eGFP for **(2d)** corresponds to a CPP concentration of 9.0µM whereas the charge ratio 10:1 with 0.25 µg for **(1a)** corresponds to a CPP concentration of 3.2 µM. Objective 20x.

In picture **A,** the positive control is presented showing high transfection efficiency for the commercially available transfection reagent Lipofectamine®2000. When looking at picture **B,** a lower transfection rate was achieved when using CPP **(2d)**. Only a few cells were transfected. On the other hand, CPP **(1a)** seemed to be as effective as the positive control. In picture **C,** numerous cells are transfected. To quantify the real number of transfected hTERT RPE-1 cells, flow cytometry studies were done, once with the addition of 100 µM chloroquine and then without. The results are displayed in figure 39. The transfection rates of CPP **(1a)** and **(2d)** by flow cytometry were normalized to the transfection efficiency of Lipofectamine®2000 which was set 100%. As a negative control, untreated cells were used.
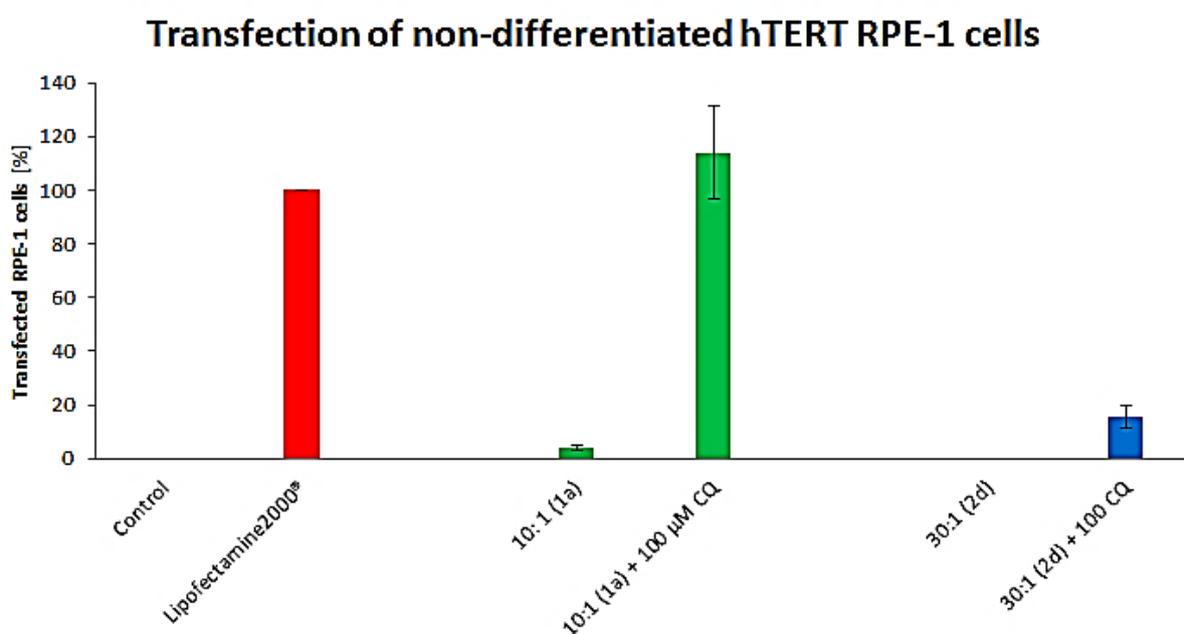
Fig.39: Quantification of the transfection rate in hTERT RPE-1 cells after 24 h. The experiment was performed at least two times in triplicate.

The flow cytometric studies are in good agreement with the fluorescence microscopy images showing poor transfection rates for CPP **(2d)** which are less than 20%. Remarkably, high transfection levels of CPP **(1a)** with the addition of 100 µM chloroquine to facilitate endosomal release were observed. Moreover, gene expression exceeded the level achieved with Lipofectamine®2000 making **(1a)** a nearly good transfection reagent as Lipofectamine®2000.

This result is even more impressive when taking into consideration that CPP **(1a)** was used with only 3.2 µM. Looking into literature and comparing the concentrations used for CPP-mediated transfection, the addition of 3.2 µM is in the lower range of applied concentrations. Li *et al.* for instance, synthesized a tetrapeptide consisting of four lysines which side chains were modified due to the introduction of guanidinocarbonylpyrrole groups. They transfected HeLa cells with 2 µg pF143-GFP plasmid and observed 24 h after incubation remarkably high transfection rates compared to PEI, which was used as a positive control. The transfection rates even exceeded those of the PEI. On the other hand, an extremely high CPP concentration of 150 µM was added to the cells making it indeed to the shortest CPP published so far, but unsuitable for *in vivo* applications since high amounts of the CPPs are needed to yield sufficient transfection results [142]. Kuchelmeister *et al.* synthesized peptidic tweezers with a lipophilic tail to transfect HEK293T cells with 2 µg pF143-GFP. The yielded transfection results for the peptides exceeded also here the results obtained by PEI or even by Lipfectamine2000® [143]. But the applied concentrations of the peptides were 240 µM which is very high compared to the concentration of CPP **(1a)**.

However, the high transfection rate could only be achieved after adding 100 µM CQ to the reaction solution. This implies again that after the endocytotic uptake a large amount of the complex is still trapped in vesicles. As already discussed earlier, the first step of the CPP/cargo internalization is the interaction of the positive charges provided by the CPP with the negatively charged proteoglycans and phospholipids on the cell surface [84]. Hence, the CPPs must have enough positive charges to interact with the cell membrane to initiate the cell entry and furthermore, to sufficient complex the nucleic acid. This would mean that CPP **(2d)** with a net charge of +15 should have the best requirements to interact with the cell membrane and to complex nucleic acid and therefore, the delivery of the cargo should be enhanced. This is not the case as the flow cytometry studies revealed. Perhaps, the interaction of the CPP with the plasmid is too strong resulting in hindered cargo dissociation and therefore, none or only a little amount of cargo reaches its target. Another possible explanation might be the loss of the cell-penetrating property due to conformational changes in the structure of **(2d)** when interacting with the cargo. Rennert *et al.* assumed that branching **(1a)** led to a separation of the nucleic acid moiety (k7 side chain) from the cell-penetrating moiety (hCT(18-32)) [144]. Hence, **(1a)** would be still able to cross the cell membrane even after cargo complexation. Besides the number of positive charges, the secondary structure of the CPP but also of the CPP/cargo is important, especially the α-helix [92]. Hoyer *et al.* proofed by CD spectroscopy that the introduction of the fusogenic peptide sequence N-E5L (GLLEALAELLE) to the

parent CPP hCT(18-32)-k7 supports a helical structure [66] which is important as the formation of amphiphilic helixes is mainly responsible for membrane interaction processes [145]. Although fluorescently-labeled **(1b)** showed good internalization rates, presumably due to its high positive net charge (+11) and the introduction of the fatty acid, which might have enhanced the membrane association, the CPP failed in transfecting hTERT RPE-1 cells. CPP **(1b)** was chosen as a possible gene delivery vector since published studies by our group revealed that an introduction of capric acid to the parent CPP hCT(18-32)-k7 led to an dramatically enhancement of the transfection efficiency *in vitro* as well as in *in vivo* studies even in challenging cell lines like primary cells [69]. Those results are in good agreement with various studies published so far. In 2001, Futaki *et al.* were able to show an improvement in gene delivery of octaarginine (R8) after stearylation [96]. The introduction of a hydrophobic fatty acid moiety showed several advantages, like a better interaction with the endosomal membrane and therefore, a better cytosolic uptake [141]. Moreover, a better stability of the CPP/ON complex is achieved probably due to shielding effects towards degradative enzymes [146]. Maybe **(1b)** is more suitable for siRNA applications since Hoyer *et al.* obtained good results in the knockdown of Y_1 receptor expression. CPP **(1b)** might be only able to deliver the cargo molecule into the cytosol but not to the nucleus, which is necessary for plasmid transfection. On the other hand, knockdown experiments require only the delivery of the siRNA to the cytosol where the RNAi machinery is present. The improved gene delivery capability of CPPs after the introduction of a fatty acid are not yet fully clarified, but it is assumed that due to lipidation the interaction between the CPP and the plasma membrane might be improved. A good and efficient interaction between the CPP/cargo complex and the cell membrane is crucial for a successful gene delivery since this process is the initial step of the cell entry as already discussed before (see transfection choanoflagellates).

4.4.5 *In Vitro* Transfection of ciliated hTERT RPE-1 cells

Next, the applicability of these delivery vectors was investigated in differentiated ciliated hTERT RPE-1 cells. Until now, no work on successfully transfected differentiated hTERT RPE-1 cells exist, as well as no method for transfecting differentiated hTERT RPE-1 cells. Cell culture studies regarding ciliary biology are hampered by the fact that differentiated ciliated cells cannot easily be transfected using current state-of-the art transfection techniques. This is due to limited efficiency and significant toxicity inducing not only cell death but also

loss of the primary cilia. Cilia development is a critical process. Cilia formation can only occur when the cells leave the cell cycle from mitosis and cell cycle into a quiescent and/or differentiated state called G0. This process can be induced by serum starvation [147].
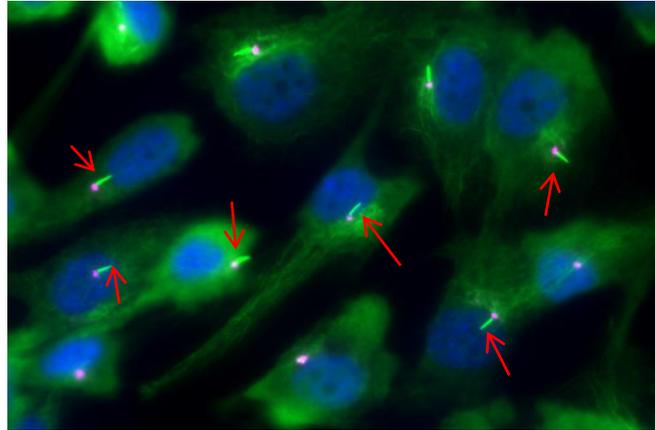
Fig. 40: Cilia staining of differentiated hTERT RPE-1 cells after fixation using antibodies. (Acetylated tubulin for cilia and Pericentrin for centrosomes). Nuclei were stained with DAPI. Objective 63x.

To examine whether cilia formation was successful, the hTERT RPE-1 cells needed to be fixed and then stained with antibodies (see methods). Figure 40 shows a successful ciliogenesis of hTERT RPE-1 cells, where usually 70% to 90% of the cells are ciliated. In order to determine if our CPPs were able to deliver the eGFP-encoding plasmid pEGFP-N1 into differentiated hTERT RPE-1 cells, the cells were serum starved for 24 h to induce ciliogenesis.
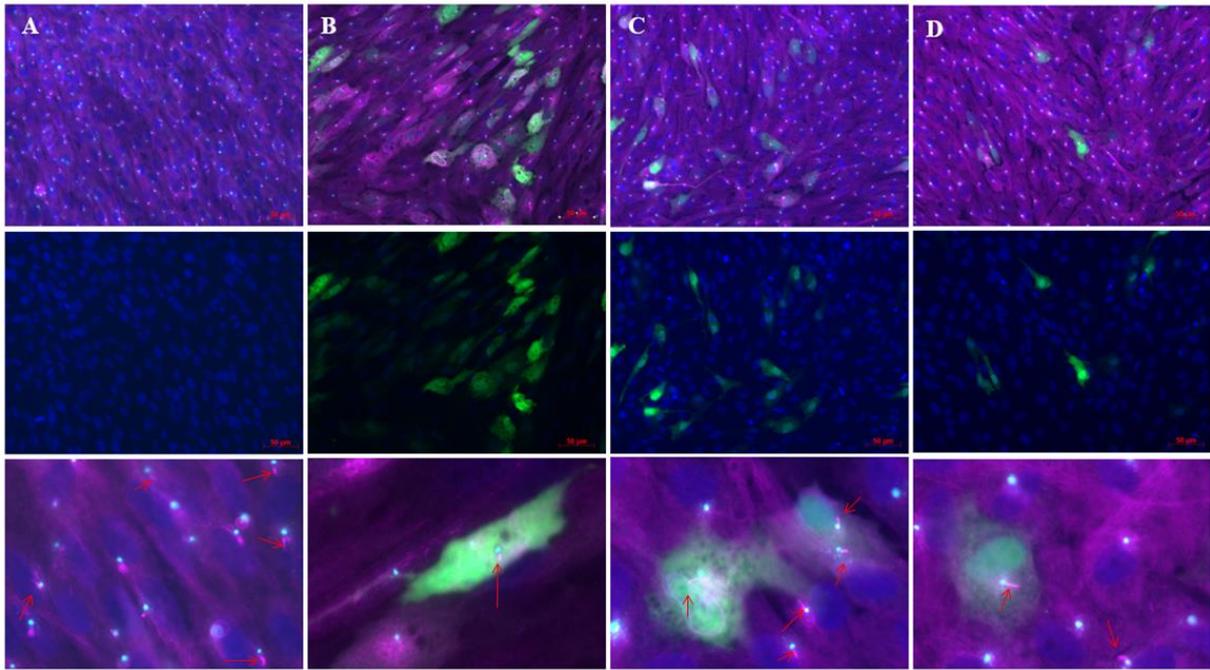
Fig. 41: Transfection of differentiated hTERT RPE-1 cells. A = Control, B = Lipofectamine; C = 10:1; 0.25 µg eGFP und (1a) and 100 µM Chloroquine, D = 30:1; 0.5 µg eGFP und (2d) und 100 µM Chloroquine. Scale bar = 50 µm. Nuclei were stained with DAPI. Upper and middle row were taken with a 20x objective whereas the lower row with a 63x objective.

The images (figure 41) in the upper and middle row where taken with a 20x objective to get an overview of the differentiated cells, whereas the lowest row shows a more detailed shot of the cells which were taken with a 63x objective. Column **A** shows the control (untreated cells) of the cilia formation. In image **A1** of figure 42**,** the cilia are nicely visible and marked with a red arrow. Almost all cells of the control exhibit a cilium indicating not only a complete and successful ciliogenesis but moreover healthy cells. Antibody staining was performed after fixation. Primary antibody anti-Pericentrin stains the centrosomes whereas acetylated tubulin antibody marks cilia. The centrosomes are then stained in cyan blue (Cy5) and the cilia in magenta (Cy3). Column **B** illustrates the transfection results of Lipofectamine®2000 showing in the middle an overlay between the green and blue fluorescence channels. Numerous cells are transfected. The cells which are not expressing GFP still exhibit a cilium as well as the cells which are positively transfected. The same results, but with less cells expressing GFP, were also obtained when transfecting the differentiated cells with the **(1a)**/DNA complex which are shown in column **C**. Nevertheless, taking a closer look at the images in the middle of **B** and **C** in figure 41, it seems as if the cells treated with Lipofectamine®2000 look unhealthy compared to the cells treated with **(1a)**. All cells in image B that are expressing GFP reveal small holes in the cytosol which are not visible in the control (image **A**) and for

(1a). Also the green fluorescence signal is brighter in **B** than in **C** possibly due to a GFP overexpression. Interestingly, the transfection efficiency of **(1a)** as well as of Lipofectamine®2000 is much lower compared to the transfection results performed on non-differentiated cells. Maybe the cell membrane of the hTERT RPE-1 cells changes upon differentiation from being more "leaky" towards "non-leaky". Another possible explanation for the different transfection efficiency might be that all energy-dependent uptake mechanisms were down-regulated to a minimum saving energy to remain in the stationary phase. The uptake efficiency of CPPs is not only dependent on the cell-type but also on the differentiation state [148]. Foerg *et al.* observed a down-regulation of CPP uptake in confluent and differentiated cells presumably due to chances of expression levels of several key factors in the Rho-family which are responsible for the endocytosis regulation [149]. Transfection using CPP **(2d)** showed only poor results but did not impact the cilia formation (see images **D**). Increasing the plasmid quantity from 0.25 µg up to 1 µg did not cause any significant improvement in the transfection rate (data not shown). Hence, for practical and toxicity reasons, the plasmid amount for **(1a)** was set at 0.25 µg and for **(2d)** at 0.5 µg. However, for both CPPs the addition of CQ was necessary to obtain positive transfection results.
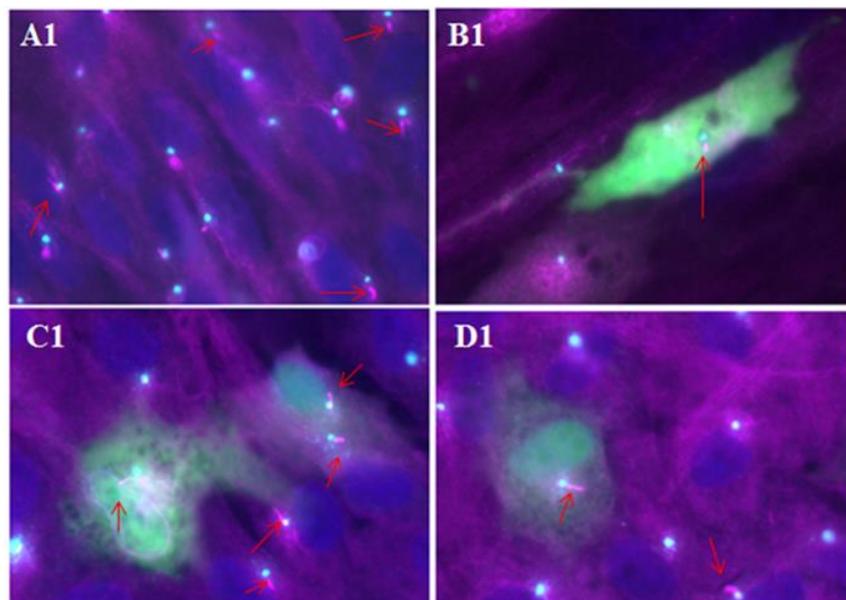
Figure 42: Closer look at the lower row of figure 41. Nuclei DAPI, magenta centrosomes, Scale bar ?

Hansson *et al.* on the other hand, transfected modified mRNA into RPE-like cells which were derived from human embryonic stem cells. These human embryonic stem cells can

differentiate *in vitro* into functional RPE-like cells and were transfected with modified and unmodified mRNA using the commercially available transfection reagent Stemfect. The delivery of modified mRNA enabled functional protein expression and negligible immune activation [150].

However, since the focus of Hansson´s *et al.* work was not the investigation of ciliogenesis or the capability of transfecting differentiated cells, it is rather difficult to compare the results with the here presented results. Therefore, to our best knowledge these are the first studies on a successful transfection of ciliated hTERT RPE-1 cells using cell-penetrating peptides.

4.4.6 *In Vitro* Transfection of ciliary plasmid 5HT6.GFP pcDNA6 in ciliated hTERT RPE-1

Here, a functionalized DNA (5HT6.GFP pcDNA6) delivery via CPP was performed successfully on differentiated hTERT RPE-1 cells. 5HT6 is a serotonin receptor 6, also known as 5-hydroxytryptamine receptor 6. It is a G protein–coupled receptor (GPCR) that localizes to the cilia. [151]. Figure 43 shows untreated differentiated cells. To determine if the cells exhibit cilia, an antibody staining was performed after fixation. The protein pericentrin is localized to the centrosomes whereas acetylated tubulin antibody marks cilia. The centrosomes are then stained in magenta (see image **B**) and the cilia in cyan blue (see image **C**). The antibody staining reveals an efficient differentiation of the hTERT RPE-1 cells which is nicely shown in the overlay of all channels (picture **E**). Channel **A** represents the GFP channel and as expected no signal for the control is visible.
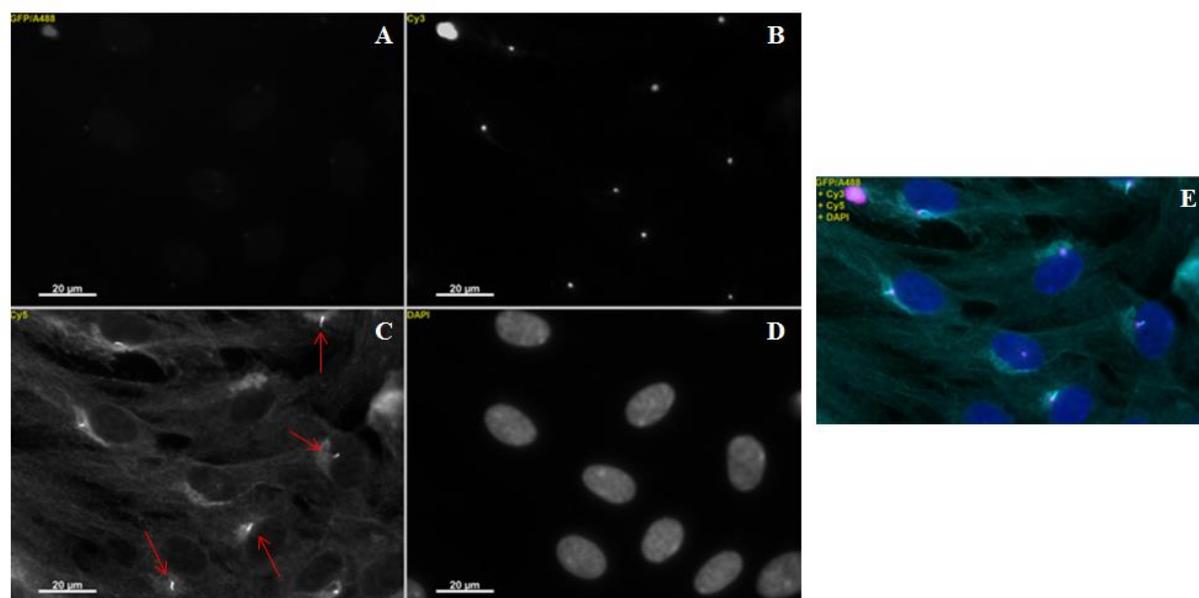
Fig. 43: Microscopic images of Control. A = GFP channel. B = Pericentrin (centrosomes). C = Acetylated tubulin (cilia). D = DAPI (nucleus). E = Overlay of all channels. 63x objective. Scale bars = 20 μM

When applying CPP **(2d)** with 0.5 μg plasmid to the differentiated hTERT RPE-1 cells, almost no cilia were found within the transfected cells. Moreover, many green vesicles in the cytosol were visible and cells looked sick (see figure 46 in the attachment). Increasing the plasmid amount at 1 μg (see figure 47 in the attachment) affected the cells even more in their viability. Interestingly, when applying the same amount of pEGFP-N1 to the differentiated hTERT RPE-1 cells, no derogation was observable. This might be due to the fact that the ciliary plasmid exhibit 6100 bp and pEGFP-N1 only 4700 bp. Hence, the concentration of **(2d)** is higher to achieve the complexation with a charge ratio of 30:1. Probably the higher concentration of **(2d)** caused the toxicity and not the plasmid amount. Again, many green vesicles could be seen in the transfected cells, but it was difficult to find green cilia. Moreover, many green floating cells were visible in the solution. Both results indicate a negative impact on the health condition of positively transfected ciliated hTERT RPE-1 cells when increasing the plasmid amount. However, the addition of the complex did not impact cilia formation of the not transfected cells as the antibody staining reveals (see C in figure 46 and C in figure 47 in the attachment).
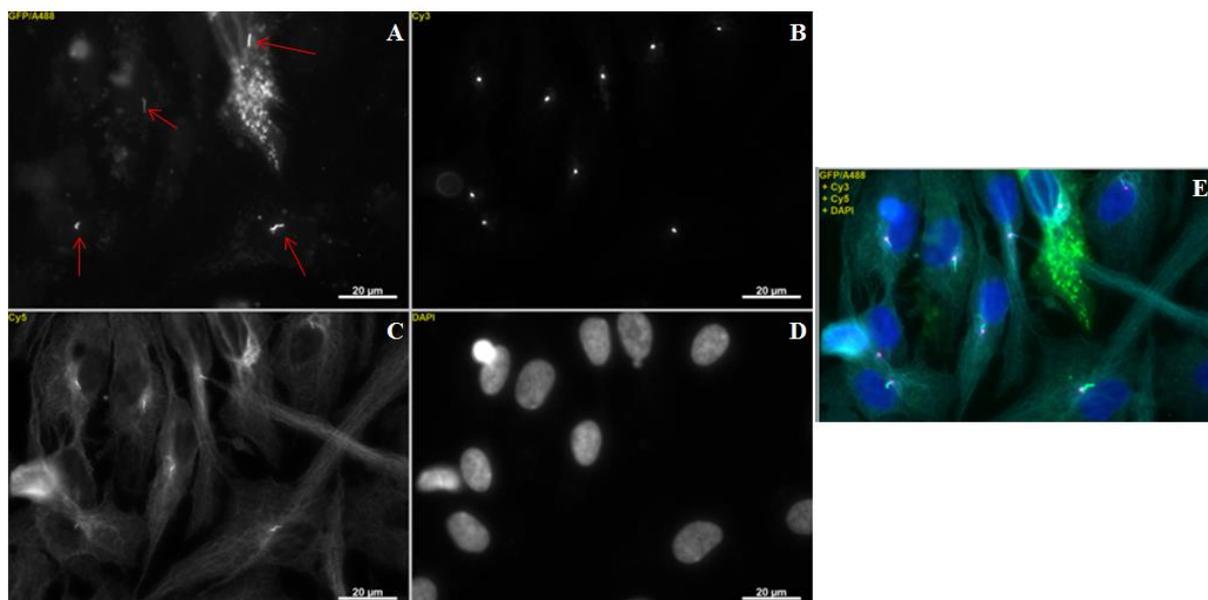
Fig. 44: Microscopic images of 10:1 (charge ratio) **(1a)** and 0.25 µg Plasmid. A = GFP channel. B = Pericentrin (centrosomes). C = Acetylated tubulin (cilia). D = DAPI (nucleus). E = Overlay of all channels. 63x objective. Scale bars = 20 µM

On the other hand, figure 44 shows the successful transfection of differentiated hTERT RPE-1 cells after the addition of only 1.6 µM CPP **(1a)** at a charge ratio of 10:1 using 0.25 µg plasmid. Taking a closer look at picture **A**, numerous positively transfected cells are visible and GFP is localized in the cilia. In addition, for a few cells the GFP signal is also apparent in the cytosol. In order to express the transfected plasmid, the cells must be healthy and moreover, the addition of the complex did not impact the cilia formation at all. In addition, it should be taken into consideration that the quality of the GFP signal is brighter than the antibody staining of cilia. Compared to the antibody staining, the transfection procedure is less laborious since only two steps are necessary, namely complexation and addition to the cells. In addition, the synthesis of the CPPs is much cheaper than buying expensive antibodies. It should be highlighted that CPP **(1a)** delivered the ciliary plasmid to the nucleus successfully and efficiently and hence, needed to overcome all before mentioned obstacles. The CPP was able to interact in an adequate manner with the cell membrane, was taken up by most likely an endocytotic uptake route and was then able to escape from the endosomes by adding CQ. Finally, the complex translocated through the nuclear envelope where the plasmid was able to disassociate from the CPP **(1a)**. The GFP signal in the cytosol might result from an overexpression of the plasmid by the cell due to an excessively amount of GFP. A correlation between the overexpression and the localization of GFP was observable. The higher the expression of GFP the less healthy cells where observable and furthermore, less

GFP could be detected in the cilium. When comparing the transfection results of figure 44 with the experiment performed with 0.5 µg ciliary plasmid (see figure 45 in the attachment) less cells with GFP localized to the cilium were detectable but the fluorescence signal in the cytosol increased. These results were also obtained with CPP (**2d**). Moreover, the GFP expressing cells looked sick, whereas all cells in figure 45 exhibited no impairment. One possible explanation for the enhanced GFP localization in the cytosol might be due to unpredictable defective processes during translation followed by an in sufficient release from the endoplasmatic reticulum. Another reason might be that the plasmid amount was too high for an adequate complexation and therefore, degradation occurred. Nevertheless, the proposed results are vital for ongoing investigations regarding ciliopathy making this delivery system to a valuable tool for future experiments since no comparable data are published so far.

4.4.7 *In Vitro* TALEn transfection of hFLCN in differentiated hTERT RPE-1 cells

Encouraged by these promising results, the delivery system was taken a step further by testing the applicability of the CPPs in generating stably integrated differentiated hTERT RPE-1 cells containing a transgenic human FLCN gene fused to a N-terminal GFP tag.

The von Hippel-Lindau (VHL) syndrome is an inherited disorder caused by mutations in the tumour suppressor gene *VHL,* characterized by the development of multiple tumors in different tissues, typically hemangioblastoma, pheochromocytoma and renal cell carcinoma. Patients that suffer from von Hippel-Lindau syndrome often develop cysts in the kidneys, pancreas, and genital tract. In 2006, Schermer *et al*. could show that the von Hippel-Lindau protein (pVHL) is localized to cilia which are specialized organelles controlling ciliogenesis in kidney cells [152]. Mutations on chromosome 17p11.2 which encodes another tumor suppressor protein folliculin (FLCN) leads to the Birt-Hogg-Dubé syndrome (BHD). People with this seldom autosomal dominant disorder develop cutaneous lesions, renal tumors and pulmonary cysts, causing spontaneous pneumothorax [153]. Since the disease characteristics of BHD are similar to those of the VHL syndrome, it is suggested that FLCN could also be located on cilia. Luijten *et al*. published in 2013 data indicating that FLCN is localized to motile and non-motile cilia, centrosomes and the mitotic spindle using antibody staining. However, the available antibodies for FLCN used in the publication are unspecific with immunofluorescence [154]. Therefore, a more specific approach to show localization of FLCN on cilia is necessary

For this purpose, a construct was generated, where FLCN is fused to GFP in a repair template vector containing homology arms for the human AAVS locus, to target a single copy integration in this locus after cleavage of genomic DNA with TALEn (Transcription activator-like effector nuclease) nucleases. These designable restriction enzymes can be inserted into plasmids and are able to cut any DNA at specific locations of the DNA sequence. Besides the sequence-specific DNA binding domain, TALEn possesses a non-specific DNA cleavage domain [155]. This technology consists of two plasmids encoding nucleases targeting the AAVS locus, and are co-transfected with one donor plasmid containing the transgene of interest flanked by homology arms for the integration locus with an overall DNA size of more than 25.000 bp.

After the addition of the CPP/DNA complex to the cells, no integration into the AAVS locus was found nor an unspecific GFP signal in the cells could be detected (result are presented in the attachment). Probably the size of the TALEn plasmids was too large to obtain a sufficient complexation with the CPP or the complex size exceeded the uptake capability since size limitation of the endosomes and cellular uptake of complexes was reported by Connor *et al.* [90]. This highly specific experiment renders many potential obstacles which have been already discussed earlier (for instance: endosomal entrapment, not reaching the nucleus, insufficient cutting of the DNA sequence by the nuclease plasmid). However, the experiment procedure needs to be improved in order to elucidate if FLCN is localized to cilia.

5. Conclusion

The focus of this thesis, was the development of appropriate *in vitro* systems as well as the investigation of novel peptide-based vectors for the nucleic acid delivery. MCF-7, HEK-293 and hTERT RPE-1 cells where chosen as *in vitro* systems to investigate the nucleic acid delivery ability of the CPPs. In addition, choanoflagellates were chosen as an *in vivo* system.

In conclusion, dimerization of the CPP sC18 as a peptide modification, led to no significant enhancement in the ability to transfect HEK-293 cells. Since unpublished data from our working group revealed an enhanced tumor cell line specifity for the derivatives, they would rather be suitable for anti cancer drug delivery or imaging. On the other hand, cyclization of sC18 led to an improved delivery of the plasmid pEGFP-N1 into MCF-7 cells. Among the three cyclic peptides, the large cycle showed the best transfection ability whereas the linear version failed. Further improvements concerning the transfection efficiency might be necessary. Moreover, performing *in vivo* experiment would be interesting as the cyclic peptides show a higher proteolytic stability compared to the linear CPP.

The development of methods to genetically manipulate choanoflagellates is mandatory as they are considered to be the closest living relatives of animals. They have the potential to serve as model organism to illuminate fundamental and ancient aspects of animal origins. For this purpose, new *in vivo* applications were generated to investigate the impact of the CPP N-E5L-hCT(18-32)-k7 and the well-described TAT(48-60) on the viability, peptide uptake and the transfection ability when in contact with three different choanoflagellate species. The obtained results where difficult to interpret and moreover not reproducible since choanoflagellates reacted extremely sensitive to slight changes in their environment. However, to our best knowledge, these were the first results on a successful gene transfection of choanoflagellates. For future experiments, it would be beneficial to eliminate the bacteria contamination in the cultures since this was one of the major problems in this thesis. For this purpose, alternative food sources might be helpful to avoid the need of bacteria as a food source. In addition, concerning uptake studies the exact composition of the theca as well as the cell membrane would simplify the experiments. Besides, the elucidation of uptake mechanisms is mandatory.

Cell culture studies regarding ciliary biology are limited due to low efficiency and significant toxicity inducing not only cell death but also loss of primary cilia. Therefore, different CPPs, which were developed in our group, were examined upon their toxicity, complex formation activity, internalization and nucleic acid delivery ability in retinal epithelium cells (hTERT

RPE-1). Fast and efficient uptake where observed for the fluorescently-labeled CPPs into non-differentiated hTERT RPE-1 cells with negligible toxicity. Furthermore, the transfection efficiency of a GFP-encoding plasmid using CPP N-E5L-hCT(18-32)-k7 exceeded the transfection rates of the widely-used reagent Lipofectamine®2000. Moreover, the delivery of a functional plasmid into differentiated hTERT RPE-1 cells was successful. For future experiments, the endosomal release of CPP (**1a**) must be improved, especially when it comes to *in vivo* studies as the addition of chloroquine is not possible. Perhaps another fusogenic sequence than the N-E5L sequence might trigger the escape out of the endosomes in a more efficient manner. Since the transfection of differentiated hTERT RPE-1 cells worked, it would be interesting to use another cell line exhibiting cilia, for instance podocytes.

6. Literature

1. Friedman.T and R. Roblin, *Gene Therapy for Human Genetic Disease.* Science, 1972. **175**(4025): p. 949-&.
2. Cepko, C.L., B.E. Roberts, and R.C. Mulligan, *Construction and Applications of a Highly Transmissible Murine Retrovirus Shuttle Vector.* Cell, 1984. **37**(3): p. 1053-1062.
3. Blaese, R.M., et al., *T-Lymphocyte-Directed Gene-Therapy for Ada(-) Scid - Initial Trial Results after 4 Years.* Science, 1995. **270**(5235): p. 475-480.
4. Somia, N. and I.M. Verma, *Gene therapy: Trials and tribulations.* Nature Reviews Genetics, 2000. **1**(2): p. 91-99.
5. Shea, J., *Gene Therapy Restores Partial Sight.* Penn Medicine, 2009/2010: p. 21-22.
6. Brown, T.R., *I am the Berlin patient: a personal reflection.* AIDS Res Hum Retroviruses, 2015. **31**(1): p. 2-3.
7. Lundberg, P. and U. Langel, *A brief introduction to cell-penetrating peptides.* Journal of Molecular Recognition, 2003. **16**(5): p. 227-233.
8. Mastrobattista, E., et al., *Artificial viruses: a nanotechnological approach to gene delivery.* Nat Rev Drug Discov, 2006. **5**(2): p. 115-21.
9. Parr-Brownlie, L.C., et al., *Lentiviral vectors as tools to understand central nervous system biology in mammalian model organisms.* Front Mol Neurosci, 2015. **8**: p. 14.
10. Boulaiz, H., et al., *Non-viral and viral vectors for gene therapy.* Cell Mol Biol (Noisy-le-grand), 2005. **51**(1): p. 3-22.
11. Glover, D.J., *Artificial viruses: exploiting viral trafficking for therapeutics.* Infect Disord Drug Targets, 2012. **12**(1): p. 68-80.
12. Mingozzi, F. and K.A. High, *Therapeutic in vivo gene transfer for genetic disease using AAV: progress and challenges.* Nat Rev Genet, 2011. **12**(5): p. 341-55.
13. Zaiss, A.K. and D.A. Muruve, *Immune responses to adeno-associated virus vectors.* Curr Gene Ther, 2005. **5**(3): p. 323-31.
14. Azzam, T. and A.J. Domb, *Current developments in gene transfection agents.* Curr Drug Deliv, 2004. **1**(2): p. 165-93.
15. Smith, A.E., *Viral vectors in gene therapy.* Annu Rev Microbiol, 1995. **49**: p. 807-38.
16. Ramamoorth, M. and A. Narvekar, *Non viral vectors in gene therapy- an overview.* J Clin Diagn Res, 2015. **9**(1): p. GE01-6.
17. Lavertu, M., et al., *High efficiency gene transfer using chitosan/DNA nanoparticles with specific combinations of molecular weight and degree of deacetylation.* Biomaterials, 2006. **27**(27): p. 4815-4824.
18. De Laporte, L., J.C. Rea, and L.D. Shea, *Design of modular non-viral gene therapy vectors.* Biomaterials, 2006. **27**(7): p. 947-954.
19. Glover, D.J., H.J. Lipps, and D.A. Jans, *Towards safe, non-viral therapeutic gene expression in humans.* Nat Rev Genet, 2005. **6**(4): p. 299-310.
20. Jin, L., et al., *Current progress in gene delivery technology based on chemical methods and nano-carriers.* Theranostics, 2014. **4**(3): p. 240-55.
21. Wang, W., et al., *Non-viral gene delivery methods.* Curr Pharm Biotechnol, 2013. **14**(1): p. 46-60.
22. Mescalchin, A., et al., *Cellular uptake and intracellular release are major obstacles to the therapeutic application of siRNA: novel options by phosphorothioate-stimulated delivery.* Expert Opinion on Biological Therapy, 2007. **7**(10): p. 1531-1538.
23. Robinson, H.L. and T.M. Pertmer, *Nucleic acid immunizations.* Curr Protoc Immunol, 2001. **Chapter 2**: p. Unit 2 14.
24. Davis, H.L., R.G. Whalen, and B.A. Demeneix, *Direct gene transfer into skeletal muscle in vivo: factors affecting efficiency of transfer and stability of expression.* Hum Gene Ther, 1993. **4**(2): p. 151-9.

25.   Wendell, D.M., et al., *The effect of jet parameters on jet injection.* Conf Proc IEEE Eng Med Biol Soc, 2006. **1**: p. 5005-8.

26.   Herweijer, H. and J.A. Wolff, *Gene therapy progress and prospects: hydrodynamic gene delivery.* Gene Ther, 2007. **14**(2): p. 99-107.

27.   Li, S.D. and L. Huang, *Gene therapy progress and prospects: non-viral gene therapy by systemic delivery.* Gene Ther, 2006. **13**(18): p. 1313-1319.

28.   Klein, T.M., et al., *High-Velocity Microprojectiles for Delivering Nucleic-Acids into Living Cells.* Nature, 1987. **327**(6117): p. 70-73.

29.   Newman, C.M.H. and T. Bettinger, *Gene therapy progress and prospects: Ultrasound for gene transfer.* Gene Ther, 2007. **14**(6): p. 465-475.

30.   Al-Dosari, M.S. and X. Gao, *Nonviral gene delivery: principle, limitations, and recent progress.* AAPS J, 2009. **11**(4): p. 671-81.

31.   Felgner, P.L., et al., *Nomenclature for synthetic gene delivery systems.* Hum Gene Ther, 1997. **8**(5): p. 511-2.

32.   Liu, Y., et al., *Cationic liposome-mediated intravenous gene delivery.* Journal of Biological Chemistry, 1995. **270**(42): p. 24864-70.

33.   Stewart, M.J., et al., *Gene transfer in vivo with DNA-liposome complexes: safety and acute toxicity in mice.* Hum Gene Ther, 1992. **3**(3): p. 267-75.

34.   Escriou, V., et al., *Cationic lipid-mediated gene transfer: analysis of cellular uptake and nuclear import of plasmid DNA.* Cell Biol Toxicol, 1998. **14**(2): p. 95-104.

35.   Escriou, V., et al., *Cationic lipid-mediated gene transfer: effect of serum on cellular uptake and intracellular fate of lipopolyamine/DNA complexes.* Biochim Biophys Acta, 1998. **1368**(2): p. 276-88.

36.   Li, W.B., et al., *Functional study of dextran-graft-poly((2-dimethyl amino)ethyl methacrylate) gene delivery vector for tumor therapy.* J Biomater Appl, 2013. **28**(1): p. 125-35.

37.   Wang, X.W., et al., *Enhanced performance of biodegradable poly(butylene succinate)/graphene oxide nanocomposites via in situ polymerization.* Langmuir, 2012. **28**(18): p. 7091-5.

38.   Chandy, T. and C.P. Sharma, *Chitosan--as a biomaterial.* Biomater Artif Cells Artif Organs, 1990. **18**(1): p. 1-24.

39.   Mourya, V.K. and N.N. Inamdar, *Chitosan-modifications and applications: Opportunities galore.* Reactive & Functional Polymers, 2008. **68**(6): p. 1013-1051.

40.   He, X.K., et al., *Low Molecular Weight Hydroxyethyl Chitosan-Prednisolone Conjugate for Renal Targeting Therapy: Synthesis, Characterization and In Vivo Studies.* Theranostics, 2012. **2**(11): p. 1054-1063.

41.   Prabaharan, M. and J.F. Mano, *Chitosan-based particles as controlled drug delivery systems.* Drug Delivery, 2005. **12**(1): p. 41-57.

42.   De Laporte, L., J. Cruz Rea, and L.D. Shea, *Design of modular non-viral gene therapy vectors.* Biomaterials, 2006. **27**(7): p. 947-54.

43.   Merkel, O.M., et al., *In vitro and in vivo complement activation and related anaphylactic effects associated with polyethylenimine and polyethylenimine-graft-poly(ethylene glycol) block copolymers.* Biomaterials, 2011. **32**(21): p. 4936-42.

44.   Kingston, R.E., C.A. Chen, and H. Okayama, *Calcium phosphate transfection.* Curr Protoc Immunol, 2001. **Chapter 10**: p. Unit 10 13.

45.   Sokolova, V.V., et al., *Effective transfection of cells with multi-shell calcium phosphate-DNA nanoparticles.* Biomaterials, 2006. **27**(16): p. 3147-53.

46.   Dunlap, D.D., et al., *Nanoscopic structure of DNA condensed for gene delivery.* Nucleic Acids Research, 1997. **25**(15): p. 3095-3101.

47.   Nimesh, S., et al., *Influence of acyl chain length on transfection mediated. by acylated PEI nanoparticles.* Int J Pharm, 2007. **337**(1-2): p. 265-274.

48.   Huang, Y.W., et al., *Delivery of nucleic acids and nanomaterials by cell-penetrating peptides: opportunities and challenges.* Biomed Res Int, 2015. **2015**: p. 834079.

49.   Raad, M., E.A. Teunissen, and E. Mastrobattista, *Peptide vectors for gene delivery: from single peptides to multifunctional peptide nanocarriers.* Nanomedicine (Lond), 2014. **9**(14): p. 2217-32.

50.   Frankel, A.D. and C.O. Pabo, *Cellular Uptake of the Tat Protein from Human Immunodeficiency Virus.* Cell, 1988. **55**(6): p. 1189-1193.

51.   Green, M. and P.M. Loewenstein, *Autonomous Functional Domains of Chemically Synthesized Human Immunodeficiency Virus Tat Trans-Activator Protein.* Cell, 1988. **55**(6): p. 1179-1188.

52.   Joliot, A., et al., *Antennapedia Homeobox Peptide Regulates Neural Morphogenesis.* Proceedings of the National Academy of Sciences of the United States of America, 1991. **88**(5): p. 1864-1868.

53.   Vives, E., P. Brodin, and B. Lebleu, *A truncated HIV-1 Tat protein basic domain rapidly translocates through the plasma membrane and accumulates in the cell nucleus.* Journal of Biological Chemistry, 1997. **272**(25): p. 16010-16017.

54.   Derossi, D., et al., *The 3rd Helix of the Antennapedia Homeodomain Translocates through Biological-Membranes.* Journal of Biological Chemistry, 1994. **269**(14): p. 10444-10450.

55.   Ruczynski, J., et al., *Cell-penetrating peptides as a promising tool for delivery of various molecules into the cells.* Folia Histochemica Et Cytobiologica, 2014. **52**(4): p. 257-269.

56.   Gupta, B., T.S. Levchenko, and V.P. Torchilin, *Intracellular delivery of large molecules and small particles by cell-penetrating proteins and peptides.* Advanced Drug Delivery Reviews, 2005. **57**(4): p. 637-651.

57.   Dietz, G.P.H. and M. Bahr, *Delivery of bioactive molecules into the cell: The Trojan horse approach.* Molecular and Cellular Neuroscience, 2004. **27**(2): p. 85-131.

58.   Mae, M. and U. Langel, *Cell-penetrating peptides as vectors for peptide, protein and oligonucleotide delivery.* Current Opinion in Pharmacology, 2006. **6**(5): p. 509-514.

59.   Ezzat, K., et al., *Solid formulation of cell-penetrating peptide nanocomplexes with siRNA and their stability in simulated gastric conditions.* Journal of Controlled Release, 2012. **162**(1): p. 1-8.

60.   Jarvert, P., et al., *Applications of cell-penetrating peptides in regulation of gene expression.* Biochemical Society Transactions, 2007. **35**: p. 770-774.

61.   Meade, B.R. and S.F. Dowdy, *Enhancing the cellular uptake of siRNA duplexes following noncovalent packaging with protein transduction domain peptides.* Advanced Drug Delivery Reviews, 2008. **60**(4-5): p. 530-536.

62.   Madani, F., et al., *Mechanisms of cellular uptake of cell-penetrating peptides.* J Biophys, 2011. **2011**: p. 414729.

63.   Pooga, M., et al., *Galanin-based peptides, galparan and transportan, with receptor-dependent and independent activities.* Ann N Y Acad Sci, 1998. **863**: p. 450-3.

64.   Pooga, M., et al., *Cell penetration by transportan.* FASEB J, 1998. **12**(1): p. 67-77.

65.   Futaki, S., et al., *Arginine-rich peptides - An abundant source of membrane-permeable peptides having potential as carriers for intracellular protein delivery.* Journal of Biological Chemistry, 2001. **276**(8): p. 5836-5840.

66.   Neundorf, I., Rennert, R., Hoyer, J., Schramm, F., Löbner, K., Kitanovic, I., Wölfl, S., *Fusion of a short HA2-derived peptide sequence to cell-penetrating peptides improved cytosolic uptake, but enhances cytotoxic activity.* Pharmaceuticals, 2009. **2**(2): p. 49-65.

67.   Morris, M.C., et al., *A new peptide vector for efficient delivery of oligonucleotides into mammalian cells.* Nucleic Acids Research, 1997. **25**(14): p. 2730-2736.

68.   Oehlke, J., et al., *Cellular uptake of an alpha-helical amphipathic model peptide with the potential to deliver polar compounds into the cell interior non-endocytically.* Biochimica Et Biophysica Acta-Biomembranes, 1998. **1414**(1-2): p. 127-139.

69.   Hoyer, J. and I. Neundorf, *Knockdown of a G protein-coupled receptor through efficient peptide-mediated siRNA delivery.* J Control Release, 2012. **161**(3): p. 826-34.

70.   Milletti, F., *Cell-penetrating peptides: classes, origin, and current landscape.* Drug Discov Today, 2012. **17**(15-16): p. 850-60.

71.   Tunnemann, G., et al., *Live-cell analysis of cell penetration ability and toxicity of oligo-arginines.* J Pept Sci, 2008. **14**(4): p. 469-76.

72.   Ragin, A.D., R.A. Morgan, and J. Chmielewski, *Cellular import mediated by nuclear localization signal Peptide sequences.* Chem Biol, 2002. **9**(8): p. 943-8.

73.   Ziegler, A., *Thermodynamic studies and binding mechanisms of cell-penetrating peptides with lipids and glycosaminoglycans.* Adv Drug Deliv Rev, 2008. **60**(4-5): p. 580-97.

74.   Morris, M.C., et al., *A new peptide vector for efficient delivery of oligonucleotides into mammalian cells.* Nucleic Acids Res, 1997. **25**(14): p. 2730-6.

75.   Ziegler, A., et al., *Protein transduction domains of HIV-1 and SIV TAT interact with charged lipid vesicles. Binding mechanism and thermodynamic analysis.* Biochemistry, 2003. **42**(30): p. 9185-94.

76.   Milletti, F., *Cell-penetrating peptides: classes, origin, and current landscape.* Drug Discovery Today, 2012. **17**(15-16): p. 850-860.

77.   Machova, Z., et al., *Cellular internalization of enhanced green fluorescent protein ligated to a human calcitonin-based carrier peptide.* Chembiochem, 2002. **3**(7): p. 672-7.

78.   Rennert, R., I. Neundorf, and A.G. Beck-Sickinger, *Calcitonin-derived peptide carriers: mechanisms and application.* Adv Drug Deliv Rev, 2008. **60**(4-5): p. 485-98.

79.   Neundorf, I. and A.G. Beck-Sickinger, *Calcitonin-derived carrier peptides.* Current Pharmaceutical Design, 2005. **11**(28): p. 3661-3669.

80.   White, J., M. Kielian, and A. Helenius, *Membrane fusion proteins of enveloped animal viruses.* Q Rev Biophys, 1983. **16**(2): p. 151-95.

81.   Heitz, F., M.C. Morris, and G. Divita, *Twenty years of cell-penetrating peptides: from molecular mechanisms to therapeutics.* British Journal of Pharmacology, 2009. **157**(2): p. 195-206.

82.   Splith, K., et al., *Specific targeting of hypoxic tumor tissue with nitroimidazole-peptide conjugates.* ChemMedChem, 2012. **7**(1): p. 57-61.

83.   Kichler, A., A.J. Mason, and B. Bechinger, *Cationic amphipathic histidine-rich peptides for gene delivery.* Biochimica Et Biophysica Acta-Biomembranes, 2006. **1758**(3): p. 301-307.

84.   Hoyer, J. and I. Neundorf, *Peptide vectors for the nonviral delivery of nucleic acids.* Acc Chem Res, 2012. **45**(7): p. 1048-56.

85.   Jarver, P. and U. Langel, *Cell-penetrating peptides - A brief introduction.* Biochimica Et Biophysica Acta-Biomembranes, 2006. **1758**(3): p. 260-263.

86.   Foerg, C., et al., *Decoding the entry of two novel cell-penetrating peptides in HeLa cells: lipid raft-mediated endocytosis and endosomal escape.* Biochemistry, 2005. **44**(1): p. 72-81.

87.   Zorko, M. and U. Langel, *Cell-penetrating peptides: mechanism and kinetics of cargo delivery.* Adv Drug Deliv Rev, 2005. **57**(4): p. 529-45.

88.   Jiao, C.Y., et al., *Translocation and Endocytosis for Cell-penetrating Peptide Internalization.* Journal of Biological Chemistry, 2009. **284**(49): p. 33957-33965.

89.   Wang, F.H., et al., *Recent progress of cell-penetrating peptides as new carriers for intracellular cargo delivery.* Journal of Controlled Release, 2014. **174**: p. 126-136.

90.   Conner, S.D. and S.L. Schmid, *Regulated portals of entry into the cell.* Nature, 2003. **422**(6927): p. 37-44.

91.   Khalil, I.A., et al., *Uptake pathways and subsequent intracellular trafficking in nonviral gene delivery.* Pharmacological Reviews, 2006. **58**(1): p. 32-45.

92.   Bechara, C. and S. Sagan, *Cell-penetrating peptides: 20 years later, where do we stand?* FEBS Lett, 2013. **587**(12): p. 1693-1702.

93.   Copolovici, D.M., et al., *Cell-Penetrating Peptides: Design, Synthesis, and Applications.* Acs Nano, 2014. **8**(3): p. 1972-1994.

94.   Aroui, S., et al., *Efficient induction of apoptosis by doxorubicin coupled to cell-penetrating peptides compared to unconjugated doxorubicin in the human breast cancer cell line MDA-MB 231.* Cancer Letters, 2009. **285**(1): p. 28-38.

95.   Pujals, S., et al., *Shuttling gold nanoparticles into tumoral cells with an amphipathic proline-rich peptide.* Chembiochem, 2009. **10**(6): p. 1025-31.

96.   Futaki, S., et al., *Stearylated arginine-rich peptides: A new class of transfection systems.* Bioconjugate Chemistry, 2001. **12**(6): p. 1005-1011.

97.   Tonges, L., et al., *Stearylated octaarginine and artificial virus-like particles for transfection of siRNA into primary rat neurons.* RNA, 2006. **12**(7): p. 1431-8.

98.   Hayashi, Y., et al., *Cell penetrating peptide-mediated systemic siRNA delivery to the liver.* Int J Pharm, 2011. **419**(1-2): p. 308-13.

99.   Nishiyama, K., et al., *Claudin localization in cilia of the retinal pigment epithelium.* Anatomical Record, 2002. **267**(3): p. 196-203.

100.   Benmerah, A., *The ciliary pocket.* Current Opinion in Cell Biology, 2013. **25**(1): p. 78-84.

101.   Hildebrandt, F., T. Benzing, and N. Katsanis, *Mechanisms of Disease: Ciliopathies.* New England Journal of Medicine, 2011. **364**(16): p. 1533-1543.

102.   Carr, M., et al., *Molecular phylogeny of choanoflagellates, the sister group to Metazoa.* Proc Natl Acad Sci U S A, 2008. **105**(43): p. 16641-6.

103.   King, N., *Choanoflagellates.* Curr Biol, 2005. **15**(4): p. R113-4.

104.   Nitsche, F., et al., *Higher level taxonomy and molecular phylogenetics of the Choanoflagellatea.* J Eukaryot Microbiol, 2011. **58**(5): p. 452-62.

105.   Thomsen, H.A., *Loricabærende choanoflaellater (Kraveflagellater). Plankton i de indre danske farvande.* Havforskning fra Miljøstyrelsen, 1992. **11**: p. 157-194.

106.   King, N., et al., *The genome of the choanoflagellate Monosiga brevicollis and the origin of metazoans.* Nature, 2008. **451**(7180): p. 783-8.

107.   Schaeffer, H.J. and M.J. Weber, *Mitogen-activated protein kinases: Specific messages from ubiquitous messengers.* Molecular and Cellular Biology, 1999. **19**(4): p. 2435-2444.

108.   King, N., *The unicellular ancestry of animal development.* Dev Cell, 2004. **7**(3): p. 313-25.

109.   Stoeck, T. and A. Stock, *The protistan gap in the eukaryotic tree of life.* Palaeodiversity, 2010: p. 151-154.

110.   Miller, W.T., *Tyrosine kinase signaling and the emergence of multicellularity.* Biochimica Et Biophysica Acta-Molecular Cell Research, 2012. **1823**(6): p. 1053-1057.

111.   Artavanis-Tsakonas, S., M.D. Rand, and R.J. Lake, *Notch signaling: Cell fate control and signal integration in development.* Science, 1999. **284**(5415): p. 770-776.

112.   Merrifield, R.B., *Solid Phase Peptide Synthesis. I. The Synthesis of a Tetrapeptide.* Journal of the American Chemical Society, 1963. **85**((14)): p. 2149.

113.   Altmann, K.H. and M. Mutter, *Chemical Synthesis of Peptides and Proteins.* Chemie in Unserer Zeit, 1993. **27**(6): p. 274-286.

114.   Kaiser, E., et al., *Color test for detection of free terminal amino groups in the solid-phase synthesis of peptides.* Anal Biochem, 1970. **34**(2): p. 595-8.

115.   Dagert, M. and S.D. Ehrlich, *Prolonged incubation in calcium chloride improves the competence of Escherichia coli cells.* Gene, 1979. **6**(1): p. 23-8.

116.   Lattig-Tunnemann, G., et al., *Backbone rigidity and static presentation of guanidinium groups increases cellular uptake of arginine-rich cell-penetrating peptides.* Nature Communications, 2011. **2**.

117.   White, C.J. and A.K. Yudin, *Contemporary strategies for peptide macrocyclization.* Nature Chemistry, 2011. **3**(7): p. 509-524.

118.   Horn, M., et al., *Tuning the properties of a novel short cell-penetrating peptide by intramolecular cyclization with a triazole bridge.* Chem Commun (Camb), 2016. **52**(11): p. 2261-4.

119.   Katsuo, S., et al., *Intermittent simulated moving bed chromatography: 3. Separation of Troger's base enantiomers under nonlinear conditions.* Journal of Chromatography A, 2011. **1218**(52): p. 9345-9352.

120.   Di Pisa, M., G. Chassaing, and J.M. Swiecicki, *Translocation mechanism(s) of cell-penetrating peptides: biophysical studies using artificial membrane bilayers.* Biochemistry, 2015. **54**(2): p. 194-207.

121.   Vorlickova, M., et al., *Circular dichroism spectroscopy of DNA: from duplexes to quadruplexes.* Chirality, 2012. **24**(9): p. 691-8.

122.   Henchey, L.K., A.L. Jochim, and P.S. Arora, *Contemporary strategies for the stabilization of peptides in the alpha-helical conformation.* Curr Opin Chem Biol, 2008. **12**(6): p. 692-7.

123.   Madden, M.M., et al., *Facile synthesis of stapled, structurally reinforced peptide helices via a photoinduced intramolecular 1,3-dipolar cycloaddition reaction.* Chem Commun (Camb), 2009(37): p. 5588-90.

124.   Muppidi, A., et al., *Synthesis of cell-permeable stapled BH3 peptide-based Mcl-1 inhibitors containing simple aryl and vinylaryl cross-linkers.* Tetrahedron, 2014. **70**(42): p. 7740-7745.

125.   Hilinski, G.J., et al., *Stitched alpha-helical peptides via bis ring-closing metathesis.* J Am Chem Soc, 2014. **136**(35): p. 12314-22.

126.   Walensky, L.D. and G.H. Bird, *Hydrocarbon-stapled peptides: principles, practice, and progress.* J Med Chem, 2014. **57**(15): p. 6275-88.

127.   Angeles-Boza, A.M., et al., *Generation of Endosomolytic Reagents by Branching of Cell-Penetrating Peptides: Tools for the Delivery of Bioactive Compounds to Live Cells in Cis or Trans.* Bioconjug Chem, 2010. **21**(12): p. 2164-2167.

128.   Hoyer, J., et al., *Dimerization of a cell-penetrating peptide leads to enhanced cellular uptake and drug delivery.* Beilstein J Org Chem, 2012. **8**: p. 1788-97.

129.   Leadbeater, B.S. and S.A. Karpov, *Cyst formation in a freshwater strain of the choanoflagellate Desmarella moniliformis Kent.* J Eukaryot Microbiol, 2000. **47**(5): p. 433-9.

130.   Erbacher, P., et al., *Putative role of chloroquine in gene transfer into a human hepatoma cell line by DNA/lactosylated polylysine complexes.* Exp Cell Res, 1996. **225**(1): p. 186-94.

131.   Schnitzer, J.E., et al., *Filipin-sensitive caveolae-mediated transport in endothelium: reduced transcytosis, scavenger endocytosis, and capillary permeability of select macromolecules.* J Cell Biol, 1994. **127**(5): p. 1217-32.

132.   Delgadillo, M.G., et al., *Transient and selectable transformation of the parasitic protist Trichomonas vaginalis.* Proc Natl Acad Sci U S A, 1997. **94**(9): p. 4716-20.

133.   Dawson, S.C., et al., *Stable transformation of an episomal protein-tagging shuttle vector in the piscine diplomonad Spironucleus vortens.* BMC Microbiol, 2008. **8**: p. 71.

134.   Dai, Y.H., et al., *Gene transport and expression by arginine-rich cell-penetrating peptides in Paramecium.* Gene, 2011. **489**(2): p. 89-97.

135.   Xu, Y., et al., *Nona-arginine facilitates delivery of quantum dots into cells via multiple pathways.* J Biomed Biotechnol, 2010. **2010**: p. 948543.

136.   Herce, H.D., et al., *Arginine-rich peptides destabilize the plasma membrane, consistent with a pore formation translocation mechanism of cell-penetrating peptides.* Biophys J, 2009. **97**(7): p. 1917-25.

137.   Reuter, M., et al., *Poly-l-lysines and poly-l-arginines induce leakage of negatively charged phospholipid vesicles and translocate through the lipid bilayer upon electrostatic binding to the membrane.* Biophys Chem, 2009. **144**(1-2): p. 27-37.

138.   Ter-Avetisyan, G., et al., *Cell entry of arginine-rich peptides is independent of endocytosis.* J Biol Chem, 2009. **284**(6): p. 3370-8.

139.   Hassane, F.S., et al., *Insights into the cellular trafficking of splice redirecting oligonucleotides complexed with chemically modified cell-penetrating peptides.* Journal of Controlled Release, 2011. **153**(2): p. 163-172.

140.   Kim, W.J., et al., *Cholesteryl oligoarginine delivering vascular endothelial growth factor siRNA effectively inhibits tumor growth in colon adenocarcinoma.* Mol Ther, 2006. **14**(3): p. 343-50.

141.   Lehto, T., et al., *Delivery of nucleic acids with a stearylated (RxR)4 peptide using a non-covalent co-incubation strategy.* J Control Release, 2010. **141**(1): p. 42-51.

142.   Li, M., et al., *A tailor-made specific anion-binding motif in the side chain transforms a tetrapeptide into an efficient vector for gene delivery.* Angew Chem Int Ed Engl, 2015. **54**(10): p. 2941-4.

143. Kuchelmeister, H.Y., et al., *Utilizing combinatorial chemistry and rational design: peptidic tweezers with nanomolar affinity to DNA can be transformed into efficient vectors for gene delivery by addition of a lipophilic tail.* Angew Chem Int Ed Engl, 2013. **52**(52): p. 14016-20.

144. Rennert, R., et al., *Generation of carrier peptides for the delivery of nucleic acid drugs in primary cells.* ChemMedChem, 2008. **3**(2): p. 241-53.

145. Korner, M. and J.C. Reubi, *NPY receptors in human cancer: a review of current knowledge.* Peptides, 2007. **28**(2): p. 419-25.

146. Andaloussi, S.E.L., et al., *Design of a peptide-based vector, PepFect6, for efficient delivery of siRNA in cell culture and systemically in vivo.* Nucleic Acids Research, 2011. **39**(9): p. 3972-3987.

147. Fliegauf, M., T. Benzing, and H. Omran, *When cilia go bad: cilia defects and ciliopathies (vol 8, pg 880, 2007).* Nature Reviews Molecular Cell Biology, 2008. **9**(1): p. 88-88.

148. Lee, S.H., B. Castagner, and J.C. Leroux, *Is there a future for cell-penetrating peptides in oligonucleotide delivery?* Eur J Pharm Biopharm, 2013. **85**(1): p. 5-11.

149. Foerg, C., et al., *Differentiation restricted endocytosis of cell penetrating peptides in MDCK cells corresponds with activities of Rho-GTPases.* Pharm Res, 2007. **24**(4): p. 628-42.

150. Hansson, M.L., et al., *Efficient delivery and functional expression of transfected modified mRNA in human embryonic stem cell-derived retinal pigmented epithelial cells.* J Biol Chem, 2015. **290**(9): p. 5661-72.

151. Berbari, N.F., et al., *Identification of ciliary localization sequences within the third intracellular loop of G protein-coupled receptors.* Mol Biol Cell, 2008. **19**(4): p. 1540-7.

152. Schermer, B., et al., *The von Hippel-Lindau tumor suppressor protein controls ciliogenesis by orienting microtubule growth.* J Cell Biol, 2006. **175**(4): p. 547-54.

153. Dal Sasso, A.A., et al., *Birt-Hogg-Dube syndrome. State-of-the-art review with emphasis on pulmonary involvement.* Respir Med, 2015. **109**(3): p. 289-96.

154. Luijten, M.N., et al., *Birt-Hogg-Dube syndrome is a novel ciliopathy.* Hum Mol Genet, 2013. **22**(21): p. 4383-97.

155. Miller, J.C., et al., *A TALE nuclease architecture for efficient genome editing.* Nat Biotechnol, 2011. **29**(2): p. 143-8.

7. Attachment

7.1 Attachment of additional figures and tables

Antibiotics used to reduce bacteria contamination

Table 16: Overview of antibiotics

Name	Used concentration
Ofloxacin	1 mg/mL
Gentamicin	1 mg/mL
Chloramphenicol	1 mg/mL
Roxythromycin	1 mg/mL
Methoxyflurane	1 mg/mL
Metronidazol	1 mg/mL
Neomycin	1 mg/mL
Polymyxin B	1 mg/mL
Tyrothricin	1 mg/mL
Bacitracin	1 mg/mL
Fusidin acid	1 mg/mL
Tobramycin	1 mg/mL

In Vitro Transfection of ciliary plasmid 5HT6.GFP pcDNA6 in differentiated hTERT RPE-1 cells
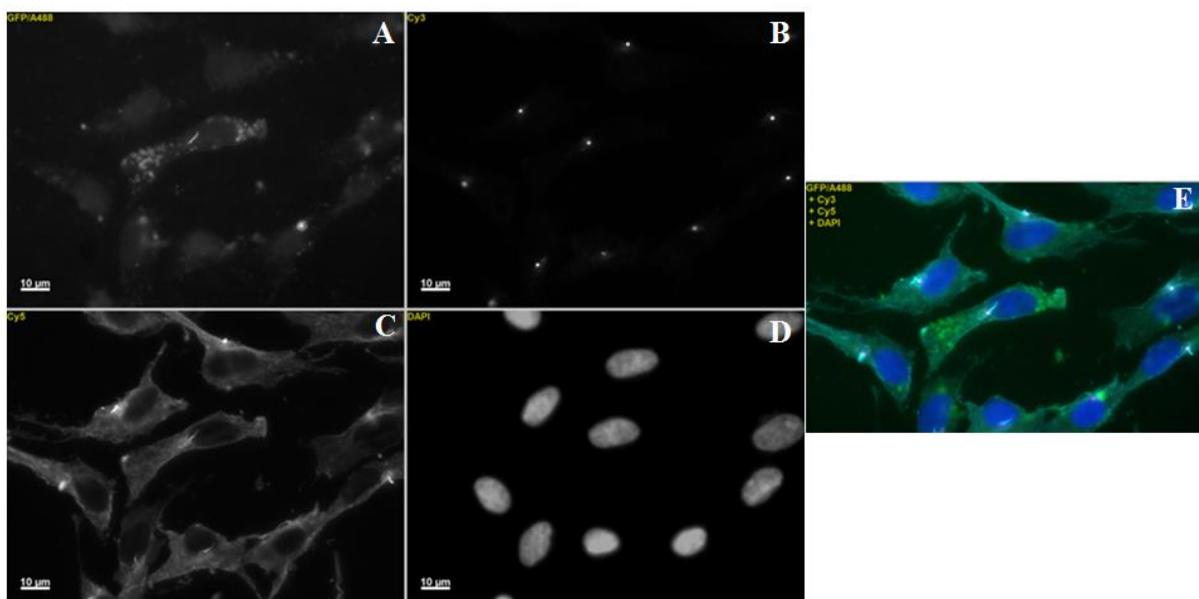
Fig. 45: Charge ratio 10:1 using 0.5 µg Plasmid and CPP **(1a)**
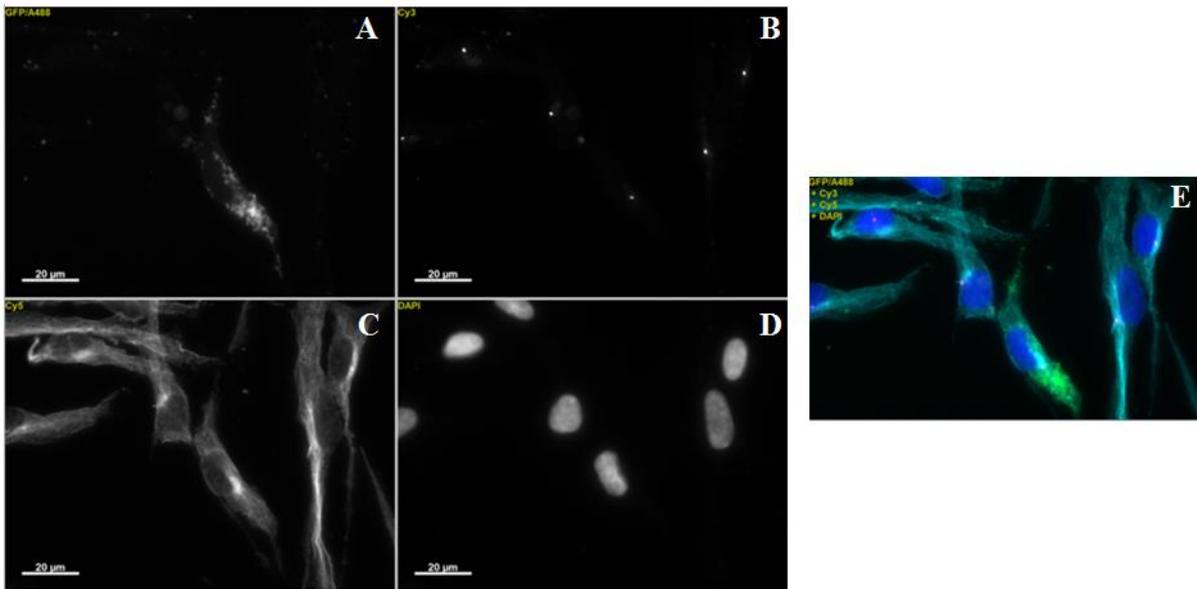
Fig. 46: Charge ratio 30:1 using 0.5 µg Plasmid and **(2d)**
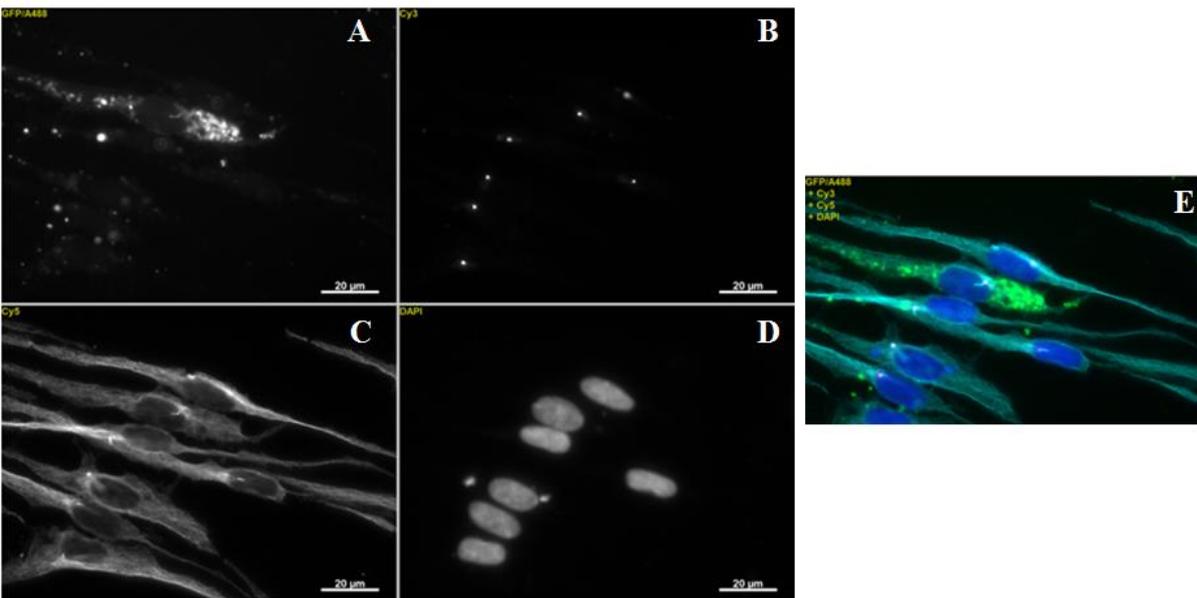
Fig. 47: Charge ratio 30:1 using 1 µg Plasmid and **(2d)**

In Vitro Transfection hFLCN (talen transfection) in differentiated hTERT RPE-1 cells
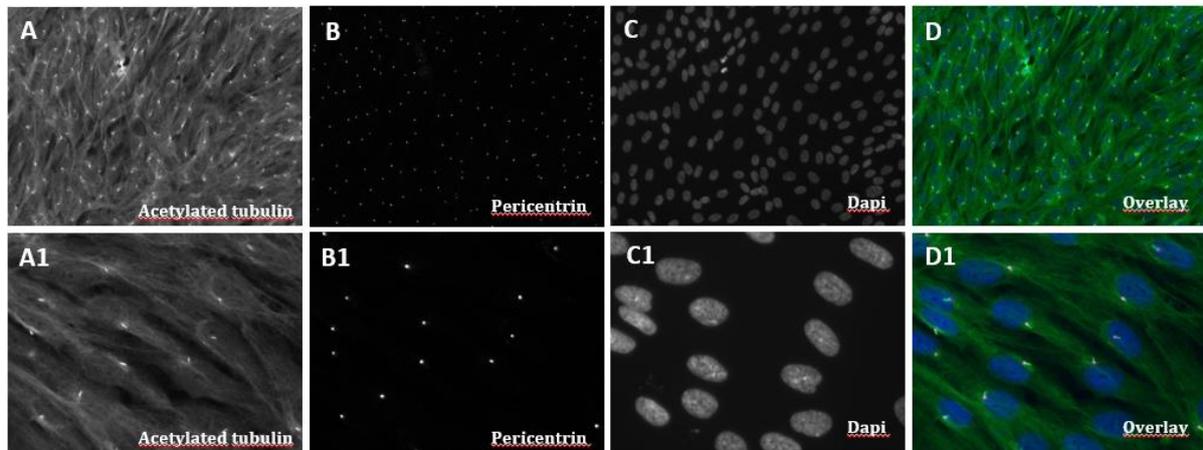
Fig. 48: Antibody Cilia staining after 24 hours serum starvation: (A-D) Axiovert 20 x objective; (A1-D1) Axiovert 60 x objective

PCR for checking integration into aavs locus

a) Empty locus amplication: product size ~1935 bp
b) Integration: product size ~1180 bp

Table 17: Overview of applied CCP concentration and plasmid amount

	Charge ratio	Peptide	Plasmid amount	[c] Peptide	Addition CQ
A	10:1	**(1a)**	Each 0.5 µg	5.7 µM	No
B	10:1	**(1a)**	Each 0.5 µg	5.7 µM	Yes, 100 µM
C	13:1	**(1a)**	Each 0.5 µg	7.4 µM	No
D	13:1	**(1a)**	Each 0.5 µg	7.4 µM	Yes, 100 µM
E	10:1	**(2d)**	Each 0.5 µg	3.1 µM	No
F	10:1	**(2d)**	Each 0.5 µg	3.1 µM	Yes, 100 µM
G	30:1	**(2d)**	Each 0.5 µg	9.3 µM	No
H	30:1	**(2d)**	Each 0.5 µg	9.3 µM	Yes, 100 µM
I	10:1	**(2a)**	Each 0.5 µg	2.7 µM	No
J	10:1	**(2a)**	Each 0.5 µg	2.7 µM	Yes, 100 µM
K	30:1	**(2a)**	Each 0.5 µg	8.1 µM	No
L	30:1	**(2a)**	Each 0.5 µg	8.1 µM	Yes, 100 µM
M	10:1	**(1a)**	Each 1.0 µg	7.6 µM	No
N	10:1	**(1a)**	Each 1.0 µg	7.6 µM	Yes, 100 µM
O	10:1	**(2d)**	Each 1.0 µg	6.1 µM	No
P	10:1	**(2d)**	Each 1.0 µg	6.1 µM	Yes, 100 µM
Q	30:1	**(2d)**	Each 1.0 µg	18.3 µM	No
R	30:1	**(2d)**	Each 1.0 µg	18.3 µM	Yes, 100 µM
S	10:1	**(2a)**	Each 1.0 µg	5.36 µM	No

T	10:1	(2a)	Each 1.0 µg	5.36 µM	Yes, 100 µM
U	30:1	(2a)	Each 1.0 µg	16:1 µM	No
V	30:1	(2a)	Each 1.0 µg	16:1 µM	Yes, 100 µM
W	10:1	(1a)	Each 1.0 µg	7.6 µM	Yes, 100 µM
X	30:1	(2d)	Each 1.0 µg	9.3 µM	Yes, 100 µM
y	30:1	(2a)	Each 1.0 µg	8.1 µM	Yes, 100 µM

Fig. 49: PCR for checking integration into aavs locus
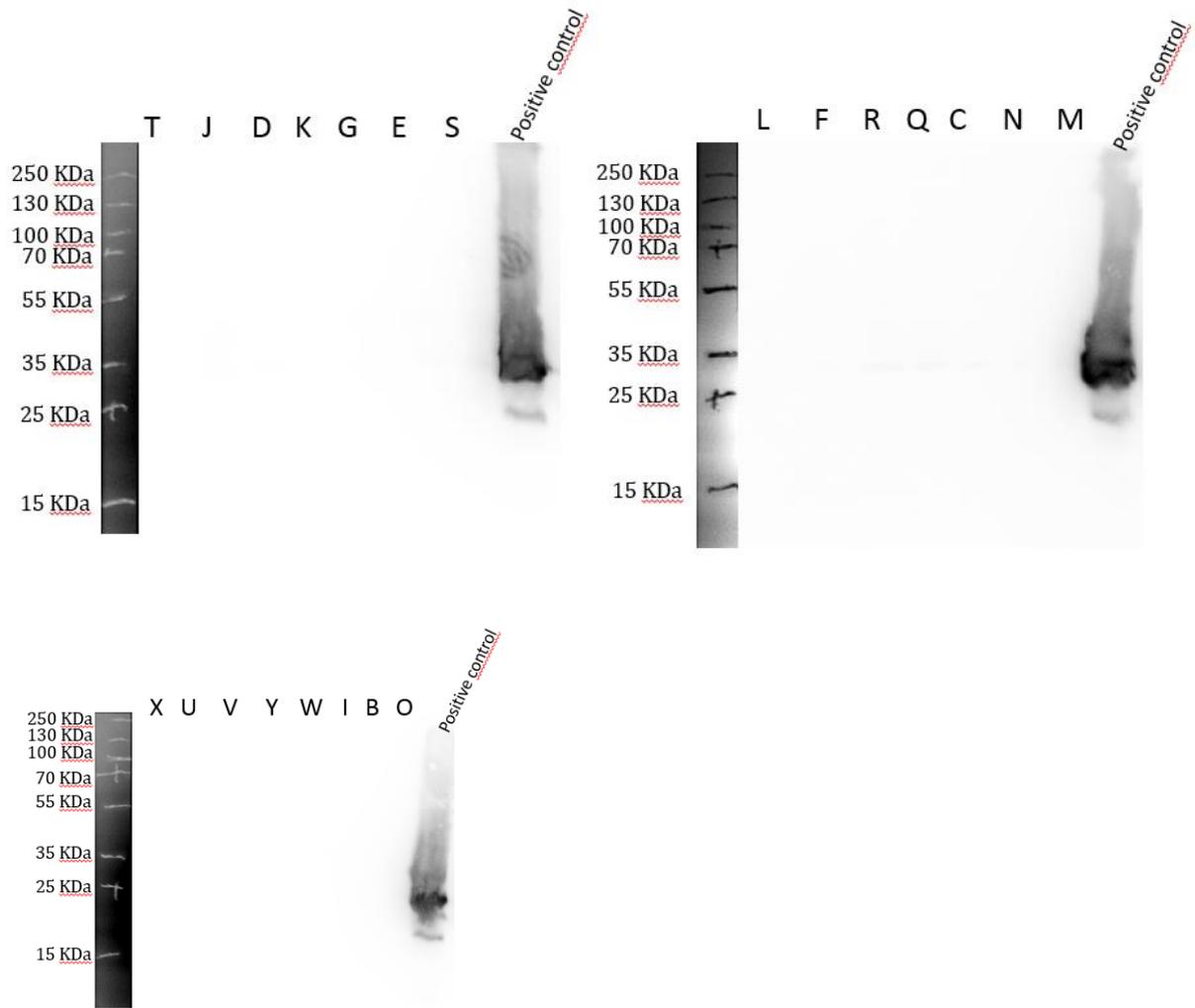
Fig. 50: Western blotting with GFP antibody

7.2 List of abbreviations

ADA-SCID	Adenosine deaminase deficiency
BOC	tert-butyloxycarbonyl
CD	circular dichroism
CF	5(6)-carboxyfluorescein
CH_2Cl_2	Dichloromethane
CPP	cell-penetrating peptide
CQ	chloroquine
CuAAC	copper-catalyzed azidealkyne cycloaddition
DCM	Dichloromethane
Dde	1-(4,4-dimethyl-2,6-d ioxacyclohexylidene)etyl
DIC	N,N'-Diisopropylcarbodiimide
DIPEA	Ethyldiisopropylamine
DMEM	Dulbecco's Modified Eagle Medium
DMF	*N,N*-Dimethylformamide
DMSO	Dimethyl sulfoxide
DNA	Deoxyribonucleic acid
DPBS	Dulbecco's phosphate buffered saline
Et_2O	Diethyl ether
EtOH	Ethanol
FACS	fluorescence-activated cell sorter
Fmoc	9-fluorenylmethoxycarbonyl
h	hour
hCT	human calcitonin
HEK-293	human embryonic kidney
HeLa	Henrietta Lacks
HIV	human immunodeficiency virus
HPLC	high performance liquid chromatrography
LC-MS	liquid chromatography mass spectrometry
MCF-7	Michigan Cancer Foundation-7
MeOH	Methanol
min	minutes
MW	Molecular weight
NLS	nuclear localization signal
NMP	N-Methyl-2-pyrrolidone
Pbf	2,2,4,6,7-Pentamethyldihydrobenzofuran-5-sulfonyl chloride

PCR	polymerase chain reaction
pDNA	plasmid DNA
PEI	polyethylenimine
PFA	para-formaldehyde
RPE	Retinal pigment epithelium
RP-HPLC	reversed phase HPLC
rpm	Revolutions per minute
RPMI	Roswell Park Memorial Institute
rt	room temperture
SDS	sodium dodecyl sulfate
siRNA	small interfering RNA
sp-Medium	Schmaltz-Pratt Medium
SPPS	solid-phase peptide synthesis
TFA	Trifluoroacetic acid
TFA	trifluoroacetic acid
TIS	Triisopropylsilane

7.3 List of figures

7.4 List of tables

Erklärung

Ich versichere, dass ich die von mir vorgelegte Dissertation selbstständig angefertigt, die benutzten Quellen und Hilfsmittel vollständig angegeben und die Stellen der Arbeit – einschließlich Tabellen, Karten und Abbildungen –, die anderen Werken im Wortlaut oder dem Sinn nach entnommen sind, in jedem Einzelfall als Entlehnung kenntlich gemacht habe; dass diese Dissertation noch keiner anderen Fakultät oder Universität zur Prüfung vorgelegen hat; dass sie – abgesehen von unten angegebenen Teilpublikationen – noch nicht veröffentlicht worden ist, sowie, dass ich eine solche Veröffentlichung vor Abschluss des Promotionsverfahrens nicht vornehmen werde. Die Bestimmungen der Promotionsordnung sind mir bekannt.

Die von mir vorgelegte Dissertation ist von Frau Prof. Dr. Ines Neundorf betreut worden.

Teilpublikationen:

- **Horn M., Reichart F., Natividad-Tietz S., Diaz D., Neundorf I. (2016)**. Tuning the properties of a novel short cell-penetrating peptide by intramolecular cyclization with a triazole bridge. *Chem Commun (Camb).*,52(11), p 2261-2264.

- **Natividad S., Nitsche, F., Neundorf I. (2014)**. First insight into cell-penetrating peptide tranlocation in choanoflagellates. Proceedings of the 33rd Eur. Pept. Symp., p 365.

- **Natividad-Tietz S., Nitsche, F., Neundorf I. (2014)**. Peptide-mediated cargo delivery in choanoflagealltes. *J Pep Sci*. 20(S1), S96-S96.

Posterpräsentationen:

- **Natividad-Tietz S., Kohli P., Schermer B., Müller R.-U., Neundorf I. (2015)**. Peptide-mediated gene delivery into ciliated cells. 12th German Peptide Symposium, Garching

- **Natividad S., Nitsche, F., Neundorf I. (2014)**. Peptide-mediated cargo delivery in choanoflagealltes. 33rd European Peptide Symposium, Sofia, Bulgarien.

—————————————   —————————————

Ort, Datum   (Stephanie Natividad-Tietz)